

2017

# Multi-scale mechanics of collagen extracellular matrix

---

<https://hdl.handle.net/2144/27042>

*"Downloaded from OpenBU. Boston University's institutional repository."*

BOSTON UNIVERSITY  
COLLEGE OF ENGINEERING

Dissertation

**MULTI-SCALE MECHANICS OF COLLAGEN EXTRACELLULAR MATRIX**

by

**HAIYUE LI**

B.S., University of Science and Technology of China, 2011

Submitted in partial fulfillment of the  
requirements for the degree of  
Doctor of Philosophy

2017

© 2017 by  
HAIYUE LI  
All rights reserved

Approved by

First Reader

---

Katherine Yanhang Zhang, Ph.D.  
Associate Professor of Mechanical Engineering  
Associate Professor of Materials Science and Engineering  
Associate Professor of Biomedical Engineering

Second Reader

---

Michael L. Smith, Ph.D.  
Associate Professor of Biomedical Engineering  
Associate Professor of Materials Science and Engineering

Third Reader

---

Dimitrije Stamenovic, Ph.D.  
Professor of Biomedical Engineering  
Professor of Materials Science and Engineering

Fourth Reader

---

Michael B. Albro, Ph.D.  
Assistant Professor of Mechanical Engineering  
Assistant Professor of Materials Science and Engineering

## **DEDICATION**

I would like to dedicate this work to my parents for their love and support.

## ACKNOWLEDGMENTS

I would like to express my thanks of gratitude to many people who helped me in last several years. First and the foremost, I would like to thank my advisor, Professor Katherine Yanhang Zhang, for her valuable suggestions, consistent patience and encouragement. Looking back over the past few years, Professor Zhang's patience and effective guidance has made me grow more and more professionally and eventually accomplish my final project. Since I don't have any experience in tissue engineering at the very beginning, Professor Zhang gives me a lot of valuable suggestions in designing experiments and analyzing results, which gradually improves my research abilities. When I meet the bottleneck of my project, it is her endless trust and encouragement that helps me get through. She even sacrifices a lot of her personal time helping me prepare my thesis. In a word, I would like to give my most sincere thanks to Prof. Zhang.

I would like to thank the rest of my dissertation committee including Professor Elise Morgan, Professor Michael Smith, Professor Dimitrije Stamenovic and Professor Michael Albro for their insightful comments and suggestions during my prospectus. I also would like to thank Dr. Enhua Zhou, Dr. Raimon Sunyer for their generous help on setting up the OMTc.

My sincere thanks also go to my lab mates and friends in the Multi-scale Tissue Biomechanics Laboratory including Ming-Jay Chow, Bin Xu, Shahrokh Zeinali-Davarani, Yunjie Wang, Jeffrey Mattson, Xunjie Yu, Hyung Jin Sun, for their inspiring suggestions and for the good time we've had together in the past years.

# **MULTI-SCALE MECHANICS OF COLLAGEN EXTRACELLULAR MATRIX**

**HAIYUE LI**

Boston University, College of Engineering, 2017

Major Professor: Katherine Yanhang Zhang, Ph.D., Associate Professor of Mechanical Engineering, Associate Professor of Materials Science and Engineering, Associate Professor of Biomedical Engineering

## **ABSTRACT**

Extracellular matrix (ECM) provides the principal avenue for mechanochemical communication between tissue and cells. ECM not only plays an important role in providing structural and biomechanical support, but also in regulating a series of cellular behaviors. However, the underlying mechanisms by which the ECM mechanics influence cell and tissue function remain to be elucidated, since this process span size scales from tissue to molecular level. Furthermore, ECM has a hierarchical 3D structure and the load distribution is highly dependent on the architecture and mechanical properties. In this thesis, the multiscale mechanics of collagen ECM was studied using both experimental and modeling approaches.

Rheological and biaxial tensile testing were performed to study the macroscopic mechanical properties. A theoretical framework was developed to determine the continuous relaxation spectrum. Investigating the spectrum in terms of number of peaks, peak intensity and time constants sheds light on the main intrinsic properties of viscoelastic materials. Material parameters from continuous relaxation spectrum were used in finite element models to simulate the dynamic rheological measurements of collagen matrix. The microscopic mechanical properties were measured using Optical

Magnetic Twisting Cytometry (OMTC). Ferromagnetic beads embedded in the matrix were used as mechanical probes. Our study on the macro- and micro-scopic mechanical properties of collagen matrix suggested several interesting differences originated from the scales of measurements. In macroscopic measurements, the storage and shear modulus increase with collagen concentration. At microscopic scale, the apparent storage and loss modulus are less sensitive to changes in collagen concentration. However, the loss modulus is more affected by the local interstitial fluid environment, leading to an increase in viscosity, especially at higher frequencies. A novel experimental approach was established to study the multi-scale ECM mechanics that allows the measurements of local ECM mechanical properties with controlled tissue-level mechanical loading by integrating the OMTC and biaxial tensile tester. Multiphoton imaging reveals structural changes in the collagen network that involve gradual straightening and collagen fiber recruitment with tissue level mechanical loading. Our study shows there is a complex interplay among structural heterogeneity, collagen fiber orientation, and fiber engagement in determining the ECM local mechanical properties.

## TABLE OF CONTENTS

<b>DEDICATION</b> .....	iv
<b>ACKNOWLEDGMENTS</b> .....	v
<b>ABSTRACT</b> .....	vi
<b>LIST OF TABLES</b> .....	xii
<b>LIST OF FIGURES</b> .....	xiii
<b>CHAPTER 1: INTRODUCTION</b> .....	1
1.1 Objectives .....	1
1.2 Collagen and its hierarchical structure.....	1
1.3 Collagen in ECM .....	3
1.4 Macroscopic mechanical measurements of collagen gel .....	5
1.5 Microscopic mechanical measurements of collagen gel.....	6
1.6 Multi-scale ECM mechanics.....	7
1.7 Outline of the research .....	8
<b>CHAPTER 2: EXPERIMENTAL METHODS</b> .....	10
2.1 Overview.....	10
2.2 Preparation of collagen matrix.....	10
2.3 Rheological test.....	11
2.4 Biaxial Tensile Testing .....	13
2.5 Optical Magnetic Twisting Cytometry (OMTC) .....	15

2.6	Integrated multi-scale OMTC – biaxial tensile testing system.....	17
<b>CHAPTER 3: EFFECT OF SLIPPAGE ON RHEOLOGICAL MEASUREMENT</b>		
<b>OF GENIPIN CROSSLINKED COLLAGEN GEL .....</b>		
		<b>19</b>
3.1	Overview.....	19
3.2	Introduction.....	19
3.3	Material and Methods .....	21
3.3.1	Sample preparation .....	21
3.3.2	Rheological test.....	21
3.3.3	Statistical Analysis.....	22
3.4	Results.....	22
3.5	Discussion.....	29
3.6	Summary.....	33
<b>CHAPTER 4: MODELING OF THE VISCOELASTIC BEHAVIOR OF</b>		
<b>COLLAGEN GEL FROM DYNAMIC OSCILLATORY SHEAR</b>		
<b>MEASUREMENTS .....</b>		
		<b>34</b>
4.1	Overview.....	34
4.2	Introduction.....	35
4.3	Theoretical framework and experimental methods.....	37
4.3.1	Discrete relaxation spectrum.....	37
4.3.2	Continuous relaxation spectrum .....	38
4.3.3	Rheological measurements .....	40
4.3.4	Finite element modeling .....	41

4.4	Results.....	42
4.5	Discussion.....	48
4.6	Summary.....	52
<b>CHAPTER 5: MULTI-SCALE MEASUREMENTS OF THE MECHANICAL</b>		
<b>PROPERTIES OF COLLAGEN MATRIX.....</b>		
5.1	Overview.....	54
5.2	Introduction.....	55
5.3	Material and methods.....	58
5.3.1	Collagen gel preparation.....	58
5.3.2	Macroscopic mechanical property measurement.....	58
5.3.3	Microscopic mechanical property measurement .....	59
5.3.4	Finite Element Modeling .....	60
5.4	Results.....	63
5.5	Discussion.....	73
5.6	Summary.....	80
<b>CHAPTER 6: INTEGRATING STRUCTURAL HETEROGENEITY FIBER</b>		
<b>ORIENTATION AND RECRUITMENT IN MULTI-SCALE ECM MECHANICS</b>		
.....		82
6.1	Overview.....	82
6.2	Introduction.....	83
6.3	Materials and methods .....	86
6.3.1	Sample preparation .....	86

6.3.2	Integrated multi-scale OMTC – biaxial tensile testing system.....	87
6.3.3	Tissue-level mechanical property measurements .....	87
6.3.4	Local mechanical property measurements.....	87
6.3.5	Multiphoton Imaging .....	88
6.4	Results.....	89
6.5	Discussion.....	99
6.6	Summary.....	105
<b>CHAPTER 7: CONCLUSIONS AND OUTLOOK.....</b>		<b>106</b>
7.1	Conclusions.....	106
7.2	Outlook .....	108
<b>BIBLIOGRAPHY.....</b>		<b>111</b>
<b>CURRICULUM VITAE.....</b>		<b>125</b>

**LIST OF TABLES**

Table 4.1: Prony series obtained from directed fitting with different fitting criteria by varying the allowable average root-mean-square fitting residual

$$\varepsilon = \sqrt{\frac{1}{m} \sum_i^m \left[ \left( \frac{G'-Z'}{G_e} \right)_i^2 + \left( \frac{G''-Z''}{G_e} \right)_i^2 \right]}$$

where m is the number of frequency levels, G' and G'' are analytical storage and loss modulus from Equation (4.2) and (4.3), Z' and Z'' are experimental measured storage and loss modulus. .... 45

Table 4.2: Prony series calculated from continuous spectrum using Equation (4.8). In addition to the peak relaxation time  $\tau_i$ , equivalent peak intensity  $G_i$ , and nondimensional quantity  $g_i$ , the integration interval (a, b) was also listed. .... 45

Table 5.1: Material parameters of collagen gel obtained by fitting the shear stress and strain responses in Figure 5.5 using the hyperelastic model in Equation 5.2. .... 70

## LIST OF FIGURES

Figure 1.1: Hierarchical structure of collagen (Gautieri & Vesentini, 2011) .....	3
Figure 1.2: Picture of Extracellular Matrix composed by mainly collagen fibers and other groundmatrix substances.....	5
Figure 2.1: Picture of a parallel plate rheometer.....	12
Figure 2.2: Picture of the biaxial tensile tester showing the sample mounted to the linear positioners with adventitia peeled from porcine thoracic aorta in zoom in view. ....	14
Figure 2.3: Picture of Optical Magnetic Twisting Cytometry System and a zoom-in view of magnetizing and twisting coil. Schematic of a ferromagnetic bead twisted by magnetic field is also shown. ....	16
Figure 2.4: (a) Picture of Optical Magnetic Twisting Cytometry combined with the biaxial tensile tester System. The samples are placed inside the magnetic twisting stage shown in (b). ....	18
Figure 3.1: Results from frequency sweep tests of 0.1% genipin crosslinked collagen gel at maximum shear strain of (a) 2%, (b) 4%, (c) 6% and (d) 8% on smooth and rough surface conditions when sandpaper (1500 grits and 400 grits) are attached to the top and bottom surfaces of the rheometer plates.....	24
Figure 3.2: Results from frequency sweep tests of 0.25% genipin crosslinked collagen gel at maximum shear strain of (a) 2%, (b) 4%, (c) 6% and (d) 8% on smooth and rough surface conditions when sandpaper (400 grits) are attached to the top and bottom surfaces of the rheometer plates.....	25

Figure 3.3: Results from frequency sweep tests of non-crosslinked and genipin crosslinked collagen gel. The maximum shear strain is 1% for non-crosslinked collagen gel and 2% for genipin crosslinked collagen gel..... 26

Figure 3.4: Comparison of storage modulus  $G'$ , loss modulus  $G''$ , and phase lag  $\delta$  from frequency sweep tests of 0.1% genipin crosslinked collagen gel on three surface conditions at 1.186Hz. (a) 2%, (b) 4%, (c) 6% and (d) 8% shear strain. \* indicates comparison is statistical significant ( $p < 0.05$ ). ..... 27

Figure 3.5: Results of (a) storage modulus  $G'$  and (b) loss modulus  $G''$  from strain sweep tests of 0.25% crosslinked collagen gel with shear strain ranges from 0.1% to 10% on smooth and rough surface conditions when sandpaper (400 grits) are attached to the top and bottom surfaces of the rheometer plates. Experiments with smooth surface conditions were performed at 1Hz, while with rough surface conditions were performed at 1Hz and 5Hz..... 28

Figure 3.6: Results from relaxation tests (a) on smooth and rough surface conditions of 0.25% crosslinked collagen gel at initial shear strain of 6%, (b) from 0.25% crosslinked collagen gel measurement at different initial shear strains of 2%, 4%, 6%, and 8% for rough surface condition when sandpaper (400 grits) are attached to the top and bottom surfaces of the rheometer plates..... 29

Figure 3.7: Comparison of the rate of relaxation of 0.25% genipin crosslinked collagen gel tested with smooth and rough surface (modified by 400 grits sandpaper) conditions at 6% of shear strain. .... 32

Figure 4.1: Dynamic storage and loss moduli of collagen gel from frequency sweep tests with angular frequency ranges from 0.3142 to 377rad/s. Maximum oscillatory shear strains are 4%, 6%, and 8%. .....	43
Figure 4.2: Continuous relaxation spectra of collagen gel obtained based on frequency sweep measurements at 4%, 6%, and 8% oscillatory shear strains. ....	44
Figure 4.3: (a) Comparison between the magnitude of shear stress output from finite element simulation and experimental measurements during frequency sweep test with 4% oscillatory shear strain; and (b) Phase lag between the shear stress and applying strain from simulation and measurements. ....	47
Figure 4.4: Comparison of G' and G'' between finite element simulations and experimental measurements. The viscous properties of collagen gel were described by using Prony series with parameters from Tables 4.1 (Fig. 4.4a–c) and Table 4.2 (Fig. 4.4d).....	48
Figure 5.1: Schematic of optical magnetic twisting cytometry. Ferromagnetic bead (Diameter $\Phi$ ) embedded in collagen matrix. The bead embedding degree is the fraction of diameter of the bead embedded in the matrix, defined as $s/\Phi$ . A homogeneous magnetic twisting field causes the bead to rotate and to displace. T is the applied specific magnetic torque. The lateral translation d is record during the OMTC measurement.....	62
Figure 5.2: Averaged storage and loss modulus from macroscopic rheometer measurements of collagen matrix of 2.0mg/ml, 3.0mg/ml, and 4.8mg/ml collagen	

concentrations from (a) strain sweep tests, and (b) frequency sweep tests. Results were averaged from four samples. Error bars represent standard error deviation. ... 64

Figure 5.3: Averaged apparent storage and loss modulus from microscopic OMTC measurements of collagen matrix of 2.0mg/ml, 3.0mg/ml, and 4.8mg/ml collagen concentrations by using (a) Streptavidin coated ferromagnetic beads, and (b) Poly-l-lysine coated ferromagnetic beads. Results were averaged from three samples and six locations on each sample. Error bars represent standard deviation..... 66

Figure 5.4: Averaged phase angle based on measurements from (a) rheometer (Figure 5.2b) and (b) OMTC (Figure 5.3a) for collagen matrix of 2.0mg/ml, 3.0mg/ml, and 4.8mg/ml collagen concentrations. Comparison between phase angles from rheometer and OMTC measurements for collagen matrix with collagen concentrations of (c) 2.0mg/ml, (d) 3.0mg/ml, and (e) 4.8mg/ml. Error bars represent standard deviation. .... 68

Figure 5.5: Averaged shear stress vs. strain curves of collagen matrix from rheometer measurements fitted by the hyperelastic constitutive model in Equation 5.2. Results were averaged from four samples. .... 69

Figure 5.6: Matrix thickness dependency study with the height of collagen matrix varies from 10 to 100 $\mu$ m in the finite element simulation. The lateral displacement at the centroid of the ferromagnetic bead is plotted with bead embedding degree varies from 5% to 90% for the 3.0mg/ml collagen matrix..... 70

Figure 5.7: Contour plots showing the strain field distribution in collagen matrix when a ferromagnetic bead is embedded in a 50 $\mu$ m-high matrix with 20% bead embedding

degree, (a) x- component, (b) z- component, (c) xz component and (d) equivalent strain..... 72

Figure 5.8: Geometric factor  $\beta$  obtained from finite element simulation with beads embedding degree varies from 5% to 90% for collagen matrix of 2.0mg/ml, 3.0mg/ml, and 4.8mg/ml collagen concentrations. Results from Mijailovich (Mijailovich, et al., 2002) with linear elastic material property assumption are shown for comparison. .... 73

Figure 6.1: (a) Average Cauchy stress vs. stretch curves of adventitial tissue samples from biaxial tensile testing (n=5). (b) Average tangent modulus in both the circumferential and longitudinal directions (n=5). Data is presented as average  $\pm$  standard error of the mean. .... 89

Figure 6.2: (a–e) Representative multiphoton images at equi-biaxial stretch levels of 1, 1.05, 1.1, 1.15, and 1.2, and (f) changes in fiber straightness parameter with equi-biaxial stretch. Data in (f) is presented as average  $\pm$  standard error of the mean. .... 90

Figure 6.3: Average normalized fiber orientation distributions with equal biaxial stretches of 1, 1.05, 1.1, 1.15 and 1.2. Fibers oriented at  $0^\circ$  and  $\pm 90^\circ$  are in the circumferential and longitudinal directions of the adventitia, respectively. .... 91

Figure 6.4: (a) Representative beads lateral displacement when the biaxial stretch is 1.15. The beads lateral displacement is oriented with the direction aligned with the arrow and the magnitude is represented by the length of the arrow ( $\times 100$ ). C and L represents the circumferential and longitudinal direction of the sample. Note that the beads are magnetized along the circumferential direction. (b) Displacement

orientation distribution of beads in (a) with multi-modal fitting. (c) Representative multi-modal fitting of beads displacement orientation distribution at different stretch levels. (d) Parameter $\pi_2$ versus stretch levels. ....	94
Figure 6.5: Complex apparent modulus from OMTC measurements located within the major and minor peaks of the beads displacement orientation distribution.....	95
Figure 6.6: Representative distributions of complex apparent modulus of sample 1 at biaxial stretch levels of (a) 1.01, (b) 1.09, and (c) 1.17. The position of median, used as a measure of the local mechanical properties in the OMTC experiment, is marked with a red line.....	96
Figure 6.7: The MAD of locally measured stiffness with increasing biaxial stretch for all adventitia samples. ....	97
Figure 6.8: Apparent storage modulus (a), loss modulus (b), complex modulus (c), and phase angle (d) measured by OMTC vs. macroscopic biaxial stretch.....	98
Figure 6.9: Apparent storage modulus (a), loss modulus (b), complex modulus (c), and phase angle (d) measured by OMTC vs. macroscopic stress.....	99

## **CHAPTER 1: INTRODUCTION**

### **1.1 Objectives**

The Extracellular Matrix (ECM) provides the principal avenue for mechanochemical communication between cells and tissue. To date, little is known about how mechanical forces are translated within the ECM and from the tissue to the cellular level. Such kind of information is critical for the understanding of cellular mechanotransduction within the context of living tissues and organisms. The mechanisms by which ECM mechanics influence cell and tissue behavior remain to be elucidated since the events associated with this process span length scales from the tissue to molecular level. To understand these mechanisms, entirely new methods are needed to measure the mechanics of ECM at multiple length scales. Type I collagen is the major component of ECM and extensively used as an ECM equivalent. The main goal of this study is to investigate the multi-scale mechanics of collagen matrix using both experimental and modeling approaches. A multi-scale magnetic tensile – twisting experimental methodology was developed by integrating the optical magnetic twisting cytometry (OMTC) with the biaxial tensile testing method (Biax). Using this methodology, we investigated the local elastic and viscoelastic properties within the collagen matrix under controlled tissue-level biaxial loading.

### **1.2 Collagen and its hierarchical structure**

Collagen is the major protein in human body, presented in skin, tendon, bone, ligaments and various connective tissues (Fratzl, 2008). It is the major component of ECM

and provides the mechanical stability and strength to many biological tissues (Alberts, et al., 2002). Of the collagen present in body, 90% is the Type I collagen. The commercial available type I collagen is soluble in acid solution, obtained by extraction from rat tail tendon, bovine calf skin and other sources (Velegol & Lanni, 2001). By controlling environmental factors (temperature, PH, ionic strength, etc.) in an appropriate manner, triple helical type I collagen molecule first self assembles to collagen fibril; bundles of collagen fibrils further aggregates to collagen fiber (Yang & Kaufman, 2009) (Gautieri & Vesentini, 2011)(Figure 1.1). With the interstitial fluid phase, a 3-D hydrogel with hierarchical structure is formed. Collagen gel has been widely used as a tissue equivalent in tissue engineering, drug delivery and wound healing because of its excellent biocompatibility, low toxicity, and easy modified chemical and mechanical properties (Xu, et al., 2011) (Lee, et al., 2001) (Lee & Yuk, 2007). Since most of these applications require the scaffolds to operate under mechanical stresses, it has been shown that the mechanical properties of collagen gel can be modified by varying the concentration (Julias, et al., 2008), fiber alignment (Guo & Kaufman, 2007) (Xu, et al., 2011) or crosslinked with genipin and glutaraldehyde (Sundararaghavan, et al., 2008) (Xu, et al., 2011).

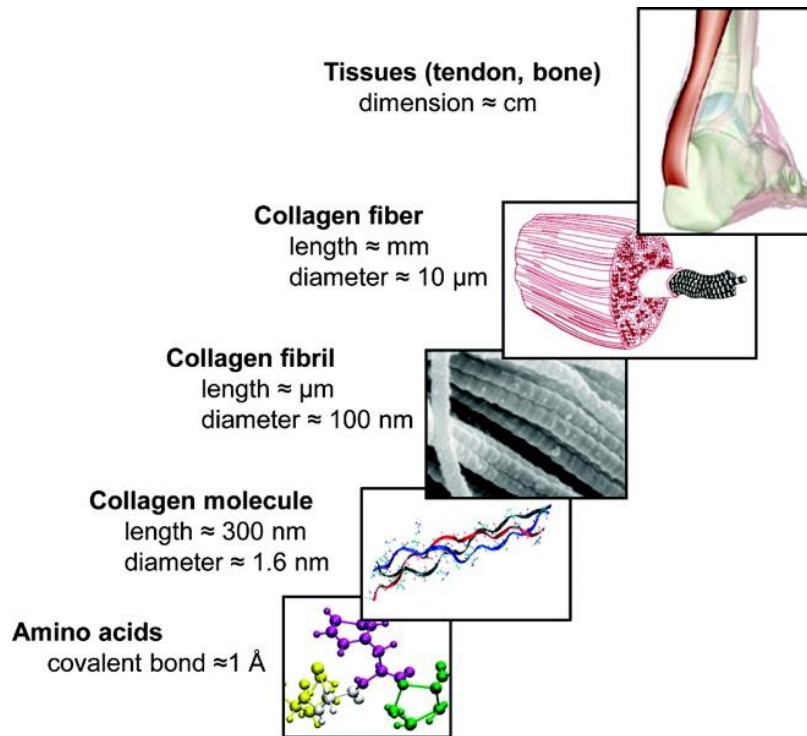
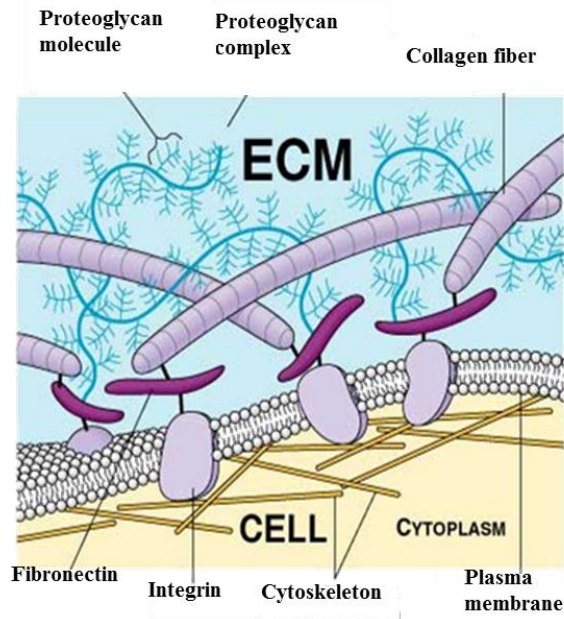


**Figure 1.1: Hierarchical structure of collagen (Gautieri & Vesentini, 2011)**

### 1.3 Collagen in ECM

The extracellular matrix is a collection of extracellular molecules secreted by cells that provides structural and biochemical support to the surrounding cells (Figure 1.2). It provides the principal avenue for mechanochemical communication between tissue and cells (Peyton, et al., 2007) (Pizzo, et al., 2005). These signals are communicated in a reciprocal manner, playing critical roles in establishing tissue structure-function relationships and controlling cell fate. For example, the stiffness of the ECM profoundly influences a series of cell behaviors including cell migration (Pelham & Wang, 1997) (Zaman, et al., 2006), cell differentiation (Engler, et al., 2006) and cell proliferation (Wang, et al., 2000). Many pathological conditions including cardiovascular disease,

tumorigenesis, metastasis, ageing of connective tissues, etc., involve significant mechanical alternations of ECM. However the mechanisms by which ECM mechanics influence cell and tissue function remain to be elucidated since the events associated with these processes span size scales from the tissue to molecular level. Furthermore, the ECM has extremely complex hierarchical three-dimensional (3-D) structures and there exists a tremendous interdependence of ECM compositional, structural, and mechanical properties. To-date it is still not well understood how mechanical forces are translated within ECM, or from the tissue- to cellular level. Such information is imperative since the magnitude of the load at the tissue level is different from that experienced by the cell (Brown, 2000), and the differential load distribution is highly dependent on the architecture and mechanical properties of the ECM (Mow, et al., 1994). As a major ECM component, collagen plays an important role in modulating cell function, in addition to providing structural support. Type I collagen gel has been used extensively to study cell-ECM interaction and cell induced ECM remodeling since it retains essential elements of cell-matrix 3D interactions, although much of the structural and molecular complexities present *in situ* are omitted.



([http://wiki.pingry.org/u/ap-biology/index.php/Extracellular\\_matrix](http://wiki.pingry.org/u/ap-biology/index.php/Extracellular_matrix))

**Figure 1.2: Picture of Extracellular Matrix composed by mainly collagen fibers and other groundmatrix substances.**

#### **1.4 Macroscopic mechanical measurements of collagen gel**

As a viscoelastic material, collagen gel behavior results from the intrinsic properties of and interaction between two component phases: a network of collagen fibrils and interstitial solution (Knapp, et al., 1997). The macroscopic mechanical properties of collagen gel have been broadly studied by using various experimental methods. Uniaxial tensile testing has been performed by Roeder et al. (Roeder, et al., 2002) to investigate the mechanical properties of Type I collagen gel under different polymerization conditions including collagen concentrations and pH values. Mechanically, all matrices exhibited a similar stress-strain curve with identifiable “toe”, “linear” and “failure” regions. Though successful, the uniaxial tensile test ignores the

multi-axial loading state under physiological conditions and cannot fully characterize the anisotropic behavior of soft tissues. Xu et al. (Xu, et al., 2011) studied the anisotropic mechanical behavior of Type I collagen gel with the effect of spatial fiber alignment and crosslinking using a planar biaxial tensile tester. Aligned collagen scaffolds were created with the aid of magnetic particles enmeshed in collagen fibrils to mimic the anisotropy seen in native tissues. To understand the frequency dependent viscoelastic behaviors, storage and loss modulus was measured using rheological measurements to characterize the frequency dependent elastic and viscous mechanical properties of collagen gel, respectively, considering the effect of collagen concentration (Julias, et al., 2008), crosslinking (Xu, et al., 2011) and polymerization temperature (Raub, et al., 2007).

### **1.5 Microscopic mechanical measurements of collagen gel**

Local mechanical properties of collagen gel have also been studied by using several microscopic measurements. Laser microrheometry technique (Velegol & Lanni, 2001) was developed to probe the local mechanical properties of collagen matrix by oscillating trapped particles. In this technique, force is exerted on one bead at a time, so the results highly depend on the local heterogeneity where the single bead locates (Leung, et al., 2007), and it could be time consuming to capture the behavior of a population of beads (Parekh & Velegol, 2007). Magnetic twisting cytometry (MTC) is capable of measuring the collective behavior of a population of beads, and has been used extensively to study the viscoelastic microrheology of living cells (Valberg PA, 1987) (Wang N, 1993) (Fabry, et al., 1999) (Maksym GN, 2000) (Laurent, et al., 2002). Since cell surface

receptors are physically linked to the cytoskeleton (CSK), mechanical properties of the CSK can be calculated from the imposed mechanical torque and measurements of bead motion. The MTC method was later adapted to measure the mechanical properties of type I collagen gel and demonstrates success on probing cellular modulation of matrix stiffness (Leung, et al., 2007). The MTC method relies on measurement of the changes in the remanent magnetic field. Fabry et al. (Fabry, et al., 1999) reported that MTC is more weighted towards weakly bound beads, resulting in overestimated mean angular bead rotation and underestimated mean shear modulus. Later, the so-called optical magnetic twisting cytometry (OMTC) method was established in which the beads' motion was measured optically via tracking the lateral displacements of the centroids of the magnetic beads (Fabry, et al., 2001) (Fabry, et al., 2003) (Smith, et al., 2003) (Deng, et al., 2004) (Trepate, et al., 2004) (Fredberg & Fabry, 2006). The OMTC method allows identifying and excluding loose beads or bead clusters from data analysis, thus the measurement is more reliable (Fabry, et al., 2001).

## **1.6 Multi-scale ECM mechanics**

To advance the current understanding on multi-scale ECM mechanics, a multiscale experimental methodology is needed to study the changes of microscopic mechanics under controlled macroscopic loading. Previous studies have studied the translation of mechanical stimuli to cells through stretchable substrate (Pourati, et al., 1998) (Brown T. , 2000) (Smith, et al., 2003) (Trepate, et al., 2004) (Rosenblatt, et al., 2004) (Rosenblatt, et al., 2007) (Throm Quinlan, et al., 2011). These studies provide

fundamental understandings on microscopic cell stiffness, deformability, cytoskeleton tension, etc., with mechanical strain. Advances in imaging techniques promote the integration of multi-scale mechanical loading and imaging modalities to provide perspectives on load induced changes in ECM microstructure, cellular morphology and alignment (Bell, et al., 2012) (Throm Quinlan, et al., 2011). An integrated mechanical loading-confocal microscopy system was developed and used to study three-dimensional (3D) mechanical strains in collagen matrix at multiple length scales in response to uniaxial (Voytik-Harbin, et al., 2003) (Roeder, et al., 2004) (Roeder, et al., 2009) and biaxial stretching (Bell, et al., 2012).

## **1.7 Outline of the research**

In Chapter 2, we introduced the experimental methods that are used in this study, including rheological testing, biaxial tensile testing, OMTC, and an integrated multi-scale OMTC – biaxial tensile testing system.

In Chapter 3 and Chapter 4, we studied macroscopic mechanical properties of collagen gel. In Chapter 3, rheological testing is performed to characterize frequency dependent storage and loss modulus with different surface conditions through frequency sweep, strain sweep, and relaxation tests. Sandpaper is attached to both top and bottom rheometer plates to modify the surface roughness and to prevent slippage between the collagen gel and the rheometer plates. In Chapter 4, the continuous relaxation spectrum is obtained from analyzing frequency dependent modulus by Tikhonov regularization method. A finite element model was created to simulate the rheological measurement, in

which the viscoelastic properties of the collagen gel was modeled as linear elastic with viscous material parameters obtained from both direct fitting and continuous spectrum.

In Chapter 5, we studied the local mechanical properties of collagen gel and compare with its macroscopic measurements. Optical Magnetic Twisting Cytometry is used to measure the local apparent storage and loss modulus of type I collagen matrix. Streptavidin coated ferromagnetic beads are used to achieve beads-matrix binding. The macroscopic (global) storage and loss modulus of collagen gel were measured using a parallel plate rheometer from frequency and strain sweep tests. A 3-D finite element model was developed to simulate the OMTC measurements, and to study the effects of nonlinear ECM material properties, matrix geometry, and beads embedding degree on the measurements.

In Chapter 6, we created a multi-scale experimental approach that combines OMTC and biaxial tensile testing techniques to study the changes in the local mechanical properties of adventitial collagen with controlled global biaxial mechanical loading. Both macro and microscopic mechanical properties were measured using this multi-scale system. Multiphoton microscopy was also used to visualize the structural changes of adventitia under external biaxial loading.

In Chapter 7, conclusions and outlook to future work are presented.

## CHAPTER 2: EXPERIMENTAL METHODS

### 2.1 Overview

This Chapter introduces the experimental methods used in the present study, including the preparation of collagen matrix, rheological test, biaxial tensile test, OMTC, and the integrated multi-scale OMTC – biaxial tensile testing system.

### 2.2 Preparation of collagen matrix

Nutragen Type I collagen solution (6mg/ml) was purchased from Advanced Biomatrix (San Diego, CA). Collagen gel was prepared following the standard procedure specified by manufacture. Briefly, neutralized collagen solution was made by quickly mixing collagen solution, 10× phosphate buffered saline (PBS) and 0.1M NaOH with a volume ratio of 8:1:1 at 4°C to reach the desired final collagen concentration. Neutralized collagen solution with a PH value between 7.2 and 7.4 was first transferred to a Petri dish and then incubated at 37°C in the incubator for 12h for gelation.

To prepare the genipin crosslinked collagen gel, collagen gel was then incubated in genipin solution for another 6h for further crosslinking. In our study, genipin concentrations of 0.1% and 0.25% were used. Finally, the gel was carefully removed from the Petri dish for rheological testing. Due to its fragility, non-crosslinked collagen gel was polymerized *in situ* by quickly loading 1ml neutralized collagen solution on a precooled Peltier stage and then raising the temperature to 37°C. During the gelation process, time sweep test at 1% oscillating strain with a frequency of 1rad/s was

performed. Once the equilibrium modulus of storage and loss modulus were reached, the development of collagen network was considered to be complete (Yang & Kaufman, 2009). The upper rheometer plate was then lowered to keep a 500um gap towards Peltier stage. Solvent trap was added to minimize dehydration during polymerization. Measurements were conducted at 37°C after allowing 2h for gelation.

### **2.3 Rheological test**

Most soft hydrogel materials are known to be viscoelastic and exhibit both viscous and elastic characteristics when subjected to mechanical loading. Their mechanical properties have been broadly studied using parallel plate rheological measurement (Nasseri, et al., 2002) (Hrapko, et al., 2006) (Mezger, 2006). Storage and loss modulus, related to the elastic and viscous behavior of the material, are determined from dynamic oscillatory tests. The time-dependent relaxation modulus under a constant strain is determined from shear stress relaxation test, and is used to describe the intrinsic relaxation behavior of viscoelastic materials. During rheological measurement, samples are sandwiched between two parallel plates with an appropriate compression. The top plate is twisted to deform the sample and the torque transmitted through the sample is measured. Dynamic oscillatory shear test is performed by using a parallel plate Rheometer. The torque (M) and rotational angle ( $\theta$ ) are related to the shear strain ( $\gamma(r)$ ) and shear stress ( $\tau(r)$ ) on the rotational plane through

$$\gamma(r) = \frac{\theta r}{H} \quad (2.1)$$

$$\tau(r) = \frac{2Mr}{\pi R^4} \quad (2.2)$$

where  $H$  is the gap between discs and  $R$  is the radius of the disc. The amplitude of the shear strain and shear stress varies linearly along the radius and reaches the maximum value when  $r = R$ :

$$\gamma_R = \frac{\theta R}{H} \quad (2.3)$$

$$\tau_R = \frac{2M}{\pi R^3} \quad (2.4)$$

The oscillatory shear strain and shear stress can be expressed as  $\gamma(\omega, t) = \gamma_R \sin(\omega t)$ , and  $\tau(\omega, t) = \tau_R \sin(\omega t + \delta)$ , where  $\omega$  is angular frequency, and  $\delta$  is the phase lag between shear strain and shear stress. The storage and loss modulus,  $G'$  and  $G''$ , are calculated as:

$$G' = \left( \frac{\tau_R}{\gamma_R} \right) \cos \delta \quad (2.5)$$

$$G'' = \left( \frac{\tau_R}{\gamma_R} \right) \sin \delta \quad (2.6)$$



**Figure 2.1: Picture of a parallel plate rheometer**

In present study, rheological test was performed using an AR-2000 parallel plate (R=20mm) rheometer (TA Instrument). The bottom plate was set to be 37°C during the test. Samples were loaded between plates. Frequency sweep, strain sweep, and relaxation tests were performed to characterize the mechanical properties of non-crosslinked or genipin crosslinked collagen gel. Details of the experimental protocol are shown in each chapter.

#### **2.4 Biaxial Tensile Testing**

Many biological tissues possess anisotropic material properties; for example, the mechanical properties of blood vessels in the circumferential and longitudinal directions are not the same. Uniaxial imposed loadings usually do not accurately reflect the state of deformation encountered in the body, and are insufficient to elaborate the structurally and mechanical anisotropy seen in biological tissues. Due to the presence of mechanical anisotropy of biological tissues, biaxial tensile testing is commonly used to fully characterize the mechanical properties. Generally, two assumptions are made in biaxial tensile test. (1) A plane stress state is assumed since the thickness of the sample is small compared to the length and width. (2) Soft biological tissues are considered to be incompressible.

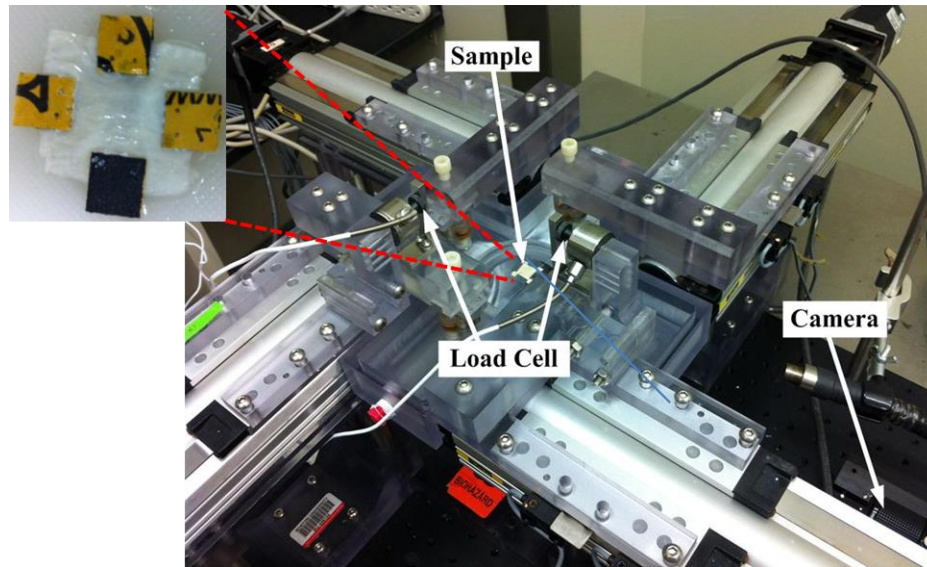


**Figure 2.2:** Picture of the biaxial tensile tester showing the sample mounted to the linear positioners with adventitia peeled from porcine thoracic aorta in zoom in view.

In present study, the macroscopic mechanical behaviors of porcine adventitia were studied using biaxial tensile test (Figure 2.2). Sandpaper tabs were attached to the top and bottom faces along the edges of a roughly square tissue samples with cyanoacrylate glue (Elmer's Products, Columbus, OH). The sutures were looped through the sandpaper fold and connected to the linear positioners of the biaxial tensile tester controlled by a custom LabVIEW program (National Instruments, Austin, TX). Load cells mounted in both circumferential and longitudinal sample directions were used to measure and record the load applied to the sample. Four carbon dots markers forming a  $5\text{mm} \times 5\text{mm}$  square were placed in the center of the testing specimen, and a CCD camera was used to track the position of markers from which the tissue strains in both directions can be determined throughout the deformation. Firstly, a preload was used to straighten the sutures. The preloaded state was used as the reference state for later strain calculation.

Sample was then preconditioned equi-biaxially for 8 cycles to achieve a repeatable material response. A half cycle time of 10 seconds was used. After preconditioning, 8 cycles of biaxial tension was applied to sample. The load and stretch in both directions collected from the last cycle used for analysis were, when the stress-stretch curves were stable. The Cauchy stresses in the direction  $x_1$  and  $x_2$  are obtained by (Zou & Zhang, 2009):

$$\sigma_1 = \frac{F_1 \lambda_1}{h L_{02}}, \quad \sigma_2 = \frac{F_2 \lambda_2}{h L_{01}} \quad (2.7)$$

where  $\sigma_i$  ( $i = 1, 2$ ) is the Cauchy stress,  $F_i$  and  $\lambda_i$  ( $i = 1, 2$ ) represents the load and stretch in the  $x_i$  direction;  $h$  and  $L_{0i}$  ( $i = 1, 2$ ) are the original thickness and length, respectively, of the sample before it was stretched.

## 2.5 Optical Magnetic Twisting Cytometry (OMTC)

A one-dimensional OMTC (EOL Eberhard, Switzerland) was used to measure the local mechanical properties of the collagen matrix (Figure 2.3). A small group of ligand-coated ferromagnetic microbeads (~4.5  $\mu\text{m}$  diameter) are bound to the collagen fibrils. Ferromagnetic microbeads are first magnetized by a brief (0.1ms), strong external magnetic pulse (>0.1T) in the horizontal plane of the collagen gel surface. A homogeneous, oscillatory weak (<0.01T) magnetic twisting field is then applied to the beads in the vertical direction. This, in turn, induces a mechanical “twisting” torque that causes the beads to rotate (Fabry, et al., 2001). The lateral translation as a result of the rotation is detected optically.

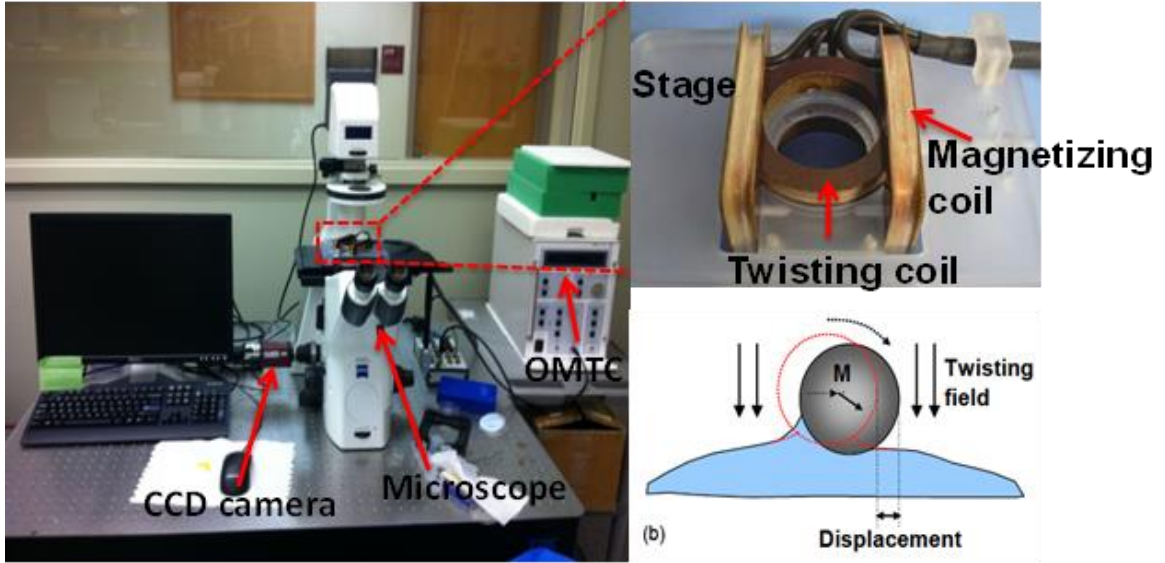


**Figure 2.3: Picture of Optical Magnetic Twisting Cytometry System and a zoom-in view of magnetizing and twisting coil. Schematic of a ferromagnetic bead twisted by magnetic field is also shown.**

The specific twisting torque  $T(t)$  is related to the applying current  $I$ , beads constant  $C_{bead}$ (Pa/G), and magnetic twisting coil constant  $C_{coil}$  as:

$$T(t) = C_{bead} * C_{coil} * I(t) \quad (2.8)$$

where  $C_{coil}$  is 35.3G/A (EOL Eberhard), the applied current is sinusoidal with magnitude  $I_0$  and oscillating angular frequency  $\omega$ , i.e.,  $I(t) = I_0 \sin \omega t$ .  $I_0 = 1.33A$  for streptavidin coated beads, and  $I_0 = 1A$  for PLL coated ferromagnetic beads in order to achieve a comparable twisting torque. The current frequency ranges from 0.1 to 31 Hz.  $C_{bead}$ , related to the intrinsic property of ferromagnetic bead, is 1.14Pa/G for streptavidin coated beads (Spherotech Co.) and 1.62Pa/G for PLL beads (Deng, et al., 2004).

Lateral bead displacement in response to the applied oscillatory torque was detected using a progressive scanning black and white CCD camera (AVT Pike F-100b,

Advanced Vision Technology Co.) mounted on an Zeiss inverted microscope (Axio Observer D1). A 10X objective was used to achieve a field of view of 714×714μm. A custom Labview (NI, Co.) program (Trepate, et al., 2003) was used to acquire 10 images every twisting cycle. Heterodyning method was used when twisting frequency was greater than 0.1Hz. Interested readers are referred to (Fabry, et al., 2003) for more details. The position of selected beads was tracked following a bead-tracking algorithm developed by (Trepate, et al., 2003). With the use of this algorithm, the bead position could be determined with an accuracy of 5nm.

Discrete Fourier transformation was then performed on both specific twisting torque  $T(t)$  and bead displacement  $d(t)$  to transfer the information from time domain to frequency domain. Only the response at fundamental frequency was considered in discrete Fourier transformation. The apparent modulus  $G_d^*$  is a function of oscillating frequency  $\omega$ , and can be calculated as:

$$G_d^*(\omega) = \frac{T(\omega)}{d(\omega)} = G_d'(\omega) + iG_d''(\omega) \quad (2.9)$$

where  $G_d'$  and  $G_d''$  represent the apparent storage and loss modulus, respectively, and have a unit of Pa/nm. Since the collagen gel is a viscoelastic material, a phase lag,  $\delta(\omega)$ , exists between the twisting torque and bead displacement response, and can be calculated as:

$$\delta(\omega) = \arctan \frac{G_d''(\omega)}{G_d'(\omega)} \quad (2.10)$$

## 2.6 Integrated multi-scale OMTC – biaxial tensile testing system

A multi-scale experimental methodology was developed by integrating a one-dimensional OMTC (EOL Eberhard, Switzerland) with a biaxial tensile tester, as shown

in Figure 2.4a. The biaxial tensile tester was set up such that the configuration will allow the access to the OMTC and microscope. Four stepper motor, ballscrew-driven linear positioners (MX80S, Parker Hannifin Corporation, Irwin PA) connected to a four-axis motion controller (DMC-4040, Galil Motion Control, Rocklin CA) were positioned so that the ECM network can be loaded biaxially at the tissue-level and maintained at the center of the field-of-view, which is  $714\mu\text{m} \times 714\mu\text{m}$  with a  $10\times$  objective (Figure 2.4b). The movements of the linear positioners were controlled by a custom LabVIEW program (National Instruments, Austin, TX). Load cells (250 g Model 31 Low, Honeywell, Golden Valley, MN) mounted in both the circumferential and longitudinal sample directions were used to measure and record the load applied to the sample. The OMTC was custom built to fit the configuration of the microscope and the biaxial tensile tester setup. The integrated magnetic tensile-twisting device was mounted on a Zeiss inverted microscope, which was placed on a vibration isolation table.

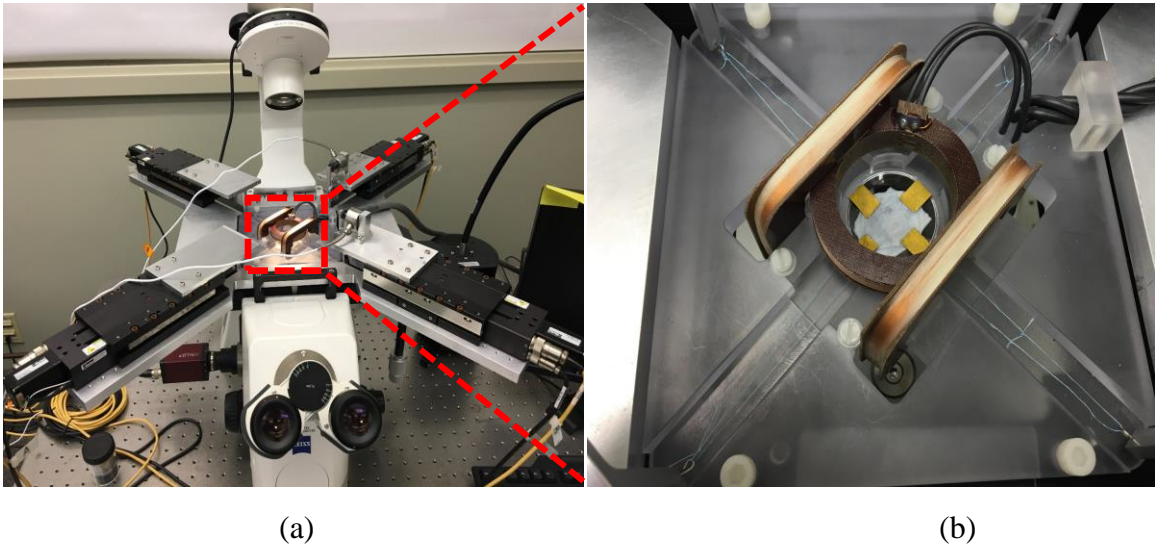


**Figure 2.4: (a) Picture of Optical Magnetic Twisting Cytometry combined with the biaxial tensile tester System. The samples are placed inside the magnetic twisting stage shown in (b).**

## **CHAPTER 3: EFFECT OF SLIPPAGE ON RHEOLOGICAL MEASUREMENT OF GENIPIN CROSSLINKED COLLAGEN GEL**

### **3.1 Overview**

Rheological measurements have been widely used to study the viscoelastic properties of hydrogels. During oscillatory shear measurements, slippage between sample and the rheometer plates will induce significant errors in measurement. Here, we studied the rheological measurement of genipin crosslinked collagen gel on different surface testing conditions through frequency sweep, strain sweep, and relaxation tests. Sandpaper is attached to both top and bottom rheometer plates to modify the surface roughness and to prevent slippage between the collagen gel and the rheometer plates. Our results consistently show that measurements of collagen gel between smooth surface condition deviate from those between rough surface conditions, with underestimated storage modulus and overestimated loss modulus and relaxation. These results suggest that it is important to achieve non-slip boundary conditions during dynamic oscillatory shear measurements.

### **3.2 Introduction**

Most soft hydrogel materials are known to be viscoelastic and exhibit both viscous and elastic characteristics when subjected to mechanical loading. Their mechanical properties have been broadly studied using parallel plate rheological measurement (Nasser, et al., 2002) (Hrapko, et al., 2006) (Mezger, 2006). Storage and

loss modulus, related to the elastic and viscous behavior of the material, are determined from dynamic oscillatory tests. The time-dependent relaxation modulus is determined from shear stress relaxation test, and is used to describe the intrinsic relaxation behavior of viscoelastic materials.

During rheological measurement, samples are sandwiched between two parallel plates with an appropriate compression. The top plate is twisted to deform the sample and the torque transmitted through the sample is measured. Due to compression, fluid inside the biological samples is likely to be squeezed out and can be regarded as a lubricant between the sample and plates, which may lead to slippage between the sample and plates and result in misestimated mechanical properties.

Collagen is a major protein in extracellular matrix and connective tissues. Collagen based gel is a highly viscoelastic material composed of a collagen network and interstitial fluid (Knapp, et al., 1997). As a broadly used biomaterial, it has excellent biocompatibility, less toxicity and easily modifiable mechanical properties (Lee, et al., 2001) (Trepatt, et al., 2004). Previous studies have used rheological measurements to study the mechanical properties of collagen gel considering the effect of collagen concentration (Julias, et al., 2008), crosslinking (Sundararaghavan, et al., 2008) (Motte & Kaufman, 2012) (Xu, et al., 2011), and polymerization temperature (Raub, et al., 2007). Here we studied the effect of slippage on rheological measurement of genipin crosslinked collagen gel using a parallel plate rheometer. Sandpapers were attached to the parallel plates of the rheometer to prevent slippage between the sample and the rheometer plates. Frequency sweep, strain sweep, and stress relaxation tests were performed with smooth

and rough surface conditions and the results were compared.

### **3.3 Material and Methods**

#### *3.3.1 Sample preparation*

Genipin crosslinked and noncrosslinked collagen matrix were prepared as described in Chapter 2.2. The collagen matrix has a concentration of 4.8mg/ml.

#### *3.3.2 Rheological test*

Rheological measurements were performed as described in Chapter 2.3. For the genipin crosslinked collagen gel, testing conditions with both smooth and rough surfaces were studied. To increase the surface roughness, sandpapers of 1500 and 400 grits were attached on the top and bottom surface of the plates in order to prevent slippage. Samples were loaded between plates with a normal compression force of about 0.2N.

Frequency sweep, strain sweep, and relaxation tests were performed to characterize the mechanical properties of genipin crosslinked collagen gel. In frequency sweep tests, oscillating shear strains of 2%, 4%, 6%, and 8% were applied to the samples with the frequency ranging from 0.05 to 50HZ. In strain sweep tests, oscillating shear strain ranging from 0.1% to 10% was applied to the sample at 1HZ for smooth surface condition; and at 1HZ and 5HZ for rough surface conditions. In relaxation tests, constant initial shear strains of 2%, 4%, 6% and 8% were applied with 0.2s strain rise time and the shear modulus were recorded over 300s. Results were averaged from three samples. For non-crosslinked collagen gel, frequency sweep test was performed at the maximum

shear strain of 1% with frequency varies from 0.05Hz to 50Hz. Results were averaged from four samples.

### 3.3.3 *Statistical Analysis*

Storage modulus ( $G'$ ) loss modulus ( $G''$ ) and phase lag ( $\delta$ ) measurements from smooth and rough surface conditions at 1.186Hz were averaged and expressed in the form of mean  $\pm$  standard deviation (SD). Statistical analysis was performed by using one-way analysis of variance (ANOVA) followed by Tukey-Kramer HSD comparisons for all pairs (JMP Pro 10.0.2, SAS Institute Inc.). Differences are considered to be significant when  $p < 0.05$ .

## 3.4 **Results**

Results from frequency sweep tests of 0.1% genipin crosslinked collagen gel are shown in Figure 3.1. Measurements from the two rough surface conditions are similar. In the tested frequency range,  $G'$  slightly increases with frequency, and is about one order of magnitude greater than  $G''$ , indicating that the cross-linked collagen gel is more solid like. Even at shear strain level of 2% (Figure 3.1a), surface conditions seem to affect the measured results. Compared with the surface conditions, measurements from smooth surface result in a lower  $G'$  and higher  $G''$ . This discrepancy between measurements from using smooth and rough surface conditions becomes more significant as the maximum shear strain increases. As the maximum oscillating shear strain increases to 4%, 6% and 8%, measurements from the two rough surface conditions remain similar (Figures 3.1b–1d). However,  $G'$  obtained from smooth surface condition is significantly

lower than that measured from rough surface conditions, especially at lower frequencies. In the meanwhile, elevated  $G''$  is observed with a crossover between  $G'$  and  $G''$  at 6% and 8% of shear strains, i.e.,  $G''$  is greater than  $G'$  at lower frequencies and this trend reverses after crossover frequency. A similar observation can be found on the frequency sweep results of 0.25% genipin crosslinked collagen gel (Figure 3.2), which indicates that the discrepancies of the results between rough and smooth surfaces are independent from crosslinking. Compared to the non-crosslinked collagen gel, genipin crosslinking increase  $G'$  by about one order of magnitude (Figure 3.3). Increasing the genipin concentration from 0.1% to 0.25% results in slightly higher  $G'$ , however the effect on  $G''$  is much more pronounced (Figure 3.3).

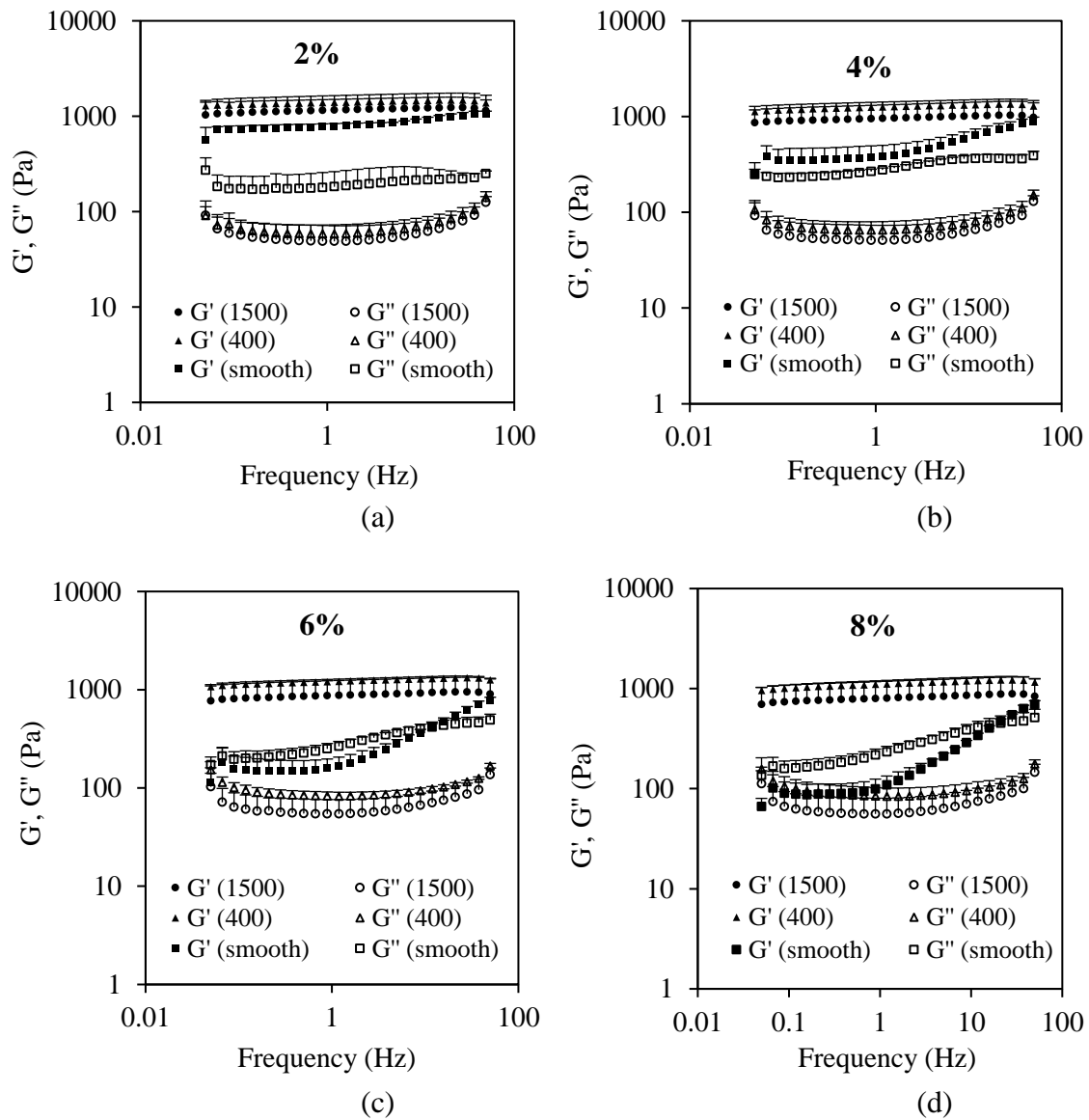


**Figure 3.1: Results from frequency sweep tests of 0.1% genipin crosslinked collagen gel at maximum shear strain of (a) 2%, (b) 4%, (c) 6% and (d) 8% on smooth and rough surface conditions when sandpaper (1500 grits and 400 grits) are attached to the top and bottom surfaces of the rheometer plates.**

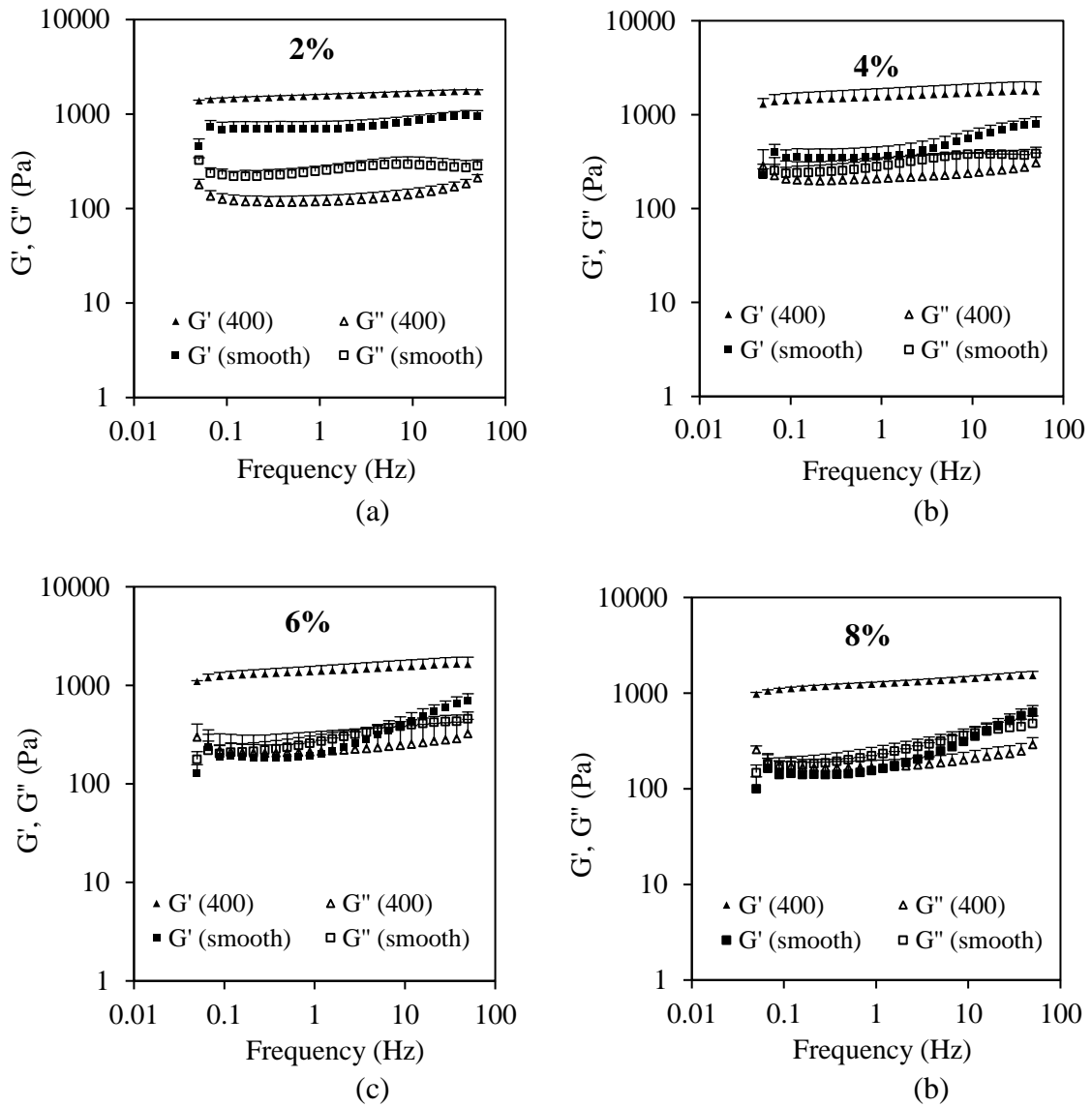


**Figure 3.2: Results from frequency sweep tests of 0.25% genipin crosslinked collagen gel at maximum shear strain of (a) 2%, (b) 4%, (c) 6% and (d) 8% on smooth and rough surface conditions when sandpaper (400 grits) are attached to the top and bottom surfaces of the rheometer plates.**

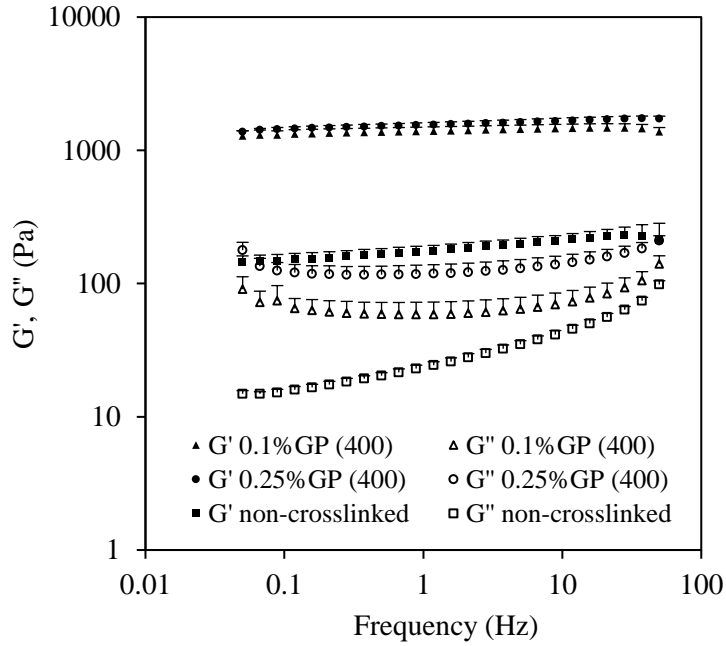


**Figure 3.3: Results from frequency sweep tests of non-crosslinked and genipin crosslinked collagen gel. The maximum shear strain is 1% for non-crosslinked collagen gel and 2% for genipin crosslinked collagen gel.**

To further quantify the effect of slippage on rheological measurements, frequency sweep results ( $G'$ ,  $G''$ , and  $\delta$ ) at 1.186 Hz were compared for 0.1% genipin crosslinked collagen gel under shear strains from 2% to 8%, as shown in Figure 3.4. Overall the differences between the results from two rough surface conditions using 400 and 1500 grits sandpaper are not significant. For shear strains higher than 2%, compared to the measurements using rough surface conditions,  $G'$  from measurements using smooth surface condition is significantly underestimated, however  $G''$  is significantly overestimated ( $p < 0.05$ ). As a result, the phase lag  $\delta = \arctan\left(\frac{G''}{G'}\right)$  from smooth surface condition appears to be significantly higher than that from rough surface conditions at all strain levels ( $p < 0.05$ ).

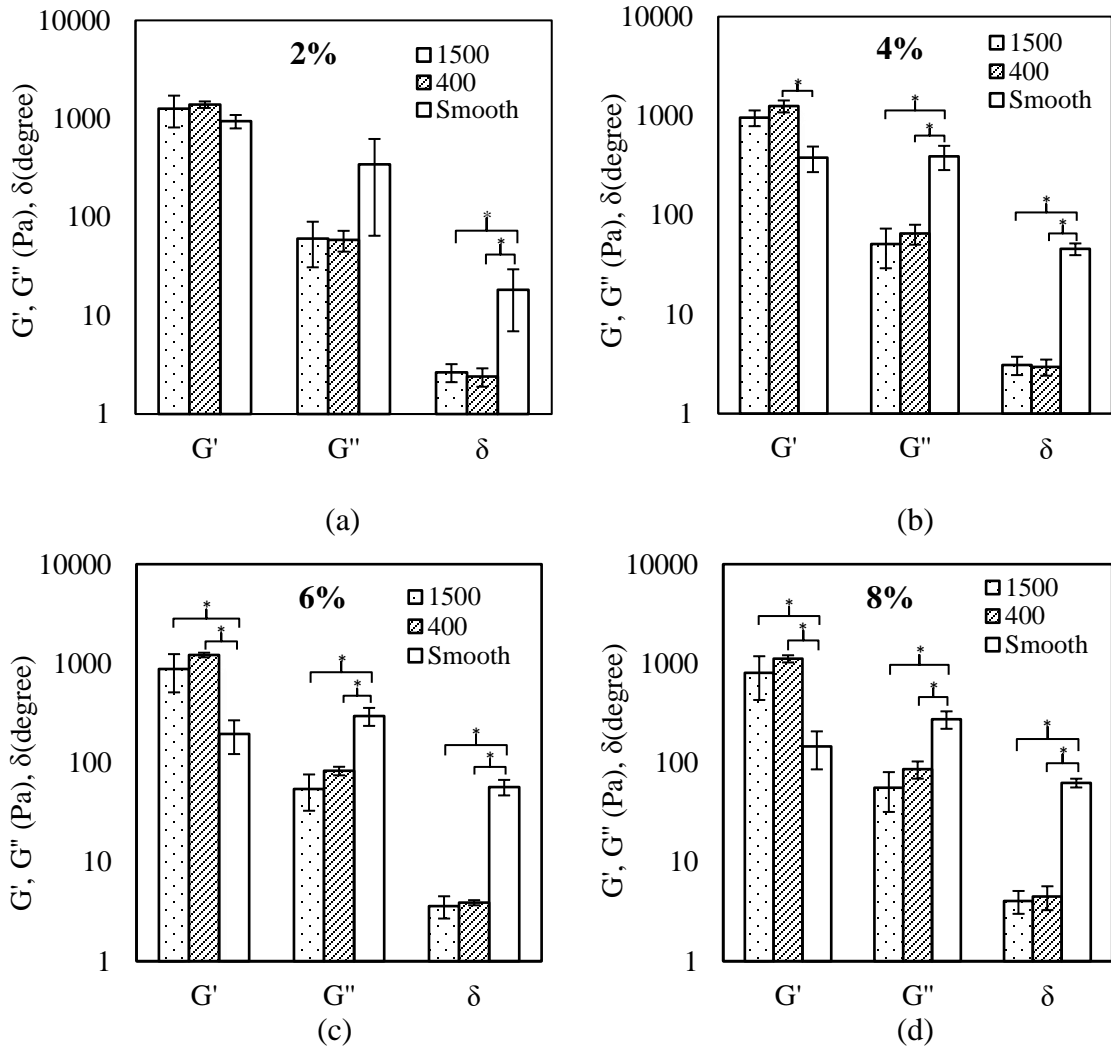


**Figure 3.4: Comparison of storage modulus  $G'$ , loss modulus  $G''$ , and phase lag  $\delta$  from frequency sweep tests of 0.1% genipin crosslinked collagen gel on three surface conditions at 1.186Hz. (a) 2%, (b) 4%, (c) 6% and (d) 8% shear strain. \* indicates comparison is statistical significant ( $p < 0.05$ ).**

Results from strain sweep tests of 0.25% genipin crosslinked collagen gel are shown in Figure 3.5. Compared with results from smooth surface, measurements from two rough surfaces are generally similar with a slight decrease of  $G'$  and a gradual increase of  $G''$  with strain, however a significant discrepancy is observed for

measurements from smooth surface condition. Specifically,  $G'$  is significantly underestimated as manifested by a dramatic drop with increasing strain. In the meanwhile,  $G''$  is overestimated as compared with the measurements from rough surface conditions.

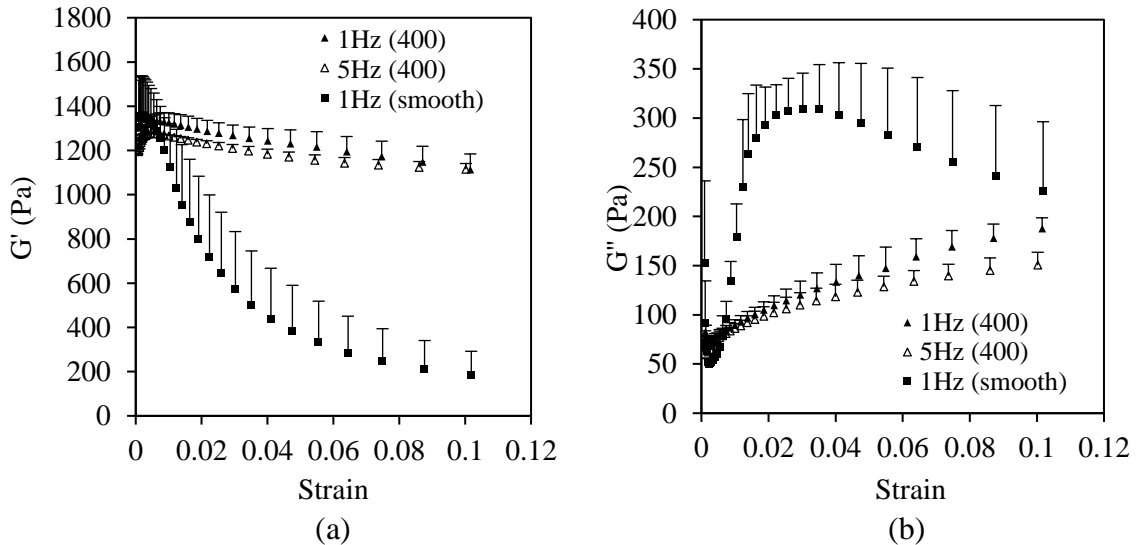


**Figure 3.5: Results of (a) storage modulus  $G'$  and (b) loss modulus  $G''$  from strain sweep tests of 0.25% crosslinked collagen gel with shear strain ranges from 0.1% to 10% on smooth and rough surface conditions when sandpaper (400 grits) are attached to the top and bottom surfaces of the rheometer plates. Experiments with smooth surface conditions were performed at 1Hz, while with rough surface conditions were performed at 1Hz and 5Hz.**

Relaxation results of 0.25% genipin crosslinked collagen gel at different surface conditions are shown in Figures 3.6a for 6% shear strain. Normalized shear modulus were obtained by dividing the measurements by the averaged shear modulus when the corresponding applying shear stress reaches peak value (ten data points before and after) to avoid sharp peaks. The normalized shear modulus decreases about 40% after a holding period of 300s based on results from the rough surface condition, however with the smooth surface, a nearly 60% drop was observed. Similar results were observed from

other strain levels. Figure 3.6b shows the comparison of relaxation curves at different initial shear strain levels for rough surface condition with 400 grit sandpaper. Overall, the relaxation modulus demonstrates minimal dependency on initial shear strain.

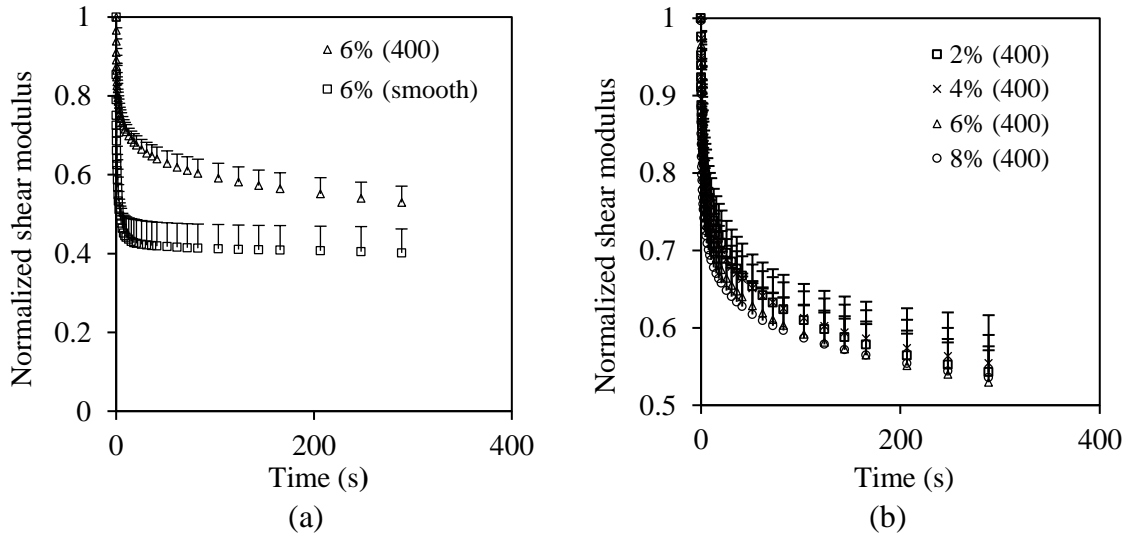


**Figure 3.6: Results from relaxation tests (a) on smooth and rough surface conditions of 0.25% crosslinked collagen gel at initial shear strain of 6%, (b) from 0.25% crosslinked collagen gel measurement at different initial shear strains of 2%, 4%, 6%, and 8% for rough surface condition when sandpaper (400 grits) are attached to the top and bottom surfaces of the rheometer plates.**

### 3.5 Discussion

In this study, we studied the effect of slippage on the rheological measurements of collagen gel. Owing to its intrinsic viscoelastic and biphasic properties, collagen gel has been broadly studied using rheological measurements. To avoid the slippage problem, in a previous study collagen gel was directly polymerized between the top and bottom plates of the rheometer (Kurniawan, et al., 2012). However this is not always an option when other post processes and/or specific environmental requirements are needed.

In our study, the polymerized samples need to be immersed in genipin solution for further crosslinking.

During rheological testing, collagen gel exudes a thin layer of fluid due to compression, which acts as a lubricant between sample and the rheometer plates. As a result, collagen gel is prone to slip. This interfacial fluid layer can lead to significant underestimation of the shear modulus (Nicolle & Paliarne, 2012). Our study shows obvious effects of slippage on rheological measurements of collagen gel. Slippage between the collagen gel and plates, which leads to less torque transmitted through the plate of the rheometer, results in large discrepancy between the measurements using smooth and rough surface conditions. As a result,  $G'$  is significantly underestimated, and such effect becomes more pronounced at shear strain higher than 2% (Figures 3.1 and 3.4). Slippage between the collagen gel and rheometer plates also leads to more phase lag between the applied shear rotation/strain and the shear stress response (Figure 3.4). As a result,  $G''$  measurements from the smooth surface condition are significantly larger than measurements from rough surface conditions (Figure 3.4).

During strain sweep test, as the maximum shear strain increases, normalized storage modulus decreases slightly (Figure 3.5). Similar “strain softening” phenomenon was reported by Kurniawan et al. (Kurniawan, et al., 2012), and it was explained as a result from the redistribution of internal stresses through progressive slippage of the physical crosslinks in the network, which can be regarded as the preparation for the strain stiffening behavior at higher strains (>20%). Such strain softening behavior has been reported to depend on the twisting frequency, degree of crosslinking, and collagen

concentration (Kurniawan et al., 2012). Results from our study show that slippage can lead to much greater drop in  $G'$  at higher strains, which dramatically magnifies the strain softening behavior (Figure 3.5).

The relaxation behavior of viscoelastic material has been studied by analyzing the relaxation spectrum to understand the intrinsic microstructural relaxation mechanisms. For example, the peak intensity indicates the amount of energy dissipated during relaxation. The number of peaks and time constants reflect the relaxation process, are often correlated with the intrinsic structure of viscoelastic materials (Bartenev, et al., 1973) (Winter, 1997) (Xu, et al., 2013). Analyzing the relaxation spectrum of collagen gel suggests that the relaxation mechanisms involve fiber, inter-fiber and fibril sliding (Xu et al., 2013) (Li & Zhang, 2014) (Gupta, et al., 2010). To achieve meaningful microstructural interpretation, it is important to ensure a reliable testing condition. The large discrepancy in the amount of relaxation from two testing conditions shown in Figure 3.6a demonstrates that slippage between the collagen gel and the rheometer plates can result in magnified relaxation behavior. The rate of relaxation, obtained by taking the derivative of the relaxation curve, shows a much faster relaxation rate for collagen gel tested between smooth surfaces at the very beginning of the relaxation period ( $<0.1$ s) (Figure 3.7). Relaxation behavior from this time period is correlated with short-time fast relaxation, or microstructurally with the sliding between collagen fibers and the surrounding fluid (Xu et al., 2013) (Li & Zhang, 2014). The magnified relaxation behavior caused by slippage will not only lead to overestimated viscosity (Brown, 1999), but also misinterpretation of the microstructural mechanisms.

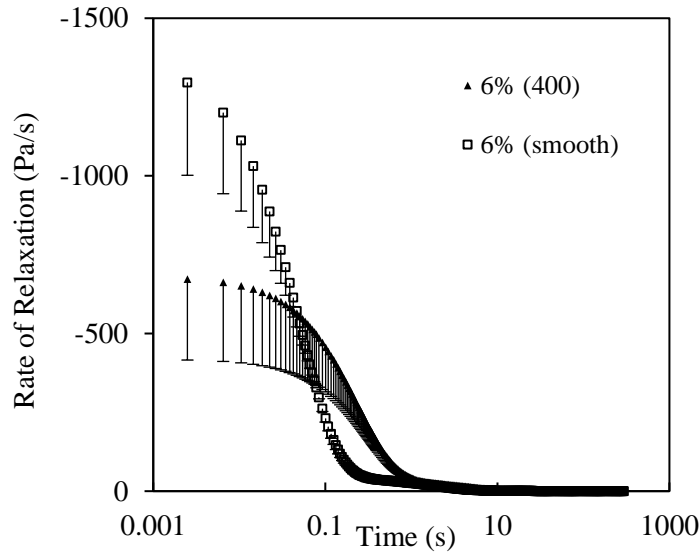


**Figure 3.7: Comparison of the rate of relaxation of 0.25% genipin crosslinked collagen gel tested with smooth and rough surface (modified by 400 grits sandpaper) conditions at 6% of shear strain.**

To avoid the slippage problem, in previous studies brain tissues have been directly glued to rheometer plates to secure a non-slip boundary condition at the interface (Nicolle, et al., 2005) (Darvish & Crabdall, 2001). Increasing surface roughness by attaching sandpaper on the plates was also shown to improve the grip between plates and tissue samples (Bilston, et al., 1997) (Bilston, et al., 2001) (Nasseri, et al., 2002), and no differences were found between these two methods suggesting both attachment methods provide a satisfactory non-slip condition (Brands, et al., 2000). However, one disadvantage of using rough surface method is that the sample must be compressed slightly prior to the shear test, and the inconsistency in compression could affect the shear measurements (Hrapko, et al., 2008). In the present study, the normal compressive forces applied prior to the shear test were carefully monitored to be around

0.2±0.01 N for all samples in order to minimize the effect. Although the results from two rough surface conditions are consistent in general, we did notice that measurements from the 400 grits surface condition show slighter higher storage modulus (Figures 3.1 and 3.4) than those from the 1500 grits surface condition. This is possibly because that the rougher grits from the coarser grid sandpaper embedding into the collagen gel may result in a slightly better grip between the surfaces of the rheometer plates and the collagen gel sample. However compared with results from smooth surface, the differences between two rough surface conditions are much smaller, which suggests the importance of achieving non-slip boundary conditions. We would also like to point out that the choice of rough surface conditions should be made carefully as very coarse surfaces may cause tearing and destroy the sample during rheological test, especially for the rather fragile collagen gel.

### **3.6 Summary**

Results from our study show that slippage between rheometer plates and samples can lead to significant error in rheological measurements. Increasing the surface roughness of the plates by attaching sandpaper seems to be a proper method to prevent such problems by achieving a secured non-slip interaction at the interface between the sample and plates. To achieve accurate mechanical measurements of hydrogel material is not only important to study its physical properties, but also to provide a foundation in further understandings of the underlying microstructural deformation mechanisms.

## **CHAPTER 4: MODELING OF THE VISCOELASTIC BEHAVIOR OF COLLAGEN GEL FROM DYNAMIC OSCILLATORY SHEAR MEASUREMENTS**

### **4.1 Overview**

Viscoelastic materials contain a continuous spectrum of relaxation time constants that cannot be measured directly from experiments. To model the viscoelastic behavior, discrete Generalized Maxwell model is usually chosen phenomenologically from direct fitting. In the present study, a theoretical framework was developed to determine the continuous spectrum of relaxation time constants, and then applied to study the dynamic rheological behavior of collagen gel using a parallel plate rheometer. Frequency sweep tests were performed to determine the storage and loss modulus of collagen gel. To obtain the continuous relaxation spectrum, Tikhonov regularization method was employed to solve the Fredholm integral equations. A finite element model (FEM) was created to simulate the rheological measurement with viscous material parameters obtained from both direct fitting and continuous spectrum. Discrete spectrum obtained by direct fitting method is not unique and highly depends on the specified fitting criteria. Continuous spectrum obtained by Tikhonov regularization effectively eliminates the possibility of getting nonunique solutions. The storage and loss modulus calculated from FEM compared well with the experimental results. Continuous relaxation spectrum can be determined based on dynamic rheological shear measurements, and incorporated into FEM to study the behavior of viscoelastic materials.

## 4.2 Introduction

Many soft biological materials exhibit viscoelastic behavior when subjected to deformation. Viscoelastic materials usually contain a continuous spectrum of relaxation time constants (Ferry, 1980). Investigating the spectrum in terms of number of peaks, peak intensity and time constants sheds light on the main intrinsic properties of viscoelastic materials. For example, the peak intensity indicates the amount of energy dissipated during relaxation. The number of peaks and time constants reflect the relaxation process, are often correlated with the intrinsic structure of viscoelastic materials (Bartenev, et al., 1973) (Winter, 1997) (Xu, et al., 2013). As a result, the continuous relaxation spectrum of viscoelastic material has been employed to study relaxation mechanism (Xu, et al., 2013), intrinsic molecular architecture (Mao, et al., 2000) and distinguish different materials (Li, et al., 2003).

The relaxation spectrum cannot be measured directly from experiments. To model the viscoelastic behavior, discrete Generalized Maxwell model (Prony series) is commonly used to obtain a discrete relaxation spectrum by fitting the experimentally measured viscoelastic behavior. However, the fitted discrete relaxation spectrum is often not unique and highly depends on the specified fitting criteria. In addition, the number of terms in the Prony series and the relaxation times are usually phenomenologically chosen and do not have any physical meanings (Laun, 1978) (Malkin, 2002) (Dealy & Larson, 2006). Recent studies (Mao, et al., 2000) (Dealy & Larson, 2006) indicated that the problem can be overcome by increasing the number of Prony series to infinity in order to avoid an arbitrary chosen number, through which the calculated continuous relaxation

spectrum reflects true material properties. Continuous relaxation spectrum, obtained by solving Fredholm integral equations of the first kind with kernel functions, has been proved to be a classical ill-posed inverse problem (Provencher, 1982) (Honerkamp, 1989) (Malkin, 1990). The solution is highly sensitive to experimental noise (Hansen, 1992) such that small perturbations in the experimental data will result in enormous differences in solution (Kontogiorgos, et al., 2009). To solve this problem, Tikhonov regularization method was employed through an objective function established by adding a regularized solution term to the fitting criteria (Groetsch, 1984) (Honerkamp & Weese, 1989) (Hansen, 1994). It effectively eliminates the possibility of getting multiple solutions.

In the present study, a theoretical framework was developed to determine both the continuous and discrete spectrum of relaxation time constants, and then applied to study the dynamic rheological behavior of collagen gel using a parallel plate rheometer. Frequency sweep tests were performed to determine the storage and loss modulus of the collagen gel. The main properties of the discrete spectrum, the number of peaks and peak intensity in the Prony series, were determined by direct fitting method. In the meanwhile, continuous relaxation spectrum was determined by using Tikhonov regularization method. Finally material parameters from both discrete and continuous relaxation spectrum was used in finite element models to simulate the oscillatory shear measurements of collagen gel using commercial finite element software ABAQUS.

### 4.3 Theoretical framework and experimental methods

#### 4.3.1 Discrete relaxation spectrum

Generalized Maxwell model consists a series of Maxwell elements and takes into account relaxation happens in a distribution of times. Each Maxwell element consists of a spring and a dashpot in series and predicts that stress decays exponentially with time constant  $\tau$ , which is determined by the stiffness of the spring and the viscosity of the dashpot. Thus the relaxation modulus,  $G_R(t)$ , can be described as (Ferry, 1980):

$$G_R(t) = G_e + \sum_{i=1}^N G_i \exp\left(-\frac{t}{\tau_i}\right) \quad (4.1)$$

where  $(G_i, \tau_i)$  are referred to as Prony series with relaxation intensity ( $G_i$ ) and relaxation time constant ( $\tau_i$ ) of the  $i^{\text{th}}$  Maxwell element,  $N$  is the total number of the Prony series pairs,  $G_e$  represents the equilibrium shear modulus at fully relaxed state, with  $G_e = 0$  for viscoelastic fluid, and  $G_e > 0$  for viscoelastic solid.

The Generalized Maxwell model can be expressed in the frequency domain through Fourier transformation of Equation (4.1) (Ferry, 1980). Dynamic storage modulus  $G'$  and loss modulus  $G''$  at each angular frequency  $\omega$  are obtained:

$$G'(\omega) = G_e + \sum_{i=1}^N G_i \frac{(\omega\tau_i)^2}{1+(\omega\tau_i)^2} \quad (4.2)$$

$$G''(\omega) = \sum_{i=1}^N G_i \frac{\omega\tau_i}{1+(\omega\tau_i)^2} \quad (4.3)$$

The discrete relaxation spectrum, represented by Prony series, is usually obtained by nonlinear least square fitting of the experimental measurements through minimizing the objective function

$$V = \sum_i [(G'_i - Z'_i)^2 + (G''_i - Z''_i)^2] \quad (4.4)$$

where  $G'(\omega)$  and  $G''(\omega)$  are the analytical results from Equations 4.2 and 4.3; and  $Z'(\omega)$  and  $Z''(\omega)$  are experimental measurements. With specified  $Z'(\omega)$ ,  $Z''(\omega)$  and  $G_e$ , the Prony series  $(G_i, \tau_i)$  are determined by nonlinear regression under restricted fitting criteria, for example the maximum number of terms  $N$  and allowable average root-mean-square fitting residual. The Prony series are expressed in the form of  $(g_i, \tau_i)$ , where  $g_i$  is a nondimensionalized Prony series parameter, defined as

$$g_i = \frac{G_i}{G_e + \sum_i^N G_i} \quad (4.5)$$

#### 4.3.2 Continuous relaxation spectrum

When the number of Maxwell elements approaches infinity, Equations (4.2) and (4.3) can be written in integral forms as (Ferry, 1980):

$$G'(\omega) = G_e + \int_0^{+\infty} H(\tau) \frac{(\omega\tau)^2}{1+(\omega\tau)^2} d\ln\tau \quad (4.6)$$

$$G''(\omega) = \int_0^{+\infty} H(\tau) \frac{\omega\tau}{1+(\omega\tau)^2} d\ln\tau \quad (4.7)$$

where  $H(\tau)$  is a non-negative density function associated with a continuous range of relaxation times  $\tau$  and is known as the continuous relaxation spectrum.

Comparing Equations (4.2) and (4.6) or (4.3) and (4.7), we have the following relation connecting Prony series parameter  $G_i$  and continuous relaxation spectrum  $H(\tau)$ . Assume the  $i$ th peak in  $H(\tau)$  spans between two valleys on the continuous spectrum defined by a time interval between  $a$  and  $b$ , we have the equivalent peak intensity calculated as:

$$G_i = \int_a^b H(\tau) d\ln\tau \quad (4.8)$$

The problem of solving for  $H(\tau)$  is sensitive to experimental noise (Hansen, 1992) such that small perturbations in the experimental data will result in enormous differences in solution (Kontogiorgos, et al., 2009). The most commonly used method to solve this ill-posed problem is Tikhonov's regularization method, in which a solution term is added to the original residual term with a regularization parameter (Hansen, 1994). The regularized solution provides a fair balance between minimizing both residual term and solution term. A FORTRAN program called FTIKREG (Weese, 1992) ([http://cpc.cs.qub.ac.uk/summaries/ACGH\\_v1\\_0.html](http://cpc.cs.qub.ac.uk/summaries/ACGH_v1_0.html)), based on Tikhonov regularization, was used to find solution of first Fredholm integral equation.

$$g(\omega) = \int K(\omega, \tau)H(\tau)d\ln\tau + \sum a_j b_j \quad (4.9)$$

To find the relaxation spectrum,  $g(\omega)$  denotes the experimentally measured dynamic modulus,  $K(\omega, \tau)$  are kernel equations for dynamic modulus as defined in Equations (4.6) and (4.7), and  $H(\tau)$  is the continuous relaxation spectrum. For storage modulus, parameter  $b_1 = 1$ , and  $a_1$  gives the estimation of long term equilibrium shear modulus  $G_e$ . The spectrum  $H(\tau)$  and equilibrium shear modulus  $G_e$  are obtained by minimizing objective function (Weese, 1992) (Sodhi, et al., 2010):

$$V(\lambda) = \sum_i \left\{ \left[ Z'_i - \left( \int_0^{+\infty} H(\tau) \frac{(\omega\tau)^2}{1 + (\omega\tau)^2} d\ln\tau + G_e \right) \right] + \left[ Z''_i - \left( \int_0^{+\infty} H(\tau) \frac{\omega\tau}{1 + (\omega\tau)^2} d\ln\tau \right) \right] \right\}^2 + \lambda \|LH(\tau)\|_2^2 \quad (4.10)$$

where  $Z'$  and  $Z''$  are experimental measurements,  $\|\cdot\|_2$  denotes the Euclidean norm of the matrix (Weese, 1992). The first term in Equation (4.10) has a traditional least square

form, called the residual term. By minimizing the residual term, solutions that are compatible with experimental data are preferred. The second term is called the solution term; operator  $L$  was defined as identity matrix in the present study to capture the standard Tikhonov regularization form, giving preference to solutions with smaller norm. An optimal regularization parameter  $\lambda$  is determined by using a self-consistent method (Weese, 1992). By minimizing the objective function, a unique regularized solution is achieved by minimizing both the residual and solution terms. It was assumed that  $H(\tau) \geq 0$  to ensure a meaningful relaxation spectrum. In addition,  $H(\tau)$  was obtained so that both the storage and loss modulus measurements were considered. For the determination of relaxation spectrum in present study, a total of 1000 data points of  $H(\tau)$  equally distributed from  $10^{-4}$ s to  $10^4$ s was calculated.

#### *4.3.3 Rheological measurements*

4.8mg/ml collagen matrix was crosslinked in 0.1% genipin following the procedure described in Chapter 2.2. Dynamic oscillatory shear test was performed by using a parallel plate Rheometer (AR-2000, TA Instrument), as described in Chapter 2.3. Sandpaper (1500 grits) was attached to both top and bottom rheological plates to prevent possible slippage between sample and plates. The bottom plate was set to be  $37^{\circ}\text{C}$  during the test. Samples were loaded between plates with a normal compression force of about 0.2N. Oscillating shear strains of 4%, 6%, and 8% was applied to the collagen gel with angular frequency ranging from 0.3142 to 377rad/s (0.05–60HZ).

#### 4.3.4 *Finite element modeling*

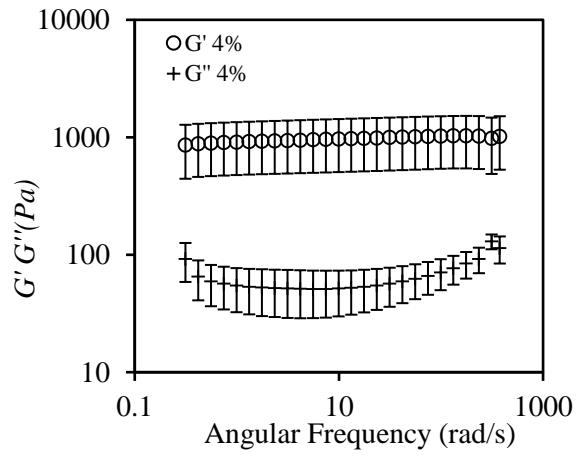
Since finite element method is broadly used to solve problems that involve material and geometric nonlinearities as well as structural complexities, here we demonstrate that the continuous relaxation spectrum can be used to define the viscoelastic properties in finite element analysis. This method can be broadly applied to other studies that need to consider the viscoelastic properties of materials. To this end, discrete spectrum from both direct fitting and calculated from continuous spectrum was used in finite element models to simulate the rheological measurement using commercial finite element software ABAQUS 6.10 (Simulia, Providence, RI). The continuous relaxation spectrum cannot be incorporated directly into the FEM simulation, instead, Prony series parameters  $G_i$  and  $\tau_i$  were obtained based on the relaxation spectrum  $H(\tau)$ .  $\tau_i$  can be directly found from spectrum since it is the time constant at the  $i$ th peak of the relaxation spectrum.  $G_i$  is calculated using Equation (4.8) assuming the  $i$ th peak in  $H(\tau)$  spans between two valleys on the continuous spectrum defined by a time interval between  $a$  and  $b$ . The model consists of a collagen gel that is in contact with an upper rheological plate. Tie constraint was used to ensure a non-slip boundary condition at the interface between collagen gel and rheological plate. The bottom plane of collagen gel was fixed during simulation. The elastic property of collagen gel was assumed to be linear elastic whereas the viscosity was characterized by Prony series. The rheological plate was modeled as a nearly rigid material compared to the collagen gel. Three-dimensional eight-node linear brick elements (C3D8R) with reduced integration were used in the model. A total of 2768 elements were used in the finite element model. We have performed mesh sensitivity

study by further reducing the element size by about 50%, however the differences in results between the meshed used in the present study and the finer mesh is minimal.

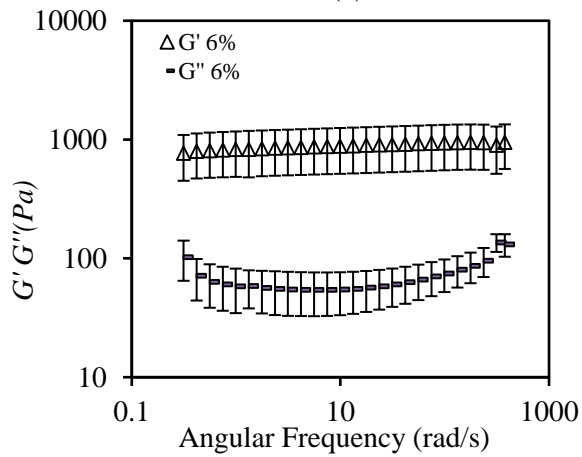
A maximum rotational strain (4%) was applied on the top plate. The distance between parallel plates was kept unchanged. A sinusoidal oscillatory rotation was applied on the top plate with frequency varying from 0.745 to 74.5rad/s. A Linear perturbation solver was used in the simulation in order to provide the steady-state solution of the collagen gel subjected to oscillatory shear rotation during the frequency sweep process. Output from the finite element simulation including shear stress, shear strain, and phase were used to obtain the storage and loss modulus based on Equations (2.5) and (2.6).

#### **4.4 Results**

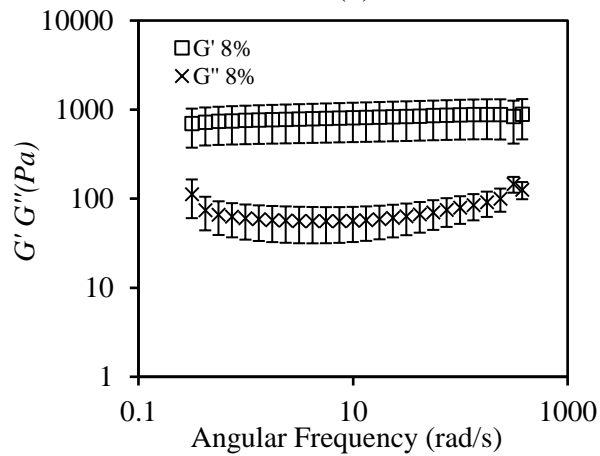
The measured storage and loss moduli at 4%, 6%, and 8% maximum shear strains are presented in Figure 4.1. Within the frequency range,  $G'$  is about one order of magnitude greater than  $G''$ , suggesting the collagen gel is a more solid-like material. Continuous relaxation spectra were obtained from experimentally measured dynamic frequency sweep results between 0.745 and 74.5rad/s, and were shown in Figure 4.2. Four peaks were uniformly observed located between 0.001–0.01s, 0.01–0.1s, 0.1–1s, and 1–10s for collagen gels tested at 4%, 6%, and 8% shear strains, although the location of the peaks and the peak intensity may vary slightly. For 4% shear strain, the four peaks are located at 0.0029s, 0.0386s, 0.1992s and 4.8382s. The estimated equilibrium shear modulus is 446Pa, 413Pa, 330Pa for 4%, 6%, and 8% shear strain, respectively.



(a)



(b)



(c)

**Figure 4.1: Dynamic storage and loss moduli of collagen gel from frequency sweep tests with angular frequency ranges from 0.3142 to 377rad/s. Maximum oscillatory shear strains are 4%, 6%, and 8%.**

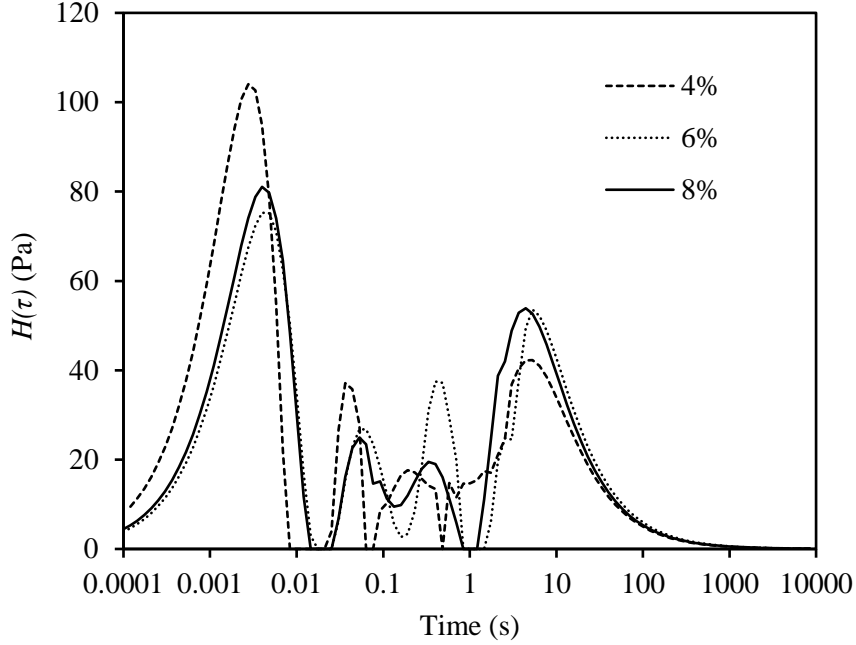


**Figure 4.2: Continuous relaxation spectra of collagen gel obtained based on frequency sweep measurements at 4%, 6%, and 8% oscillatory shear strains.**

The Prony series determined from nonlinear regression are presented in Table 4.1. Experimental results at 4% shear strain were used in the calculation. The maximum number of terms  $N$  was assumed to be 13 and the allowable average root-mean-square

residual,  $\varepsilon = \sqrt{\frac{1}{m} \sum_i^m \left[ \left( \frac{G' - Z'}{G_e} \right)_i^2 + \left( \frac{G'' - Z''}{G_e} \right)_i^2 \right]}$ , where  $m$  is the number of frequency levels

and varies from 0.001 to 0.007. As we can see that the obtained Prony series are not unique and highly dependent on fitting criteria. Using Equation (4.8), discrete spectrum was calculated from the continuous spectrum numerically. The equivalent peak intensity  $G_i$ , integration interval, nondimensional quantity  $g_i$ , together with the location of peaks are presented in Table 4.2.

**Table 4.1: Prony series obtained from directed fitting with different fitting criteria by varying the allowable average root-mean-square fitting residual  $\varepsilon = \sqrt{\frac{1}{m} \sum_i^m \left[ \left( \frac{G' - Z'}{G_e} \right)_i^2 + \left( \frac{G'' - Z''}{G_e} \right)_i^2 \right]}$ , where  $m$  is the number of frequency levels,  $G'$  and  $G''$  are analytical storage and loss modulus from Equation (4.2) and (4.3),  $Z'$  and  $Z''$  are experimental measured storage and loss modulus.**

$\varepsilon = 0.001$			$\varepsilon = 0.002$			$\varepsilon = 0.007$		
$G_i(\text{Pa})$	$\tau_i(\text{s})$	$g_i$	$G_i(\text{Pa})$	$\tau_i(\text{s})$	$g_i$	$G_i(\text{Pa})$	$\tau_i(\text{s})$	$g_i$
966.49	0.0004	0.6059	175.86	0.0028	0.2214	91.94	0.0087	0.1324
31.74	0.0284	0.0199	33.36	0.0521	0.0420	40.07	0.1766	0.0577
23.45	0.1527	0.0147	31.37	0.4329	0.0395	116.38	4.5986	0.1676
28.39	0.8388	0.0178	107.71	6.0472	0.1356			
99.06	6.0472	0.0621						

**Table 4.2: Prony series calculated from continuous spectrum using Equation (4.8). In addition to the peak relaxation time  $\tau_i$ , equivalent peak intensity  $G_i$ , and nondimensional quantity  $g_i$ , the integration interval (a, b) was also listed.**

Relaxation time $\tau_i$ (s)	Integration interval (s)	Equivalent peak intensity $G_i$ (Pa)	$g_i$
0.0029	0.0001 – 0.0075	224.7963	0.2663
0.0386	0.0248 – 0.0750	26.6211	0.0315
0.1992	0.0837 – 0.4567	23.6784	0.0281
4.8382	0.4652 – 10000	122.9047	0.1456

Finite element modelling was employed to simulate the frequency sweep test. Discrete spectra with parameters from Tables 4.1 and 4.2 were used to characterize the viscous behavior of collagen gel. Figure 4.3 shows the magnitude of shear stress  $\tau$  and

phase lag  $\delta$  when Prony series under  $\varepsilon = 0.002$  from Table 4.1 was chosen to model viscoelasticity. The storage and loss modulus were calculated using Equations (2.5) and (2.6) and comparisons with experimental measurements are shown in Figure 4.4. In general, comparison between simulated and experimental storage and loss moduli show that simulations with all parameters from Tables 4.1 and 4.2 provide reasonably good fittings to the experimental measurements. We can see that simulations with parameters determined from nonlinear regression (Table 4.1) provide slightly better fit. This is because that these parameters are obtained by minimizing the RMS fitting residual, which characterizes the difference between the fitting and the experimental results. However the parameters are very sensitive to the fitting criteria, as can be seen in Table 4.1 that a slight variation in the fitting criteria can result in a completely different set of parameters. The parameters in Table 4.2, however, are determined from continuous relaxation spectrum, which is obtained based on objective function defined by Equation (4.10). A unique regularized solution is achieved by balancing both the residual and solution terms. For this reason, the fitting using parameters based on continuum relaxation spectrum is not necessary to achieve the smallest RMS fitting residual, however the fitting is unique with parameters determined directly from continuous relaxation spectrum.

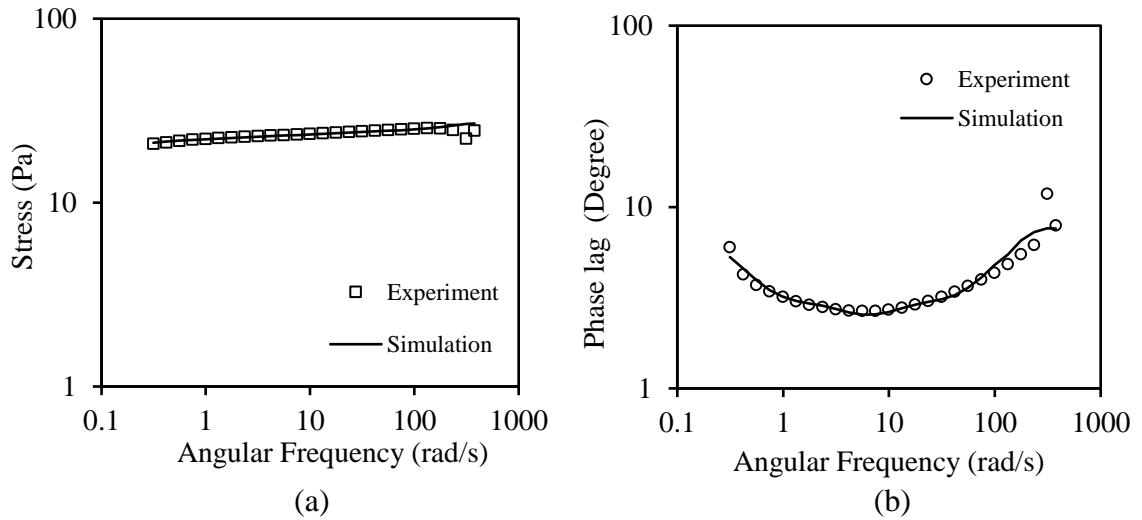


**Figure 4.3:** (a) Comparison between the magnitude of shear stress output from finite element simulation and experimental measurements during frequency sweep test with 4% oscillatory shear strain; and (b) Phase lag between the shear stress and applying strain from simulation and measurements.

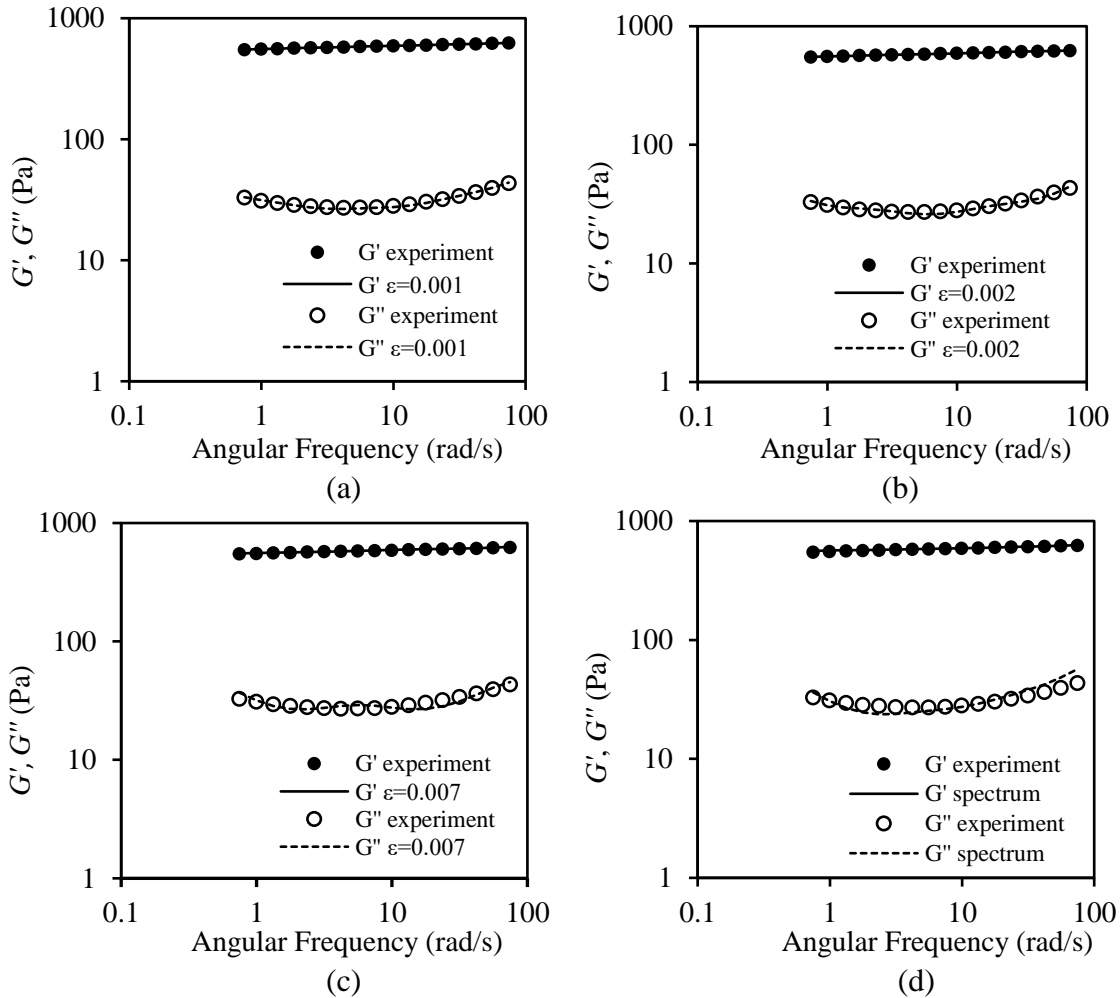


**Figure 4.4: Comparison of  $G'$  and  $G''$  between finite element simulations and experimental measurements. The viscous properties of collagen gel were described by using Prony series with parameters from Tables 4.1 (Fig. 4.4a–c) and Table 4.2 (Fig. 4.4d).**

## 4.5 Discussion

In the present study, a theoretical framework was established to obtain both discrete and continuous relaxation spectrum of collagen gel from oscillatory rheological measurements. We have shown that the discrete relaxation spectrum obtained by a direct fitting was not unique and highly dependent on constrained fitting criteria. This problem can be overcome by obtaining the continuous relaxation spectrum using Tikhonov

Regularization method. The nonuniqueness problem of discrete relaxation spectrum has been shown in previous studies. Efforts have been made to obtain unique spectrum with a small number of Prony Series. A method to achieve discrete spectrum by nonlinear regression (the so called Interactive Rheology Information Systems (IRIS) method) was provided by Baumgaertel and Winter (Baumgaertel & Winter, 1989), and Jackson et al. (Jackson, et al., 1994). They obtained a converged parsimonious discrete spectrum by choosing the number of Prony Series terms  $N$  as the fewest number of terms beyond which fitting is not improved significantly. Furthermore, they propose that the ill-posedness of the problem will completely vanish when simultaneously performing inversion on both storage and loss modulus. However, this statement was challenged later on by Malkin (Malkin, 2006) as it was not strictly proven. Moreover, Orbey (Orbey & Dealy, 1991) compared discrete spectrum obtained by IRIS method and continuous spectrum, although all Prony Series terms fell on the continuous spectrum, these terms did not show up at the peak. In other words, discrete spectra from direct fitting are not reliable to characterize the intrinsic properties of a viscoelastic material. Similar findings were also shown by Mustapha and Phyllips (Mustapha & TN, 2000), in which the discrete spectrum was determined by Marquardt–Levenberg procedure.

The continuous relaxation spectrum can be obtained from measurements in both the time and frequency domain. Stress relaxation experiment in the time domain, during which the stress decay under constant strain with respect to time is measured, has been performed broadly to study the viscoelastic material behaviors. Stress relaxation data has been used as experimental source to obtain a continuous spectrum in previous studies (Xu,

et al., 2013) (Li, et al., 2003) (Kontogiorgos, et al., 2009) (Kontogiorgos & Kasapis, 2010). In the frequency domain, dynamic oscillatory shear measurement is also widely used to characterize the viscoelastic material behavior (Nasseri, et al., 2002) (Mezger, 2006) (Kontogiorgos, 2010) (Xu, et al., 2011). Compared with stress relaxation test, dynamic rheological measurements do not involve sudden increase of strain. The measured frequency-dependent dynamic moduli have been used for the calculation of continuous relaxation time spectrum (Honerkamp & Weese, 1989) (Kontogiorgos, 2010) (Elster, et al., 1991) (Roths, et al., 2000) (Hansen, 2008) (Bhattacharjee, et al., 2012). In the present study, continuous relaxation spectrum was obtained through solving ill-posed inversion problem with Tikhonov regularization. It is proved to be reliable in terms of keeping the main properties (number of peaks, relaxation time constant and peak intensity) of a continuous spectrum, because more data points are used in the calculation to prevent the danger of ill-posedness (Orbey & Dealy, 1991). It is also believed to be a true representation of material properties (Dealy & Larson, 2006). Moreover, both storage and loss modulus were used in the calculation for relaxation spectrum, increasing the accuracy in the obtained relaxation spectrum (Winter, 1997).

The calculated relaxation spectra show four obvious peaks (Figure 4.2). Previous studies (Ptaszek & Grzesik, 2007) (Ptaszek, et al., 2009) inferred the presence of multiple peaks owing to the heterogeneous structure of the investigated biopolymers. It is well known that collagen-based materials are organized into hierarchical structures, where hierarchical levels consist of collagen molecules, fibrils, and fibers (Fratzl, 2008) (Gautieri & Vesentini, 2011). The stress relaxation behavior of collagen based material

can be well modeled by three exponential decay terms which reflecting the short, medium and long-term relaxation in the tissue (Toms, et al., 2002) (Wagenseil, et al., 2003) (Komatsu, 2010). In relation to the structure, the three relaxation processes are likely correlated with relaxation mechanisms involving fiber, inter-fibril, and fibril sliding, respectively (Xu, et al., 2013) (Gupta, et al., 2010). In our previous biaxial tensile stress relaxation tests of collagen network (Xu, et al., 2013), three peaks at the short (0.3s ~ 1s), medium (3s ~ 90s), and long relaxation time (>200s) were observed in the relaxation spectrum. Intra fibril crosslinks is the most stable structure under long term load (Gupta, et al., 2010) (Bailey, 2001), therefore the fibril relaxation is likely to be the slowest (Xu, et al., 2013). The difference between the spectrum obtained from biaxial tensile tests and rheological shear measurements may indicate differences in relaxation mechanisms involved. The spectrum from rheological shear measurements consist a high intensity peak between 0.001 and 0.1s, suggesting that the relaxation is mostly dominated by fast relaxation process, however this peak is absent from the tensile stress relaxation data. The fast relaxation is likely related to the unstable interactions that prone to relax at short time scales. Similar phenomena have been observed in previous studies using rheological shear measurements (Sodhi, et al., 2010) (Ptaszek & Grzesik, 2007) (Ptaszek, et al., 2009). Since in rheological shear relaxation both collagen fiber network and interstitial fluid play important roles, we suspect the fast relaxation was due to the interaction between collagen fibers and surrounding fluid.

We would like to point out some limitations in our study. With dynamic rheological measurement, the frequency-dependent data are obtained only at a certain

number of discrete frequencies and data are available only between maximum and minimum frequencies that are imposed by the capabilities of the instrument. According to Davies and Anderssen (Davies & Anderssen, 1997), storage and loss moduli over this frequency range yields information of relaxation spectrum over the range of 0.064–0.28s and spectrum obtained outside this range should be considered as suspicious. This theory has been applied to determine the range of relaxation spectrum based on experimental data (Jensen, 2002), however the relaxation spectra obtained based on sampling localization theorem are poor and have met some difficulties in fitting the experimental results were pointed out by earlier studies (Mustapha & TN, 2000) (Jensen, 2002). Although not shown here, we have similar problems. In the meanwhile, several previous studies (Sodhi, et al., 2010) (Ptaszek & Grzesik, 2007) (Ptaszek, et al., 2009) obtained the relaxation spectrum outside the experimental time frame. Time-temperature superposition analysis (Kontogiorgos & Dahunsi, 2014) by studying frequency dependent properties of collagen gel at various temperatures could potentially extend the timeframe of observation and be used to verify the spectrum calculated in this study.

#### **4.6 Summary**

A theoretical framework was developed to calculate both the discrete and continuous relaxation spectrum of viscoelastic soft biological material based on dynamic rheological measurements. A finite element model was developed to simulate the rheological experiments considering the viscoelastic properties of the material. Using collagen gel as an example, we have shown that the discrete spectrum, Prony Series,

obtained by a nonlinear regression procedure, is not unique and highly dependent on the fitting criteria. The continuous relaxation spectrum, obtained through solving ill-posed inversion problem with Tikhonov regularization, however, is more reliable when studying the main properties (number of peaks, relaxation time constant and peak intensity) of a continuous spectrum, which is important when correlating with intrinsic structural properties and relaxation mechanisms of viscoelastic materials. In terms of finite element modeling, parameters from both the discrete and continuous spectrum provide good fittings of experimental data.

## **CHAPTER 5: MULTI-SCALE MEASUREMENTS OF THE MECHANICAL PROPERTIES OF COLLAGEN MATRIX**

### **5.1 Overview**

Extracellular matrix (ECM) provides the principal avenue for mechanochemical communication between tissue and cells. ECM not only plays an important role in providing structural and biomechanical support but also in regulating a series of cellular behaviors such as cell differentiation, proliferation and mobility. Many pathological conditions are related to mechanical alternations in the ECM. However, the underlying mechanisms by which the ECM mechanics influences cell and tissue function remain to be elucidated since the events associated with this process span size scales from tissue to molecular level. Furthermore, ECM has an extremely complex hierarchical 3D structure and the load distribution is highly dependent on the architecture and mechanical properties of ECM. Collagen gel has been broadly used as an ECM equivalent. In the present study, the macro and microscale mechanical properties of collagen gel were studied. Dynamic rheological testing was performed to study the macroscale mechanical properties of collagen gel. The microscale mechanical properties of collagen gel were measured using Optical Magnetic Twisting Cytometry (OMTC). Ferromagnetic beads embedded in the matrix were used as mechanical probes. Our study on the multi-scale mechanical properties of collage matrix suggests several interesting differences between macro and micro-scale mechanical properties originated from the scales of measurements. In the rheometer measurements, the storage and loss moduli increase with collagen

concentrations. The nonaffine collagen fibril structural network deformation plays an important role in determining the macroscopic mechanical properties of the collagen matrix. At the microscopic scale, however, the local apparent storage and loss modulus are less sensitive to changes in collagen concentration due to the more immediate/direct deformation of collagen fibrils in the OMTC measurements through forces exerted by locally attached ferromagnetic beads. The apparent loss modulus is more affected by the local interstitial fluid environment, leading to a rather dramatic increase in viscosity with frequency, especially at higher frequencies ( $>10$  Hz). A finite element model was developed to study the geometric factors in the OMTC measurements when the collagen matrix was considered to be hyperelastic. Our results show that the geometric factors are dependent on collagen concentration, or the stiffness of matrix, when nonlinear material properties of the matrix are considered, thus interpretation of the apparent modulus from OMTC measurements should be conducted carefully.

## **5.2 Introduction**

The Extracellular Matrix (ECM) provides the principal avenue for mechanochemical communication between tissue and cells (Peyton, et al., 2007) (Pizzo, et al., 2005). These signals are communicated in a reciprocal manner, playing critical roles in establishing tissue structure-function relationships and controlling cell fate. For example, the stiffness of ECM not only provides structural support but also plays an important role in regulating a series of cell activities such as differentiation (Engler, et al., 2006), proliferation (Wang, et al., 2000) and migration (Pelham & Wang, 1997) (Zaman,

et al., 2006). On the other hand, cells sense the local forces exerted by ECM and then modulate the structure and composition of the ECM. Many pathological conditions including cardiovascular diseases, tumorigenesis, metastasis, ageing of connective tissues, etc., involve significant biological and mechanical alternations of ECM. However the mechanisms by which ECM mechanics influence cell and tissue function remain to be elucidated since the events associated with these processes span size scales from the tissue to molecular level. Furthermore, the ECM has extremely complex hierarchical three-dimensional (3-D) structures and there exists a tremendous interdependence of ECM compositional, structural, and mechanical properties (Pizzo, et al., 2005). To date it is still not well understood how mechanical forces are translated within ECM, or from the tissue- to cellular level. Such information is imperative since the magnitude of the load at the tissue level is different from that experienced by the cell (Pizzo, et al., 2005) (Brown, 2000), and the differential load distribution is highly dependent on the architecture and mechanical properties of the ECM (Pizzo, et al., 2005) (Mow, et al., 1994).

As a major ECM component, collagen plays an important role in modulating cell function, in addition to providing structural support. Type I collagen gel has been used extensively to study cell-ECM interaction and cell induced ECM remodeling since it retains essential elements of cell-matrix 3D interactions, although much of the structural and molecular complexities present *in situ* are omitted. By controlling environmental factors (temperature, pH, ionic strength, etc.) in an appropriate manner, triple helical type I collagen molecules first self-assemble to form collagen fibril; bundles of collagen fibrils further aggregate to collagen fibers (Motte & Kaufman, 2012) (Yang & Kaufman, 2009).

Together with the interstitial fluid, a 3-D collagen matrix with hierarchical structure is formed. The macroscopic mechanical properties of collagen gel have been broadly studied by using rheological testing method. Storage and loss moduli were measured to characterize the elastic and viscous mechanical properties of collagen gel, respectively, considering the effect of collagen concentration (Julias, et al., 2008), crosslinking (Xu, et al., 2011) and polymerization temperature (Raub, et al., 2007). Local mechanical properties of collagen gel have also been studied by using several microscopic measurement methods. Laser microrheometry technique (Velegol & Lanni, 2001) was developed to probe the local mechanical properties of collagen matrix by oscillating a trapped particle. In this technique, force is exerted on one bead at a time, so the results could depend on the local heterogeneity (Leung, et al., 2007), and it would be time consuming to capture the behavior of a population of beads (Parekh & Velegol, 2007). Magnetic twisting cytometry (MTC) is capable of measuring the collective behavior of a population of beads, and has been used extensively to study the viscoelastic microrheology of living cells (Valberg PA, 1987) (Wang, et al., 1993) (Fabry, et al., 1999) (Maksym, et al., 2000) (Laurent, et al., 2002). Since receptors at cell surfaces are physically linked to the cytoskeleton (CSK), mechanical properties of the CSK can be inferred. The MTC method was later adapted to measure the mechanical properties of type I collagen gel and demonstrated success on probing cellular modulation of matrix stiffness (Leung, et al., 2007). The MTC method relies on measurement of the changes in the remanent magnetic field. Fabry (Fabry, et al., 1999) reported that the method is more weighted towards weakly bound beads, resulting in overestimated mean angular bead

rotation and underestimated mean shear modulus. Later, the so-called optical magnetic twisting cytometry (OMTC) method was established in which the beads rotation was measured optically via tracking the lateral displacements of the centroids of the magnetic beads (Fabry, et al., 2001) (Fabry, et al., 2003) (Smith, et al., 2003) (Deng, et al., 2004) (Trepate, et al., 2004) (Fredberg & Fabry, 2006). The OMTC method allows identifying and excluding loose beads or bead clusters from data analysis, thus the measurement is more reliable (Fabry, et al., 2001). In the present study, the OMTC method was used to measure the local mechanical properties of type I collagen matrix. Streptavidin and poly-L-lysine (PLL) coated ferromagnetic beads were used to achieve beads-matrix binding. The macroscopic mechanical properties of collagen gel were measured using a parallel plate rheometer. A 3-D finite element model was developed to simulate the OMTC measurements, and to study the effects of nonlinear ECM material properties, matrix geometry, and beads embedding degree on the measurements.

### **5.3 Material and methods**

#### *5.3.1 Collagen gel preparation*

Collagen matrix were prepared as described in Chapter 2.2 to reach the final concentration of 2.0, 3.0 and 4.8mg/ml.

#### *5.3.2 Macroscopic mechanical property measurement*

Rheological testing was performed by using a parallel-plate (R=2cm) AR-2000 Rheometer (TA Instruments), as described in Chapter 2.3. Frequency and strain sweep

tests were performed to characterize the viscoelastic mechanical properties of collagen gel. In frequency sweep tests, oscillating shear strains of 1% were applied to the samples with frequencies ranging from 0.05 to 30HZ. In strain sweep tests, oscillating shear with maximum strain ranging from 0.1% to 35% was applied to the sample at 1Hz. Results from rheological testing were averaged from four samples.

### *5.3.3 Microscopic mechanical property measurement*

Two types of ferromagnetic beads with different binding mechanisms were used in local mechanical property measurement. Streptavidin coated ferromagnetic beads (Spherotech Co., 4.7um in diameter) were used to achieve bonding via bio-conjugation between the beads and the collagen fibrils. Streptavidin contains an Arg-Tyr-Asp (RYD) amino acid sequence that mimics the Arg-Gly-Asp (RGD) receptor domain of fibronectin. A tight binding is formed between streptavidin and collagen under complex interactions including specific biochemical affinity, charge polarity, complementary shapes and hydrophobicity (Chen, et al., 2012) (Guo & Kaufman, 2007) (Herath, et al., 2014). For a second type of magnetic beads, ferromagnetic beads (~4.1um-diameter, provided by Dr. Jeffery Fredburg's group at Harvard) coated with poly-l-lysine (PLL) (Sigma Co.) following procedures by Zhou et al. (Zhou, et al., 2009) were used. PLL contains a positively charged hydrophilic amino group, which enhances the attachment with negative charged collagen fibrils due to electrostatic interaction. Beads solution of 0.05mg/ml was poured on collagen gel surface followed by incubation at 37°C for 20 min for Streptavidin beads and 40 min for PLL beads to allow binding between beads and

collagen fibrils. The sample was then washed twice with DI water to remove unbound beads.

Local mechanical properties of collagen matrix were measured using OMTC, as described in Chapter 2.5. Results from three samples were averaged, and for each sample six different locations were measured to minimize the effect of heterogeneity.

The apparent storage and loss modulus in Equation 2.9 have a dimension of Pa/nm. To obtain storage and loss modulus, a geometric factor  $\beta$  is required (Fabry, et al., 2001). The storage and loss modulus,  $G$ , is related to the apparent modulus  $G_d$  as (Mijailovich, et al., 2002):

$$G_d = \frac{k\beta}{R} G \quad (5.1)$$

Where  $k$  is a shape factor (6 for spherical beads) and  $R$  is the radius of beads.

#### 5.3.4 Finite Element Modeling

A three-dimensional finite element model was developed using ABAQUS 6.10 (Simulia, Providence, RI) to simulate the local mechanical property measurements using OMTC. The ferromagnetic bead was modeled as a rigid material. Collagen matrix was modeled as a nearly incompressible isotropic hyperelastic material with strain energy function defined as (Gasser, et al., 2006):

$$U = C_{10}(\bar{I}_1 - 3) + \frac{k_1}{2k_2} \sum_{\alpha=1}^N \{ \exp[k_2 \langle \bar{E}_\alpha \rangle^2] - 1 \} + \frac{1}{D} \left( \frac{(J^{el})^2 - 1}{2} - \ln J^{el} \right) \quad (5.2)$$

where  $\bar{I}_1$  is the first invariant of modified counterpart right Cauchy-Green tensor  $\bar{C}$  (Gasser, et al., 2006), and the stress like parameter  $C_{10}$  relates to the initial stiffness of the matrix. The second term captures the behavior of dispersed collagen fibrils. Parameter  $k_1$

is another stress like parameter and  $k_2$  is a dimensionless parameter.  $N$  is the number of fiber families. In our model,  $N = 2$  to define the two mean directions of collagen fibrils. The dispersed collagen fibrils are distributed about each mean direction. Parameter  $\kappa$  defines the level of dispersion and is thus related to the anisotropic behavior. The collagen gel without any preferred fibril alignment can be regarded as an isotropic material so  $\kappa = 1/3$ . The strain-like quantity  $\overline{E}_\alpha \stackrel{\text{def}}{=} \kappa(\overline{I}_1 - 3) + (1 - 3\kappa)(\overline{I}_{4(\alpha\alpha)} - 1)$  characterizes the deformation of each family of fibers along the mean direction. The third term is related to the compressibility of the sample.  $D$  is the inverse of bulk modulus and  $J^{el}$  is the elastic volume ratio. In our study, the collagen matrix is assumed to be incompressible with the values of  $D$  and  $J^{el}$  to be 0 and 1, respectively. Material parameters of the collagen matrix with different collagen concentrations were determined by fitting the shear stress-strain measurements with FEM simulations of rheological measurements, which consists of a collagen gel sandwiched between two parallel plates (Li & Zhang, 2014). These material parameters were then used in simulations of the OMTC experiments.

To simulate the OMTC experiment, a single rigid bead ( $\Phi=4.5\mu\text{m}$ ) embedded in the collagen matrix was modeled. A tie constraint non-slip boundary condition at the interface between collagen matrix and the bead was applied. Considering the beads density, the average area occupied by a single bead, and the symmetric geometry and loading conditions, half of the collagen matrix of  $36\mu\text{m}\times 18\mu\text{m}\times 50\mu\text{m}$  was used in the model with periodic boundary conditions. The height of the collagen matrix was determined from thickness dependency study, which will be presented later. The collagen

matrix was modeled using 3-D, 8-node hybrid linear brick C3D8H elements. A total of 34439 elements were used in the finite element model, after a mesh dependency study. Zero displacements boundary condition was imposed on the bottom surface of the collagen matrix. A twisting torque, calculated by multiplying the specific twisting torque by the volume of single bead, was applied at the centroid of the ferromagnetic beads along the y axis and the resulted lateral displacements were recorded. In this study, the twisting torque was  $1.28 \times 10^{-12}$  N mm for streptavidin coated beads and  $1.36 \times 10^{-12}$  N mm for PLL coated beads. The beads embedding degree refers to the degree to which the bead is embedded (Figure 5.1). It was calculated as the fraction of the diameter of the bead embedded in the matrix to the total diameter of the bead (Mijailovich, et al., 2002). In this study, the beads embedding degree was varied from 5% to 90%. The effect of matrix height was also studied by varying the height of the collagen matrix at 10, 25, 50, and  $100 \mu\text{m}$ . The lateral displacement of the centroid of the bead was used to calculate the local apparent modulus  $G_d$ .

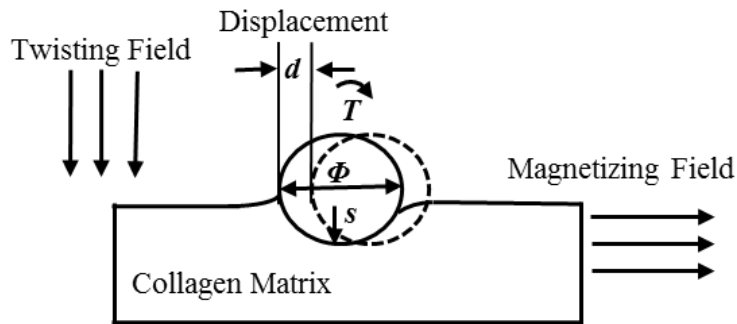
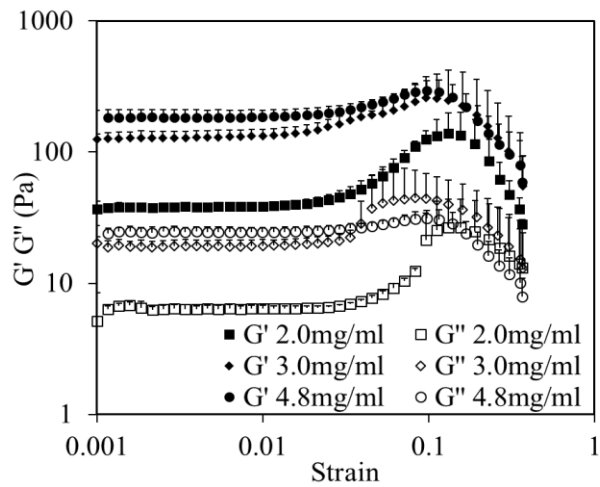


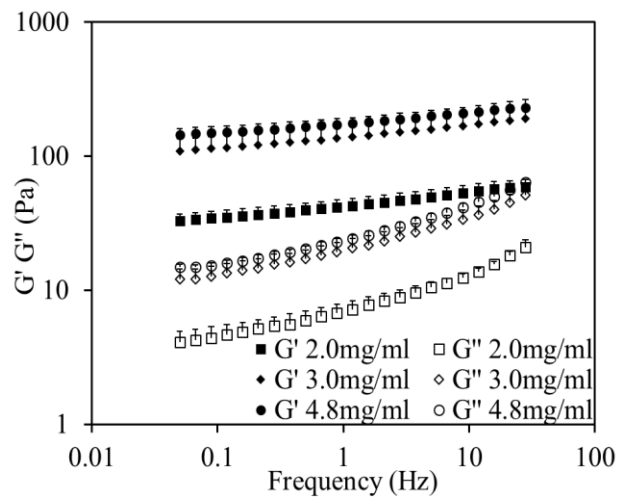
**Figure 5.1: Schematic of optical magnetic twisting cytometry. Ferromagnetic bead (Diameter  $\Phi$ ) embedded in collagen matrix. The bead embedding degree is the fraction of diameter of the bead embedded in the matrix, defined as  $s/\Phi$ . A homogeneous magnetic twisting field causes the bead to rotate and to displace.  $T$  is the applied specific magnetic torque. The lateral translation  $d$  is record during the OMTC measurement.**

## 5.4 Results

Strain and frequency sweep tests were performed to characterize the macroscopic mechanical properties of collagen matrix. For all collagen concentrations,  $G'$  and  $G''$  appears to be constant below 1~2% shear strain, followed by gradual strain stiffening and finally failure at about 10% shear strain (Figure 5.2a). Both storage and loss moduli increase with collagen concentrations, however the increase is more obvious when collagen concentration increases from 2.0mg/ml to 3.0mg/ml. Results of frequency sweep tests (Figure 5.2b) show that for all collagen concentrations,  $G'$  increases as a power of frequencies within the frequency range from 0.05 to 30Hz, as shown by the linear relationship between  $G'$  and frequency in the log-log plot.  $G''$  first increases as a power of frequencies less than 10Hz and then shows a stronger frequency dependency in the high frequency domain. Similar as the strain sweep tests, collagen gel becomes stiffer as the concentration increases from 2.0mg/ml to 3.0mg/ml, however the storage and loss moduli do not increase as much when the collagen concentration is further increased to 4.8mg/ml.



(a)

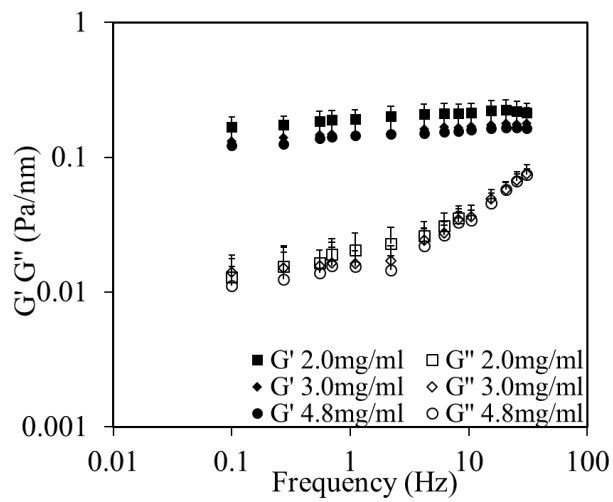


(b)

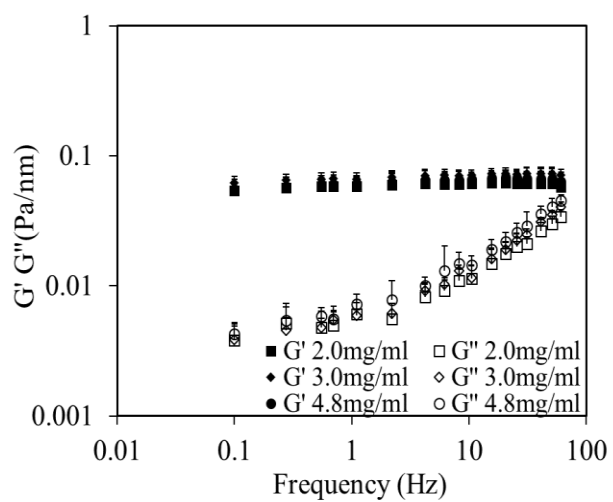
**Figure 5.2: Averaged storage and loss modulus from macroscopic rheometer measurements of collagen matrix of 2.0mg/ml, 3.0mg/ml, and 4.8mg/ml collagen concentrations from (a) strain sweep tests, and (b) frequency sweep tests. Results were averaged from four samples. Error bars represent standard error deviation.**

Figure 5.3 shows the apparent storage and loss modulus from local mechanical property measurements using both streptavidin and PLL coated ferromagnetic beads. The different binding mechanisms do not seem to affect the local mechanical property

measurements, as the results in Figures 5.3a and 5.3b are similar. Compared with the macroscopic frequency sweep measurements in Figure 5.2b, however, there are several striking differences: first of all, the local mechanical measurements do not show obvious dependency on collagen concentration, i.e., the apparent storage modulus appears to be similar for all collagen concentrations. Further, there is no obvious frequency dependency of the apparent storage modulus. The apparent loss modulus, however, has a much stronger dependency on frequency, especially at higher frequencies ( $>10\text{Hz}$ ).



(a)



(b)

**Figure 5.3: Averaged apparent storage and loss modulus from microscopic OMTC measurements of collagen matrix of 2.0mg/ml, 3.0mg/ml, and 4.8mg/ml collagen concentrations by using (a) Streptavidin coated ferromagnetic beads, and (b) Poly-l-lysine coated ferromagnetic beads. Results were averaged from three samples and six locations on each sample. Error bars represent standard deviation.**

Further comparisons between macroscopic and microscopic measurements are made by comparing the dimensionless quantity, phase lag angle, from both the rheometer and OMTC measurements (Figure 5.4). The phase angle measured using rheometer, which captures the macroscopic material behavior, shows a decreasing trend as the collagen concentration increases, especially from 2 to 3mg/ml (Figure 5.4a). However, this trend is absent from the OMTC measurements (Figure 5.4b). Similar to the apparent loss modulus measurements in Figure 5.3, the phase angle appears to have a strong frequency dependency, especially when the frequency is higher than 10Hz.

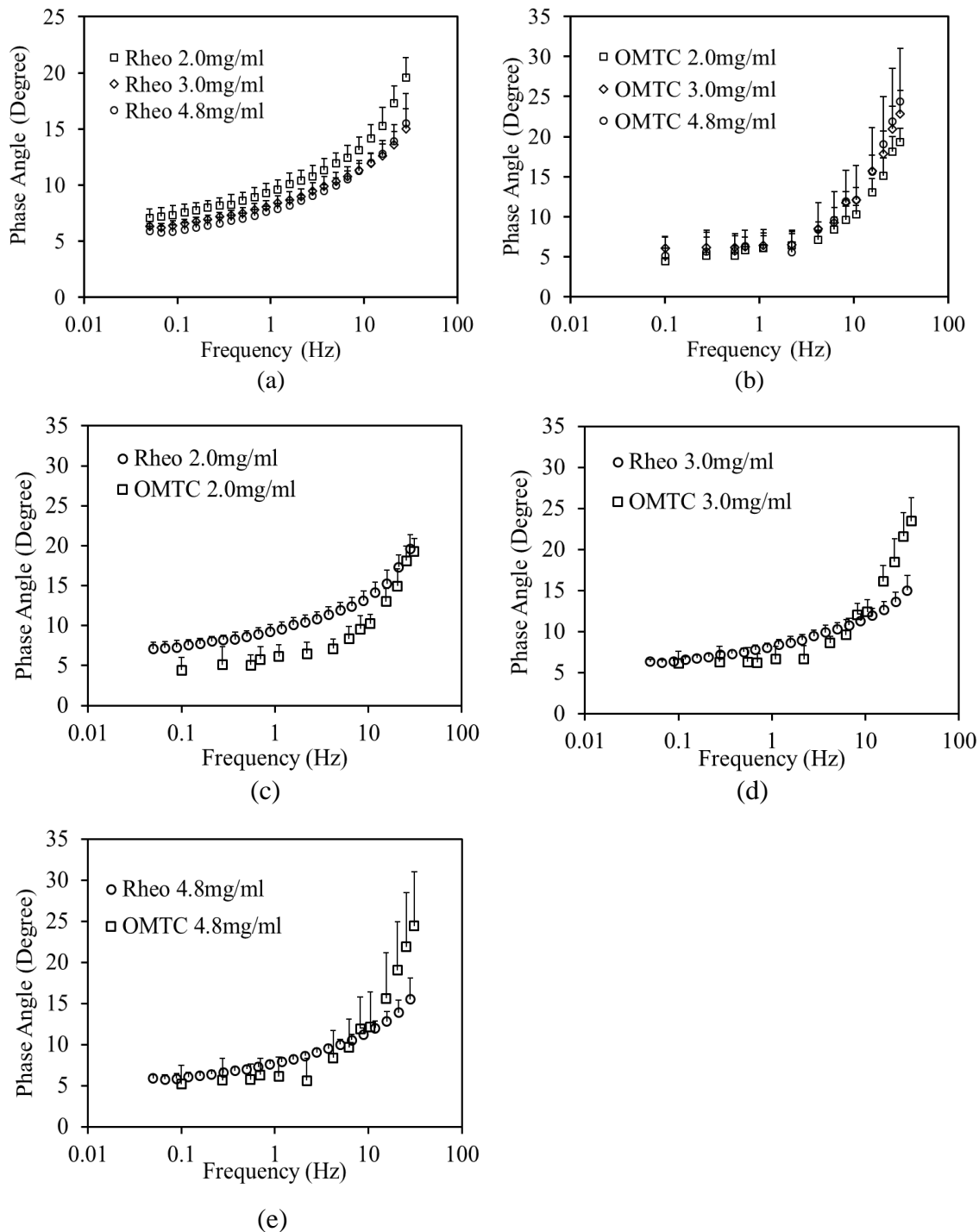


**Figure 5.4:** Averaged phase angle based on measurements from (a) rheometer (Figure 5.2b) and (b) OMTC (Figure 5.3a) for collagen matrix of 2.0mg/ml, 3.0mg/ml, and 4.8mg/ml collagen concentrations. Comparison between phase angles from rheometer and OMTC measurements for collagen matrix with collagen concentrations of (c) 2.0mg/ml, (d) 3.0mg/ml, and (e) 4.8mg/ml. Error bars represent standard deviation.

The material parameters in the constitutive model (Equation 5.2) of the collagen matrix, obtained by fitting a finite element model of rheological testing (Li & Zhang, 2014) to the shear stress-strain curves in Figure 5.5, are summarized in Table 5.1. Figure 5.6 shows the relationship between the lateral displacement of the beads and the beads embedding degree when the thickness of the matrix increases from 10 to 100  $\mu\text{m}$ . The lateral displacement of the beads centroid decreases exponentially with higher bead embedding degree. Overall, the effect of matrix thickness on the lateral beads displacement diminishes when the thickness is greater than 50 $\mu\text{m}$ . Thus, a matrix height of 50 $\mu\text{m}$  is used in further simulations in our study.

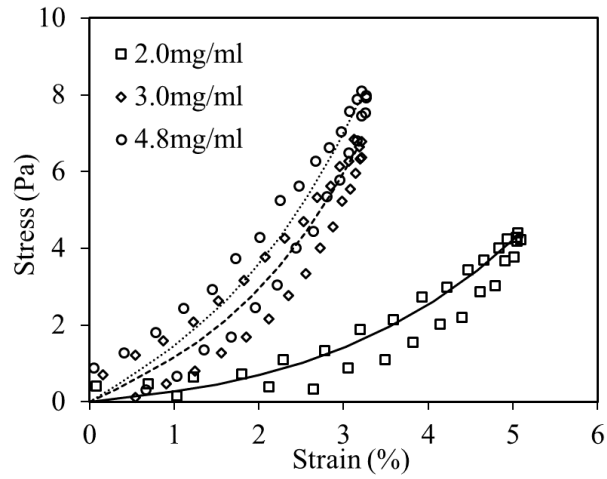


**Figure 5.5: Averaged shear stress vs. strain curves of collagen matrix from rheometer measurements fitted by the hyperelastic constitutive model in Equation 5.2. Results were averaged from four samples.**

**Table 5.1: Material parameters of collagen gel obtained by fitting the shear stress and strain responses in Figure 5.5 using the hyperelastic model in Equation 5.2.**

Collagen concentration (mg/ml)	$C_{10}$ (Pa)	$K_1$ (Pa)	$K_2$
2.0	12.5	$5.80 \times 10^4$	$8 \times 10^2$
3.0	53	$2.45 \times 10^5$	$8 \times 10^2$
4.8	68	$2.60 \times 10^5$	$8 \times 10^2$

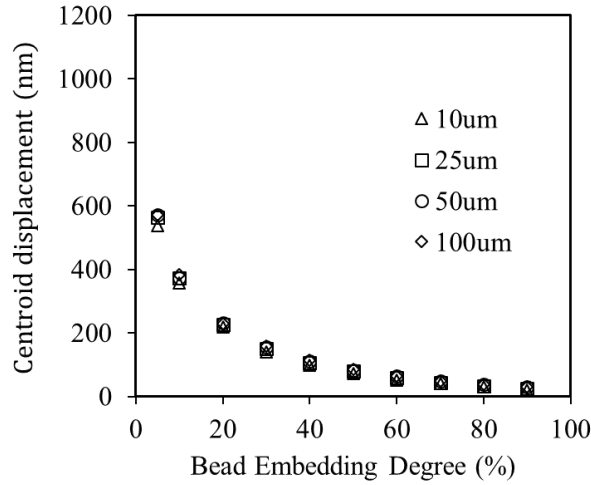


**Figure 5.6: Matrix thickness dependency study with the height of collagen matrix varies from 10 to 100 $\mu$ m in the finite element simulation. The lateral displacement at the centroid of the ferromagnetic bead is plotted with bead embedding degree varies from 5% to 90% for the 3.0mg/ml collagen matrix.**

To understand the spatial distributions of strain within the matrix, Figure 5.7 shows the strain contour plots of collagen matrix with 20% bead embedding degree. Here a clockwise twisting torque is applied about the y- axis. The logarithm strain components  $LE_{11}$  and  $LE_{33}$  show opposite signs on each side of the vertical plane containing the bead rotational axis. The shear component  $LE_{13}$  distributes symmetrically with the greatest shear strain found at the bottom of the bead. The equivalent strain, defined as  $LE^{eff} =$

$\sqrt{\frac{2}{3} \mathbf{LE}^{dev} : \mathbf{LE}^{dev}}$ , where  $\mathbf{LE}^{dev} = \mathbf{LE} - \frac{1}{3} \text{tr}(\mathbf{LE}) \mathbf{I}$  is the deviatoric strain in Cartesian system, is also presented to provide an overall measure of the maximum shear strain (Mijailovich, et al., 2002).  $\mathbf{LE}$  is the logarithm strain tensor defined as  $\mathbf{LE} = \frac{1}{2} \ln(\mathbf{C})$ , where  $\mathbf{C}$  is the right Cauchy-Green deformation tensor. We can see that the equivalent strain distribution is highly non-uniform, and the maximum effective strain appears near the interface between the bead and the free apical surface of the matrix, and the bottom of the bead. The strain decays rapidly in the radial direction, which manifests the nature of local deformation. Although not shown here, under the same magnetic torque, increasing the bead embedding degree leads to lower magnitude in strain.

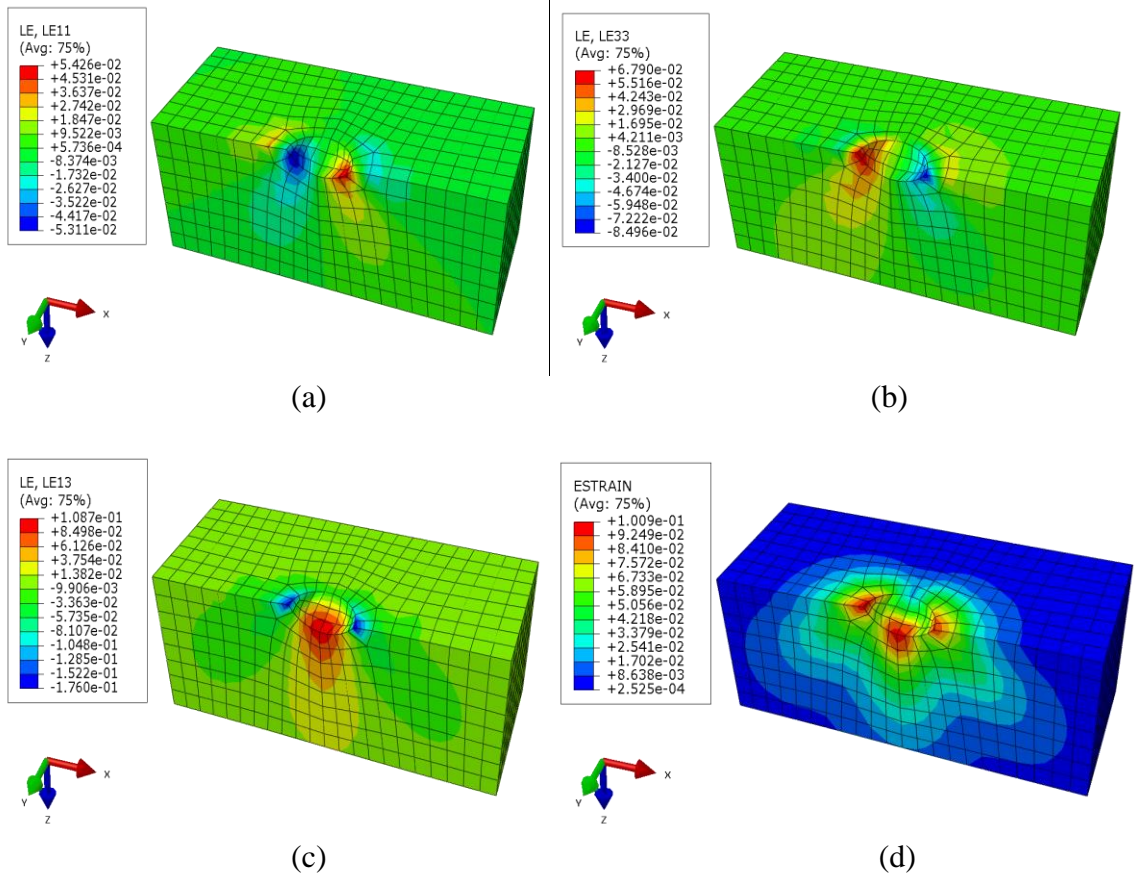


**Figure 5.7: Contour plots showing the strain field distribution in collagen matrix when a ferromagnetic bead is embedded in a  $50\mu\text{m}$ -high matrix with 20% bead embedding degree, (a) x- component, (b) z- component, (c) xz component and (d) equivalent strain.**

The geometric factors were calculated for each bead embedding degree based on Equation 5.1 and plotted in Figure 5.8. Here the initial shear modulus estimated from the shear stress-strain curves in Figure 5.5 was used as the shear modulus  $G$  of the collagen matrix. Results from Mijailovich (Mijailovich, et al., 2002) were also plotted for comparison. As we can see, by considering the nonlinear hyperelastic mechanical properties of the collagen matrix, the geometric factors obtained from our study deviate from the results by Mijailovich (Mijailovich, et al., 2002), in which linear elastic material

property of the matrix was considered. The discrepancy is more obvious at smaller bead embedding degrees. The geometric factor also shows dependency on collagen concentration, or the stiffness of the matrix when hyperelastic material property of the matrix is considered. At the same bead embedding degree, the geometric factor decreases as collagen concentration increases.

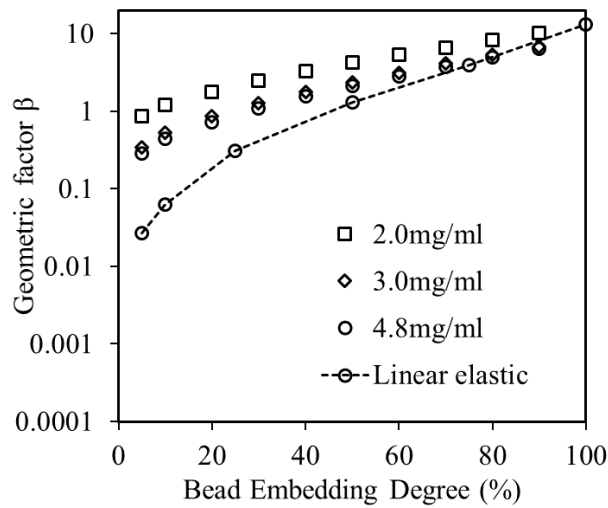


**Figure 5.8: Geometric factor  $\beta$  obtained from finite element simulation with beads embedding degree varies from 5% to 90% for collagen matrix of 2.0mg/ml, 3.0mg/ml, and 4.8mg/ml collagen concentrations. Results from Mijailovich (Mijailovich, et al., 2002) with linear elastic material property assumption are shown for comparison.**

## 5.5 Discussion

Understanding the differences between global and local mechanical properties of the hierarchical 3-D ECM network is important to study the mapping of mechanical forces from tissue to cellular level. Using rheometer and OMTC measurements, the current study reveals several interesting differences between the macro and microscopic mechanical properties of collagen matrix, suggesting the importance of the scales of

measurements. Collagen gel contains a collagen fiber network and interstitial fluid, which are referred to as solid and fluid phases, and both contribute to its viscoelastic mechanical behavior (Knapp, et al., 1997). Its frequency and strain dependent properties have been widely studied using rheological testing. Within the range of collagen concentrations in this study, collagen gel is a more solid-like viscoelastic material, as shown in Figure 5.2 that the storage modulus is about 10 times of the loss modulus, which is consistent with other studies (Hsu, et al., 1994) (Yang & Kaufman, 2009) (Velegol & Lanni, 2001). Collagen gel possesses strain-stiffening behavior under shear (Figure 2a), as also reported by others (Motte & Kaufman, 2012) (Stein, et al., 2010) (Arevalo, et al., 2011) (Kurniawan, et al., 2012). The strain stiffening behavior was suggested to emerge from nonaffine deformation and rearrangement of collagen fibrils within the fibrous network through both numerical simulations (Onck, et al., 2005) (Kang, et al., 2009) (Stein, et al., 2010) and imaging studies (Vader, et al., 2009) (Arevalo, et al., 2011) (Tower, et al., 2002). In the undeformed state, the wavy collagen fibrils distribute randomly. When subjected to strain, the wavy collagen fibrils start to uncrimp, and rearrange in the loading direction, inducing a transition from bending-dominated response at small strains to a stretching-dominated response at large strains, and thus the strain stiffening behavior (Onck, et al., 2005).

Since no crosslinking agent was used in our experiment, the interaction between collagen fibrils is most likely to be transient, and originated from entanglements and weak noncovalent interactions between fibrils (Shayegan & Forde, 2013). The macroscopic measurements (Figure 5.2) capture a combined response from both elastic

and viscous phases (Knapp, et al., 1997). The elastic contributions are related to the solid phase in the network (Kurniawan, et al., 2012) (Xu & Craig, 2011). The viscous contributions mainly arise from two parts. Due to the formation of collagen gel with weak noncovalent interactions and entanglements, the rearrangement and disentanglement of collagen fibrils contribute to the relaxation of fibril network under deformation. In addition, the viscous contribution also arises from the movement of interstitial fluid, which is linearly proportional to the rate of deformation, and turns out to be small except at high frequencies (Fabry, et al., 2003). Under oscillatory shear at low frequency levels, there is enough time for collagen fibrils to rearrange and disentangle so the measured properties are dominated by the equilibrium elastic deformation of the network. Physical disentanglements between collagen fibrils happen rather quickly compared to the low oscillatory shear frequency so they do not contribute much to elastic energy (Grillet, et al., 2012). As the frequency increases (Figure 5.2b), however, there is not enough time for microstructural rearrangement and the collagen fibrils are prone to stay entangled and create the so-called “pseudo-crosslinks” (Wu, et al., 2005), which leads to an increase in storage and loss modulus (Grillet, et al., 2012). At higher frequencies (>10Hz), the contribution of viscous fluid becomes dominant and leads to a faster increase in loss modulus.

Within the range of testing frequency, the local frequency dependent behavior measured using OMTC in present study follow a similar trend as that measured on a 0.5mg/ml collagen gel using optical tweezers (Shayegan & Forde, 2013). The fact that the apparent storage and loss moduli from OMTC measurements (Figure 5.3) are not

affected by the collagen concentration suggests a dependency on the scale of measurements. In local mechanical property measurements, micro-scale ferromagnetic beads (averaged diameter  $4.7\mu\text{m}$ ) are used as probes to locally deform the attached collagen fibrils. The diameter of the beads is comparable to the averaged mesh size of the collagen matrix, which was reported to range from  $2.3\text{--}3.2\ \mu\text{m}$  for the collagen concentration used in our study (Yang, et al., 2009). Since the averaged mesh size characterizes the averaged distance between the neighboring collagen fibrils, the number of collagen fibrils attached by single bead is nearly the same among the three collagen concentrations at microscale. Thus the dependency on collagen concentration is reduced when decreasing the measurement scales from macro to microscale.

The observation that local properties do not always match global properties has been shown numerically using discrete network models (Chandran & Barocas, 2005) (D'Amore, et al., 2014) (Huisman, et al., 2007) (Stein, et al., 2010). These studies found the deformation of the interconnected fibrils in a fibrous network are dominated by nonaffine deformation and the fibrils always reorient to the loading direction gradually. Chandran (Chandran & Barocas, 2005) and D'Amore (D'Amore, et al., 2014) also showed that fibril strains are contained by extensive reorientation and a large portion of fibrils have nearly zero fibril strains since they are reoriented without stretching during deformation. Thus, only a small fraction of fibrils contributes to the mechanics of a fibrous network. In studies on the remodeling of fibrous ECM by contractile cell forces, fiber alignment and long force transmission was observed (Rowe, et al., 2015) (Baker, et al., 2015) (Babaei, et al., 2016) (Abhilash, et al., 2014). The aggregated thick bundles of

aligned fibers reach out across very long distances to enhance the ECM networks and affect the viscoelasticity of the matrices (Marquez, et al., 2006) (Wang, et al., 2014) (Aghvami, et al., 2013). Our study suggests that the scales of measurements are important when studying the ECM properties, however the relevance of the scales to cellular behavior remain to be understood.

The non-dimensional quantity phase angle provides a more direct comparison between the measurements at macro and microscopic scales (Figure 5.4). The phase angle provides a measure of the dissipated energy relative to the stored energy. A change of phase angle in the frequency domain usually accompanies with the changes of elastic and viscous contributions as frequency varies. Within the testing frequency range, the phase angle from the macroscopic rheometer measurements shows a decreasing trend as the concentration increases. Using confocal reflectance method, it has been shown that the fibril density increases with collagen concentration (Yang & Kaufman, 2009) (Jordan, et al., 2010) (Arevalo, et al., 2010) (Motte & Kaufman, 2012). A decrease in phase angle with increasing collagen concentration from the rheometer measurements (Figure 5.4a) implies that there is more energy stored relative to that dissipated, resulting from an increase of the fibril density. However, the phase angle from OMTC measurements shows independency on collagen concentration (Figure 5.4b). This further proves that the dependency on collagen concentration is reduced in the microscopic mechanical property measurements. Interestingly, when the twisting frequency increases to above 10Hz, the viscous contribution becomes more significant, resulting in a rapid increase in the phase angle from the OMTC measurements. This suggests that the contribution of the viscous

effect is more significant in the OMTC measurements since the beads bound to collagen fibrils are surrounded by matrix interstitial fluid and are more exposed/sensitive to the high frequency dependency of the microscopic local fluid environment.

The local measurements tend to have a smaller phase angle compared to that at macro scales at low frequencies, especially for the 2.0mg/ml and 3.0mg/ml collagen matrix (Figures 5.4c, 5.4d). This is likely due to the more immediate/direct deformation of collagen fibrils in OMTC measurements through forces exerted by locally attached ferromagnetic beads, as opposed to the nonaffine fiber network deformation in macroscopic measurements that typically involves fiber reorientation, which precludes the development of fibril strain (Chandran & Barocas, 2005) (D'Amore, et al., 2014) (Huisman, et al., 2007). The discrepancy in phase angle between macro and microscopic measurements at low frequencies diminishes as the collagen concentration increases to 4.8mg/ml, as the nonaffinity decreases with higher collagen concentration (Onck, et al., 2005) due to the formation of a denser network that limits the room available for reorientation.

Geometric factor in Equation 5.1 plays an important role in translating the apparent modulus (Figure 5.3) to shear modulus in OMTC measurement. The geometric factor has been shown to be affected by beads embedding degree, thickness of the matrix (Mijailovich, et al., 2002), and beads radius (Ohayon & Tracqui, 2005). Measurement of bead embedding degree is usually a very challenging task. Previous studies quantified bead embedding degree experimentally via spatial reconstruction of the matrix issued from confocal microscopy (Laurent, et al., 2002). Ohayon suggested estimating the bead

embedding degree from self-built FEM model if both the bead rotation and bead lateral displacement were known (Ohayon & Tracqui, 2005). In previous finite element modeling, linear elastic material properties were used (Mijailovich, et al., 2002). In this study, the collagen matrix was modeled as a nonlinear hyperelastic material. As a comparison, the geometric factor curves deviate from Mijailovich's results (Mijailovich, et al., 2002) (Figure 5.8), especially at smaller beads embedding degrees. As we know that for the same magnetic torque, the strain in the matrix associated with beads twisting is higher with smaller beads embedding degree. Thus, the effect of the nonlinear hyperelastic material consideration becomes more significant, as the discrepancies between a hyperelastic and linear elastic model become more significant at larger strains. As shown in Figure 5.7, the effective strain is about 10% for 20% beads embedding degree. This strain is large enough that the nonlinear stress-strain behavior will deviate significantly from the linear regime (See Figure 5.5, for example). At higher beads embedding degree, or much smaller strain, the discrepancy between the results using linear and nonlinear material properties becomes smaller (Figure 5.8). Our study also shows that the geometric factors are dependent on collagen concentration, or the stiffness of the matrix, if nonlinear hyperelasticity is considered (Figure 5.8). Such dependency on material property is absent when the matrix is modeled as a linear elastic material (Mijailovich, et al., 2002). These results show that the nonlinear material properties of the matrix have an effect on determining the geometric factor, thus interpretation of the apparent modulus from OMTC measurements should be conducted carefully.

We would like to point out several limitations of the current study. The collagen

matrix in the FEM model in this model was assumed to be elastic. However, it is worth mentioning that our results may be extended to viscoelastic collagen matrix, as supported by (Ohayon & Tracqui, 2005) (Kamgoue, et al., 2007), under the assumption that the viscoelasticity of the collagen matrix is strain independent. The FEM model allows an estimation of the geometric factors at different bead embedding degrees. With the geometric factor, the shear modulus can then be obtained based on the apparent modulus measurements from OMTC using Equation 5.1. Given the fact that the bead embedding degree is unknown in the current study, we can't make quantitative comparisons between rheological and OMTC measurements. In addition, collagen matrix was assumed to be a homogeneous continuum in the FEM model, thus the local and global mechanical properties are the same (Mijailovich, et al., 2002) (Ohayon & Tracqui, 2005). Discrete network models have been developed to study the mechanical and structural behaviors of the fibrous network (Stein, et al., 2010) (Onck, et al., 2005) (Chandran & Barocas, 2005) (D'Amore, et al., 2014) (Huisman, et al., 2007) (Aghvami, et al., 2013) (Abhilash, et al., 2014) (Hatami-Marbini, et al., 2013). To better understand the nonaffine matrix reorganization and fiber alignment due to a local mechanical excitation, a discrete network model is required. These limitations remain to be addressed before we have a better understanding on the link between local and global ECM properties.

## **5.6 Summary**

Our study on the multiscale mechanics of collage matrix suggested several interesting differences between the macro and microscopic mechanical properties

originated from the scales of measurements. In the macroscale rheometer measurements, the storage and loss moduli increase with collagen concentration. The nonaffine deformation of the fibril structural network plays an important role. At the microscopic scale, the apparent storage and loss modulus are less sensitive to changes in collagen concentration. However, the apparent loss modulus is more affected by the local interstitial fluid environment, leading to an increase in viscosity at high frequencies. Nonlinear hyperelastic material properties should be considered when transforming the apparent modulus, measured from OMTC, to shear modulus. The present study sheds light on understanding the multi-scale mechanics of ECM, which is important when studying the force translation from tissue to cellular level.

## **CHAPTER 6: INTEGRATING STRUCTURAL HETEROGENEITY FIBER ORIENTATION AND RECRUITMENT IN MULTI-SCALE ECM MECHANICS**

### **6.1 Overview**

The extracellular matrix (ECM) provides the principal avenue for mechanochemical communication between tissue and cells, which plays critical roles in establishing tissue structure-function relationships and controlling cell fate. However, the mechanisms by which ECM mechanics influence cell and tissue behavior remain to be elucidated since the events associated with this process span length scales from tissue to molecular level. Entirely new methods are needed in order to better understand the multi-scale mechanics of ECM. In this study, a multiscale experimental approach was established by integrating Optical Magnetic Twisting Cytometry (OMTC) with a biaxial tensile tester to study the microscopic (local) ECM mechanical properties under controlled tissue-level (global) loading. Porcine adventitial layer was used as a collagen-based ECM. Multiphoton microscopy imaging was performed to capture the changes in ECM fiber structure during biaxial deformation. As visualized from multiphoton microscopy images, biaxial stretch involves gradual fiber straightening and the fiber families become evident at higher mechanical loading. The OMTC measurements show that the median of the local apparent storage and loss modulus increases with the global biaxial stretch, however there exist a complex interplay among local ECM mechanical properties, ECM structural heterogeneity, and fiber distribution and engagement. Dimensionless quantity phase lag does not change significantly with global biaxial

stretch. Our results also show a much faster increase in global tissue tangent modulus compared to the local apparent complex modulus with biaxial stretch, indicating the scale dependency of ECM mechanics.

## **6.2 Introduction**

The extracellular matrix (ECM) provides the principal avenue for mechanical and biochemical communications between tissue and cells. Cells actively sense the external mechanical forces applied through the ECM and also their surrounding local stiffness (Throm Quinlan, et al., 2011). External mechanical forces and ECM stiffness have been shown to play important roles in regulating fundamental cellular morphology (Wells, 2008) and functions, such as proliferation (Wells, 2008) (Schrader, et al., 2011), differentiation (Engler, et al., 2006) (Even-Ram, et al., 2006) and mobility (Pelham & Wang, 1997) (Zaman, et al., 2006). Many pathological conditions involve significant alternations of ECM mechanical properties (Baker, et al., 2009) (Janmey & Miller, 2011) (Lu, et al., 2012) (Engler, et al., 2008) (Chaturvedi, et al., 2010) (Georges, et al., 2007) (Wells, 2008), (Shkumatov, et al., 2015) (White, 2015). Understanding the translation of mechanical forces from tissue to cellular level is crucial and a requisite bridge between research in the fields of cell and tissue mechanics. However, the force translation in ECM is inherently a multiscale process ranging from the macroscopic to microscopic level. The mechanical properties of ECM, known to have a 3D hierarchical structure, have been shown to be highly dependent on the scale of measurement (Aifantis, et al., 2011) (Li, et al., 2017). As a result, the distribution of mechanical force in the ECM is highly

dependent on the hierarchical structure and the multiscale mechanical properties (Pizzo, et al., 2005) (Mow, et al., 1994).

The mechanical properties of ECM have been broadly studied. Various experimental methods, such as uniaxial tension (Roeder, et al., 2002) (Feng, et al., 2003) (Duan & Sheardown, 2006) (Van Oosten, et al., 2016), biaxial tension (Jhun, et al., 2009) (Sander, et al., 2009) (Xu, et al., 2011), and rheological tests (Vader, et al., 2009) (Xu, et al., 2011) (Kurniawan, et al., 2012) (Li & Zhang, 2014) (Motte & Kaufman, 2012) have been performed to investigate the macroscopic mechanical properties of collagen matrix. In microscopic mechanical measurement, controlled mechanical forces were applied using a variety of techniques including indentation (Wenger, et al., 2007) (Aifantis, et al., 2011) (Mckee, et al., 2011), laser tracking microrheology (Velegol & Lanni, 2001) (Parekh & Velegol, 2007) (Sun, et al., 2004) (Shayegan & Forde, 2013), magnetic twisting cytometry (Leung, et al., 2007), and optical magnetic twisting cytometry (OMTC) (Li, et al., 2017).

Previous studies have focused on ECM local strain measurements. In traction force microscopy, the macro-scale mechanical properties of substrate are usually used in calculation of local traction forces (Franck, et al., 2011) (Toyjanova.J, et al., 2014). To date, there has been limited understanding on the multi-scale ECM mechanical properties. Several previous studies have attempted to measure the local mechanical properties of ECM and showed that the local mechanical properties of an interconnected network do not always match its global properties. Microscopic mechanical properties of ECM measured by laser trap microscopy (Velegol & Lanni, 2001) and AFM (Gautreau, et al.,

2006) (Throm Quinlan & Billar, 2012) yield consistently greater stiffness measurements than those obtained from macroscopic rheometry and uniaxial tensile test. Significant difference in the mechanical properties of ECM were shown ranging from macro to nano scales as  $E_{\text{tendon}} < E_{\text{fiber}} < E_{\text{fibril}}$  (Aifantis, et al., 2011). The microscopic mechanical properties were found to be less sensitive to changes in collagen concentration, as compared to the macroscopic mechanical properties (Li, et al., 2017) (Baniasadi & Minary-Jolandan, 2015). The scale of measurements was found to play an important role in multiscale ECM mechanical properties. The differences in multiple ECM mechanical properties emerge when the probe size is comparable to or smaller than the average pore size of the sample (Costa, et al., 2003).

In the present study, we created a multi-scale experimental approach that combines optical magnetic twisting cytometry and biaxial tensile testing techniques to study the changes in local ECM mechanical properties with controlled global biaxial mechanical loading. The biaxial tensile test considers the multi-axial loading state under physiological conditions and has shown promises in fully characterizing the anisotropic nature of soft biological tissues (Sacks & Sun, 2003) (Nerurkar, et al., 2010) (Bell, et al., 2012). By oscillating microscale ferromagnetic beads bound to collagen fibers, OMTC was used to measure the local stiffness of collagen matrix. It allows the measurements of a population of beads and can effectively eliminate the unbound or loosely bound bead (Fabry, et al., 2001). Both macro and microscopic mechanical properties were measured using this multi-scale system. Porcine adventitia layer was used as an ECM equivalent due to several reasons: 1) Porcine adventitia is the outmost layer of the artery and

consists primarily of type I collagen fibers organized into thick collagen bundles. 2) It is semi-transparent so it is possible to make optical measurements using OMTC. 3) Compared to collagen gel, it is not fragile and easier to work with when biaxial loading is applied. Multiphoton microscopy was also used to visualize the structural changes of adventitia under external biaxial loading.

## **6.3 Materials and methods**

### *6.3.1 Sample preparation*

Porcine thoracic aortas were harvested at a local abattoir and transported to the laboratory on ice. Before experiments, the aortas were cleaned of adherent tissues and fat and rinsed in deionized water. All samples were taken from the same longitudinal region of the aorta to avoid changes in mechanical properties along the longitudinal anatomic position. The adventitial layer was carefully peeled from the porcine artery and cut into squares of about  $1\text{ cm} \times 1\text{ cm} \times 0.3\text{ mm}$  ( $n = 5$ ).

The primary constituents of adventitia layer are thick bundles of type I collagen fibers (Chow, et al., 2014). Streptavidin coated ferromagnetic beads (Spherotech Co.) with an average diameter of  $4.7\text{ }\mu\text{m}$  were used. Tight binding between streptavidin and collagen is formed via bio-conjugation (Chen, et al., 2012) (Guo & Kaufman, 2007). A bead solution of  $0.4\text{ mg/ml}$  was poured onto the adventitia surface and then the sample was incubated at  $37\text{ }^{\circ}\text{C}$  for  $\sim 40\text{ min}$  to allow beads to bind to collagen. The sample was then washed twice with deionized water to remove unbound beads.

### 6.3.2 *Integrated multi-scale OMTC – biaxial tensile testing system*

A multi-scale experimental methodology was developed by integrating a one-dimensional OMTC (EOL Eberhard, Switzerland) with a biaxial tensile tester, as described in Chapter 2.5. To apply biaxial loading, sandpaper tabs were glued to the sides of the adventitia sample. Sutures were looped through the sandpaper and connected to the linear positioners of the biaxial tensile tester. The local mechanical properties were then measured using OMTC and the global mechanical properties were measured using the biaxial tensile tester.

### 6.3.3 *Tissue-level mechanical property measurements*

The mechanical properties of adventitia were studied using the biaxial tensile tester, refer to Chapter 2.4 for details. Particular experimental settings for this study include 8-cycles equal biaxial loadings of 60g during preconditioning. After preconditioning, 8 cycles of equal biaxial tension with a load of 100g was applied to the sample. A synchronized biaxial response from the last cycle was used for further data analysis. The Cauchy stress in the direction  $x_1$  and  $x_2$  are calculated by equation 2.7.

### 6.3.4 *Local mechanical property measurements*

Equi-biaxial loading of 5, 10, 20, 30g, 40, 60 and 80g were applied to the tissue sample. The local mechanical properties of adventitia were measured using the OMTC, refer to Chapter 2.5 for details. In present study, the circumferential direction of adventitia was aligned with the direction of the magnetizing field. The bead constant  $C_{bead}$  (Pa/G) is 1.14Pa/G (Spherotech Co) and the magnetic twisting coil constant  $C_{coil}$  is

35.3G/A. The ferromagnetic beads were remagnetized after each increase of tissue-level mechanical loading to ensure beads magnetization was kept aligned throughout the experiment. At each loading level, local mechanical properties were measured at three or four different locations, and the average value of the locations was used to represent the local mechanical properties.

### 6.3.5 *Multiphoton Imaging*

Multiphoton imaging was performed to assess the collagen fiber network structure in the adventitia during mechanical loading. A multiphoton microscope (Carl Zeiss LSM 710 NLO microscope with Coherent Chameleon Vision-S laser set to 800 nm) illuminates the collagen via second harmonic generation passed through an emission filter at 417 nm, 80 nm width. For each sample, images of  $425 \times 425 \mu\text{m}^2$  at five locations were recorded and for each location, z-stacks images in 2  $\mu\text{m}$  increments allowed for maximum intensity projections to be used for analysis. All samples were aligned so that  $0^\circ$  and  $\pm 90^\circ$  represent the aorta's circumferential (C) and longitudinal (L) directions, respectively. Samples were imaged at 1, 1.05, 1.1, 1.15, and 1.2 equi-biaxial grip-to-grip stretches using a custom-made biaxial loading device (Chow, et al., 2014).

Adventitial collagen fiber waviness was defined by a straightness parameter,  $P_s = L_o/L_f$ , where end-to-end distance ( $L_o$ ) and total fiber length ( $L_f$ ) were traced with NeuronJ ([imagescience.org/meijering/software/neuronj](http://imagescience.org/meijering/software/neuronj)). As collagen fibers become less wavy,  $P_s$  increases until being equal to 1 for a straight line. In addition to  $P_s$ , fiber orientation was quantified with the directionality plug-in in FIJI ([fiji.sc/Fiji](http://fiji.sc/Fiji), Ashburn, VA) using two-dimensional fast Fourier transform analysis (FFT).

## 6.4 Results

Figure 6.1a shows the average Cauchy stress vs. stretch curves from biaxial tensile testing of the tissue sample, which is highly nonlinear with the longitudinal direction stiffens slightly earlier than the circumferential direction. To better compare the mechanical properties in the longitudinal and circumferential directions, tangent modulus was obtained by differentiating the Cauchy stress-stretch curves in Figure 6.1a. As shown in Figure 6.1b, a dramatic increase in tangent modulus was observed when the stretch is beyond 1.1. The large error bar at higher stretches is due to the variations in tissue stiffening among tissue samples.

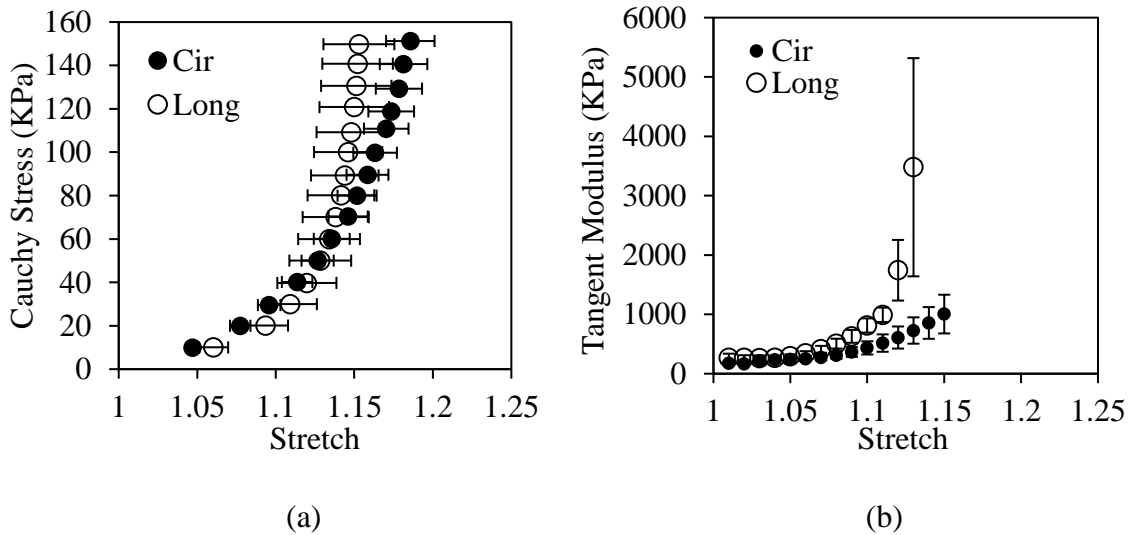


**Figure 6.1:** (a) Average Cauchy stress vs. stretch curves of adventitial tissue samples from biaxial tensile testing (n=5). (b) Average tangent modulus in both the circumferential and longitudinal directions (n=5). Data is presented as average  $\pm$  standard error of the mean.

Representative Multiphoton images under equi-biaxial stretches are presented in Figure 6.2a–e. The collagen fibers have a wavy configuration at the undeformed state. As the equi-biaxial stretch increases, the collagen fibers are gradually straightened, resulting

in an increase of the straightness parameter of the collagen fibers, as shown in Figure 6.2f. When the stretch increases to 1.2, the fibers are approximately straightened.

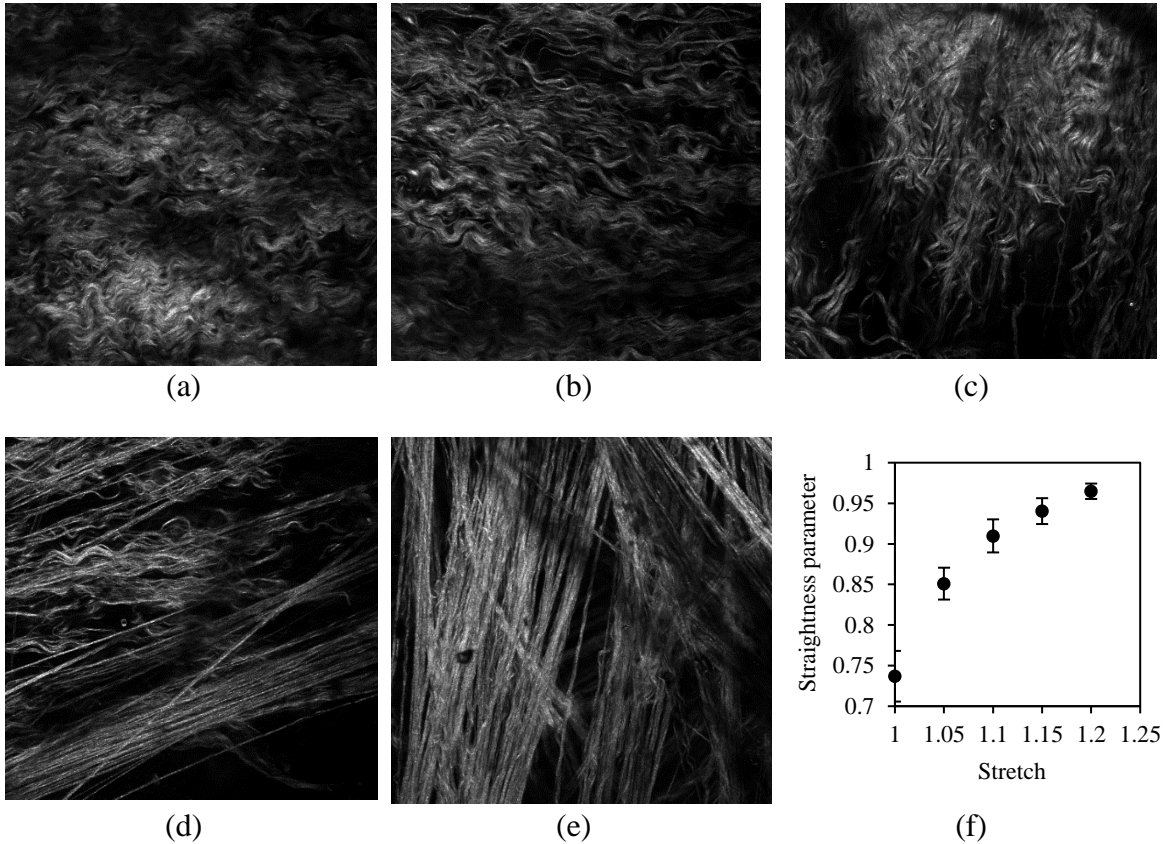


**Figure 6.2: (a–e) Representative multiphoton images at equi-biaxial stretch levels of 1, 1.05, 1.1, 1.15, and 1.2, and (f) changes in fiber straightness parameter with equi-biaxial stretch. Data in (f) is presented as average  $\pm$  standard error of the mean.**

Figure 6.3 shows collagen fiber distribution at different biaxial stretches. The x-axis represents the fiber angle ( $0^\circ$  is circumferential and  $\pm 90^\circ$  is longitudinal direction) and the corresponding frequency of fiber count is shown on the y-axis. At low equi-biaxial stretch levels (1 and 1.05), a single peak centers at the circumferential direction indicating a preferred circumferential distribution of the fibers. As the biaxial stretch increases, there is a decrease in circumferentially oriented fibers and multiple peaks

appear. The fiber orientations at 1.15–1.2 equi-biaxial stretches consist of multiple peaks revealing the existence of multiple collagen families.

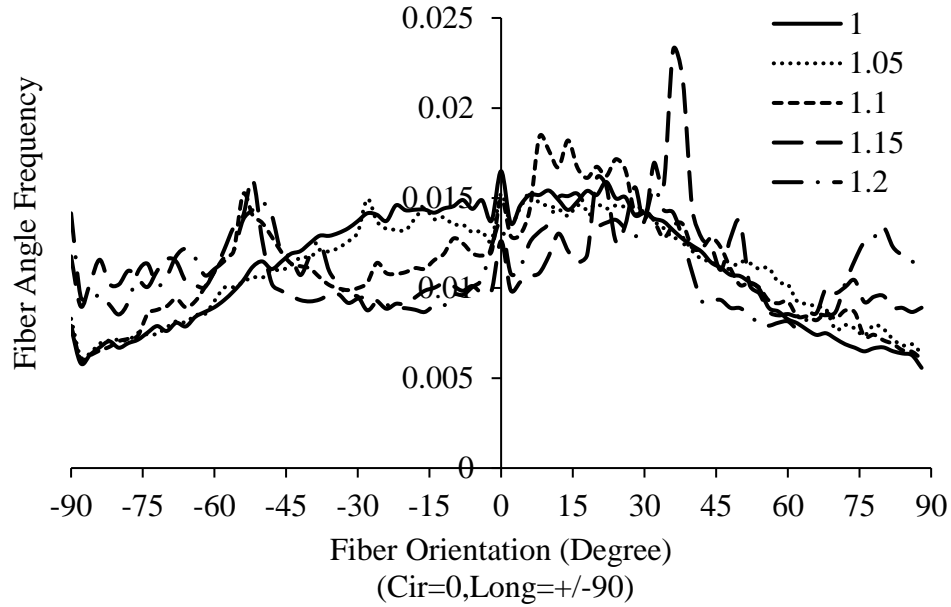
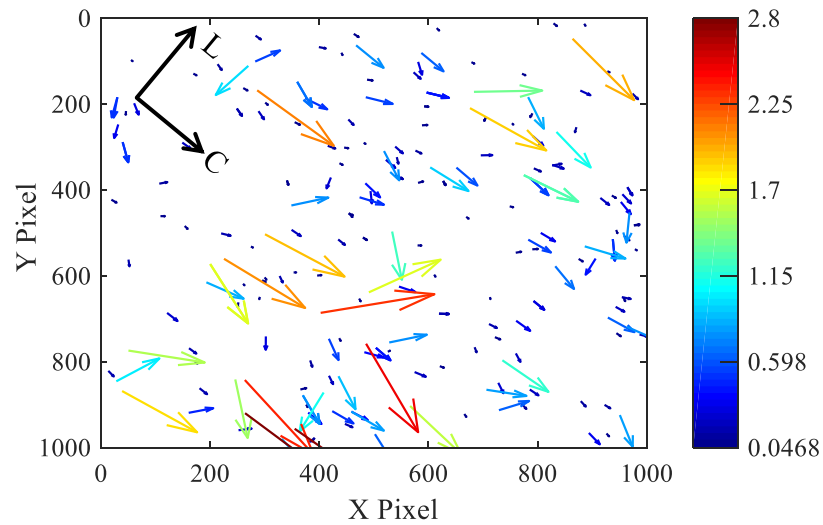


**Figure 6.3: Average normalized fiber orientation distributions with equal biaxial stretches of 1, 1.05, 1.1, 1.15 and 1.2. Fibers oriented at 0° and +/- 90° are in the circumferential and longitudinal directions of the adventitia, respectively.**

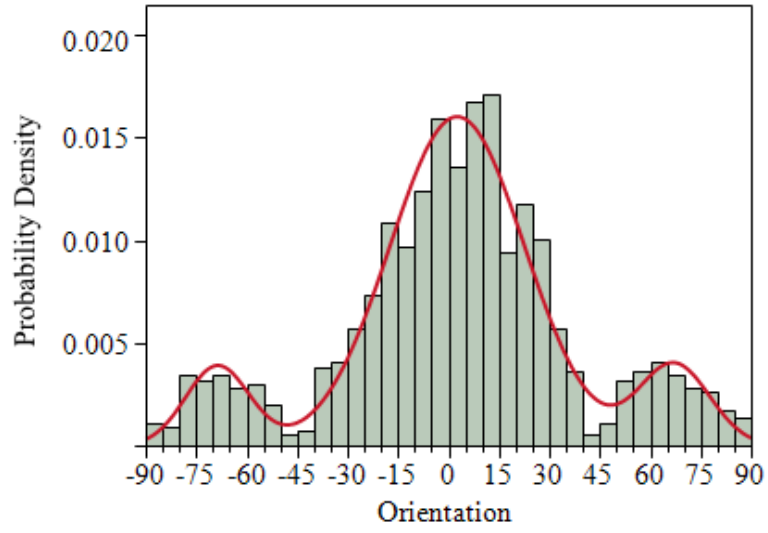
Figure 6.4a shows the beads lateral displacement from the OMTC measurement with the direction and magnitude ( $\times 100$ ) of the arrows. Majority of the beads lateral displacement distributed between  $-40^\circ$  to  $40^\circ$  from the circumferential direction since the magnetizing direction was always kept consistent with the circumferential direction of adventitia. A probability density function of tri-modal distribution was then fit to the orientation distribution of bead displacement in Figure 6.4b, and the function is defined as:

$$\text{Probability Density Function (PDF): } \sum_{i=1}^3 \frac{\pi_i}{\sigma_i} \Phi\left(\frac{x-\mu_i}{\sigma_i}\right) \quad (6.1)$$

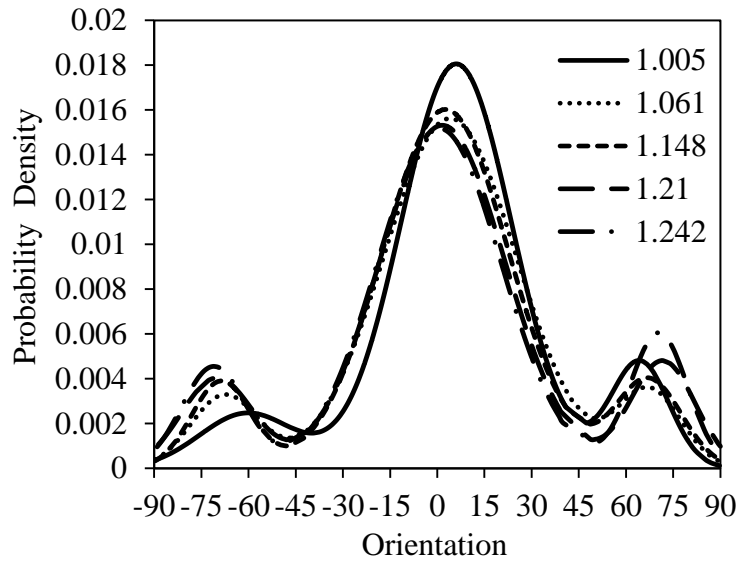
where  $\mu_i$ ,  $\sigma_i$  and  $\pi_i$  are the respective mean, standard deviation and proportion for the  $i^{\text{th}}$  modal; and  $\pi_1 + \pi_2 + \pi_3 = 1$ .  $\Phi(\cdot)$  is the standard normal PDF, and is defined as  $\Phi(x) = \frac{1}{\sqrt{2\pi}} e^{-\frac{x^2}{2}}$ . Figure 6.4c shows the distribution of bead displacement orientation with increasing equi-biaxial stretch. The portion of beads moving along the circumferential direction (twisting direction) is decreasing, while there is an increasing trend of beads moving with +70 or -70 degree deviation from the circumferential direction. This can be further verified by a decrease in the fitting parameter  $\pi_2$  since  $\pi_2$  represents the proportion of beads moving along the circumferential direction (Fig 6.4d).



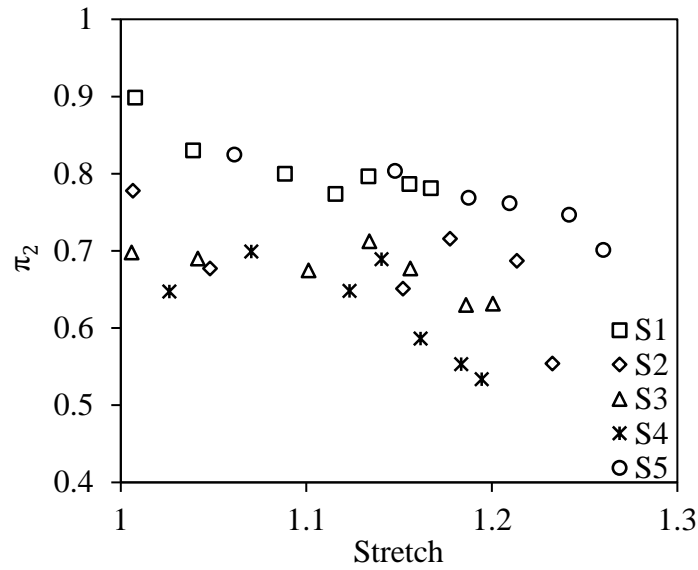
(a)



(b)



(c)



(d)

**Figure 6.4:** (a) Representative beads lateral displacement when the biaxial stretch is 1.15. The beads lateral displacement is oriented with the direction aligned with the arrow and the magnitude is represented by the length of the arrow ( $\times 100$ ). C and L represents the circumferential and longitudinal direction of the sample. Note that the beads are magnetized along the circumferential direction. (b) Displacement orientation distribution of beads in (a) with multi-modal fitting. (c) Representative multi-modal fitting of beads displacement orientation distribution at different stretch levels. (d) Parameter  $\pi_2$  versus stretch levels.

The complex apparent modulus from OMTC measurements located within the major and minor peaks of the beads displacement orientation distribution were plotted separately in Figure 6.5. We can see that the modulus measured within the major peak shows a stronger dependency on stretch. Interestingly, the discrepancy between the results from major and minor peaks increases at higher stretch levels.

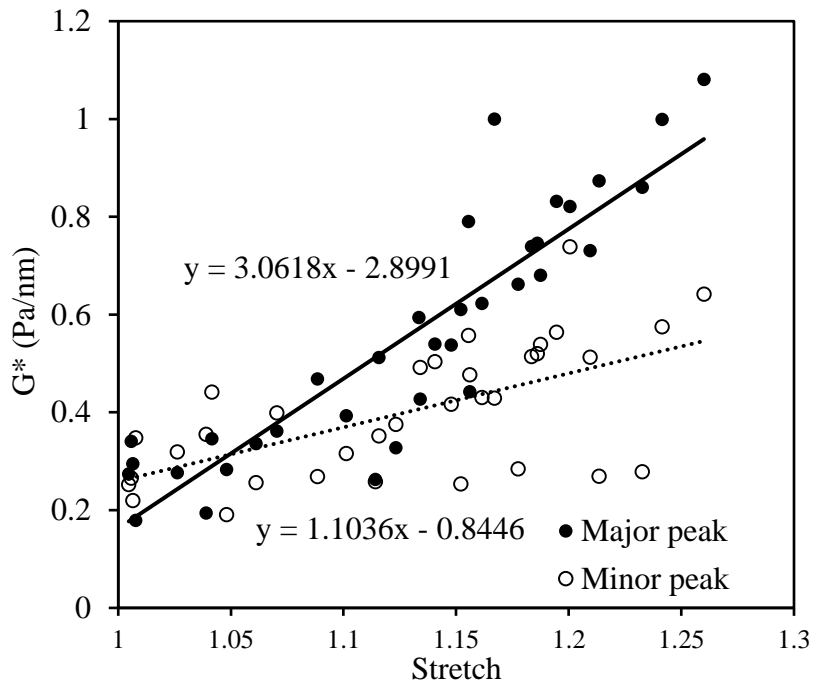
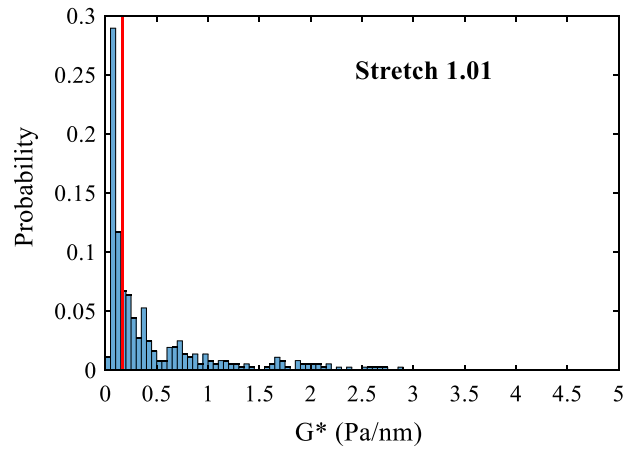


**Figure 6.5: Complex apparent modulus from OMTC measurements located within the major and minor peaks of the beads displacement orientation distribution.**

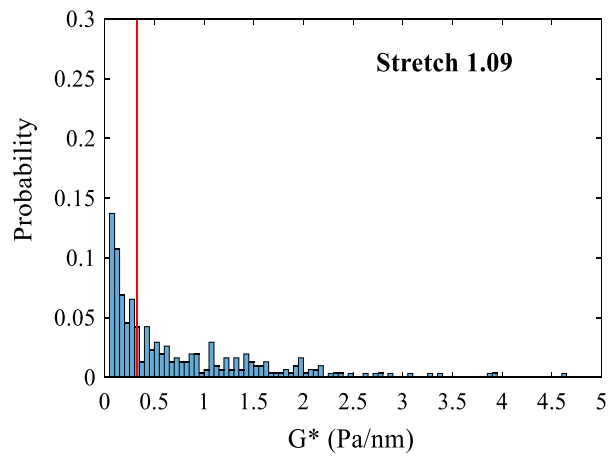
More than 100 beads are tracked during the OMTC measurement. To demonstrate the heterogeneity in local mechanical properties, representative distribution of complex apparent modulus at different loading levels are shown in Figure 6.6. The red dashed line indicates the position of the median, which is used as a measure of the local mechanical properties in the OMTC experiment. As we can see, the position of the median tends to move toward higher modulus as the tissue level stretch increases. The median absolute deviation (MAD), defined by Equation (6.2), is calculated at different stretch levels to characterize the variability of the dispersed data (Rousseeuw & Croux, 1993). Figure 6.7 shows that the MAD increases with the global equal stretch levels for all samples, suggesting increased heterogeneity in local mechanical properties with global loading.

$$\text{MAD} = \text{median} (|X_i - \text{median}(X)|)$$

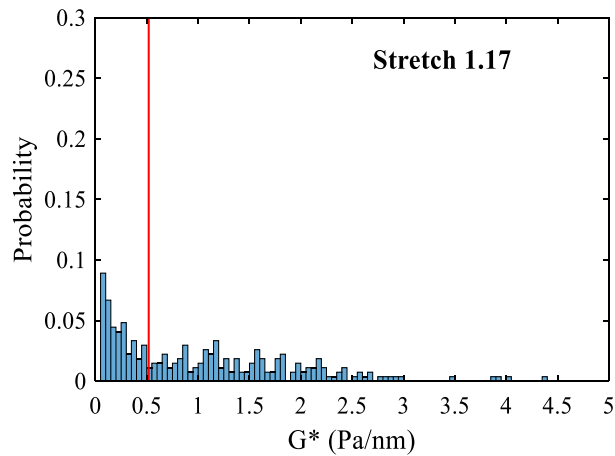
(6.2)



(a)



(b)



(c)

Figure 6.6: Representative distributions of complex apparent modulus of sample 1 at biaxial

stretch levels of (a) 1.01, (b) 1.09, and (c) 1.17. The position of median, used as a measure of the local mechanical properties in the OMTC experiment, is marked with a red line.

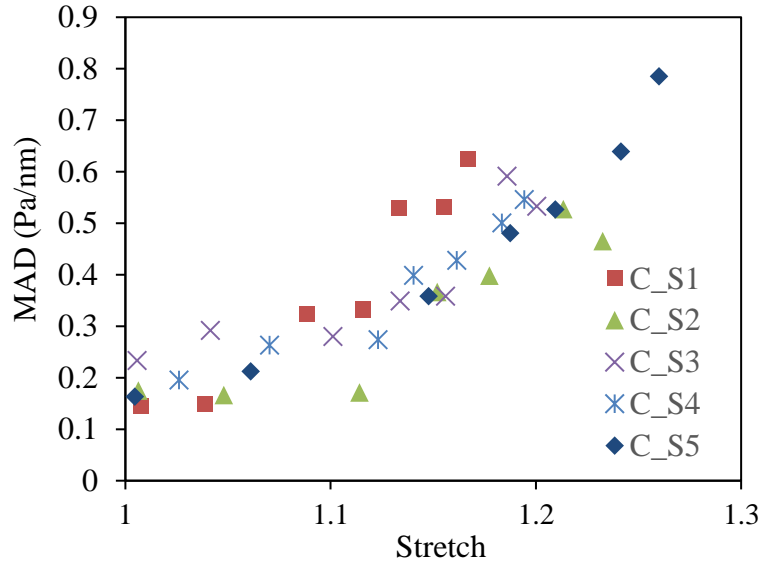


**Figure 6.7: The MAD of locally measured stiffness with increasing biaxial stretch for all adventitia samples.**

Figures 6.8 and 6.9 show the changes in local mechanical properties with macroscopic mechanical loading. The local apparent modulus consistently increases with tissue stretch up to about 1.2–1.3 (Figures 6.8a–c). Similar trend is observed in the local modulus vs. stress plots (Figures 6.9a–c). However this trend seems to plateau when stresses are higher than 100kPa. The phase angle does not change with global stretching or stress within the testing range (Figures 6.8d and 6.9d).

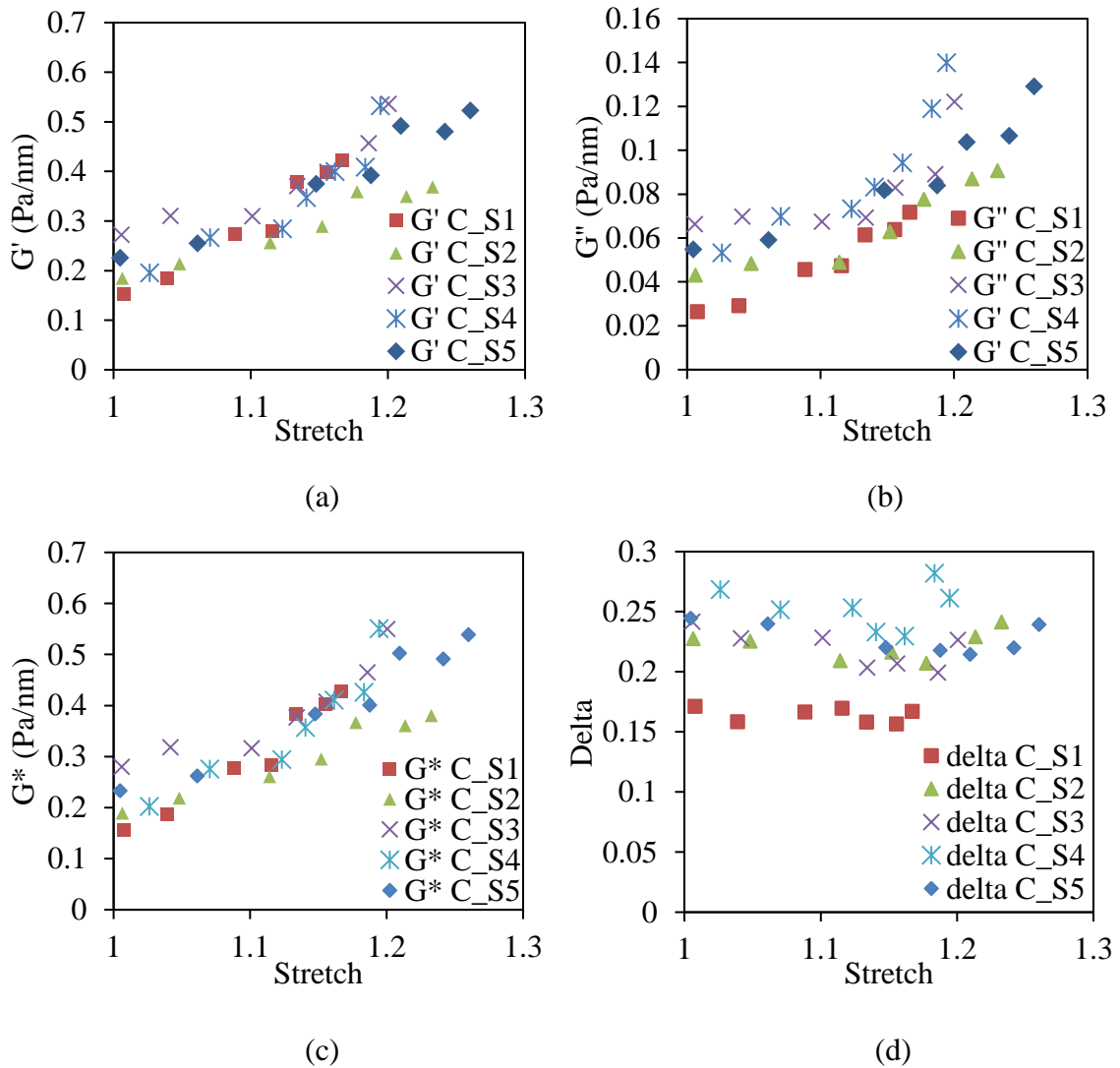
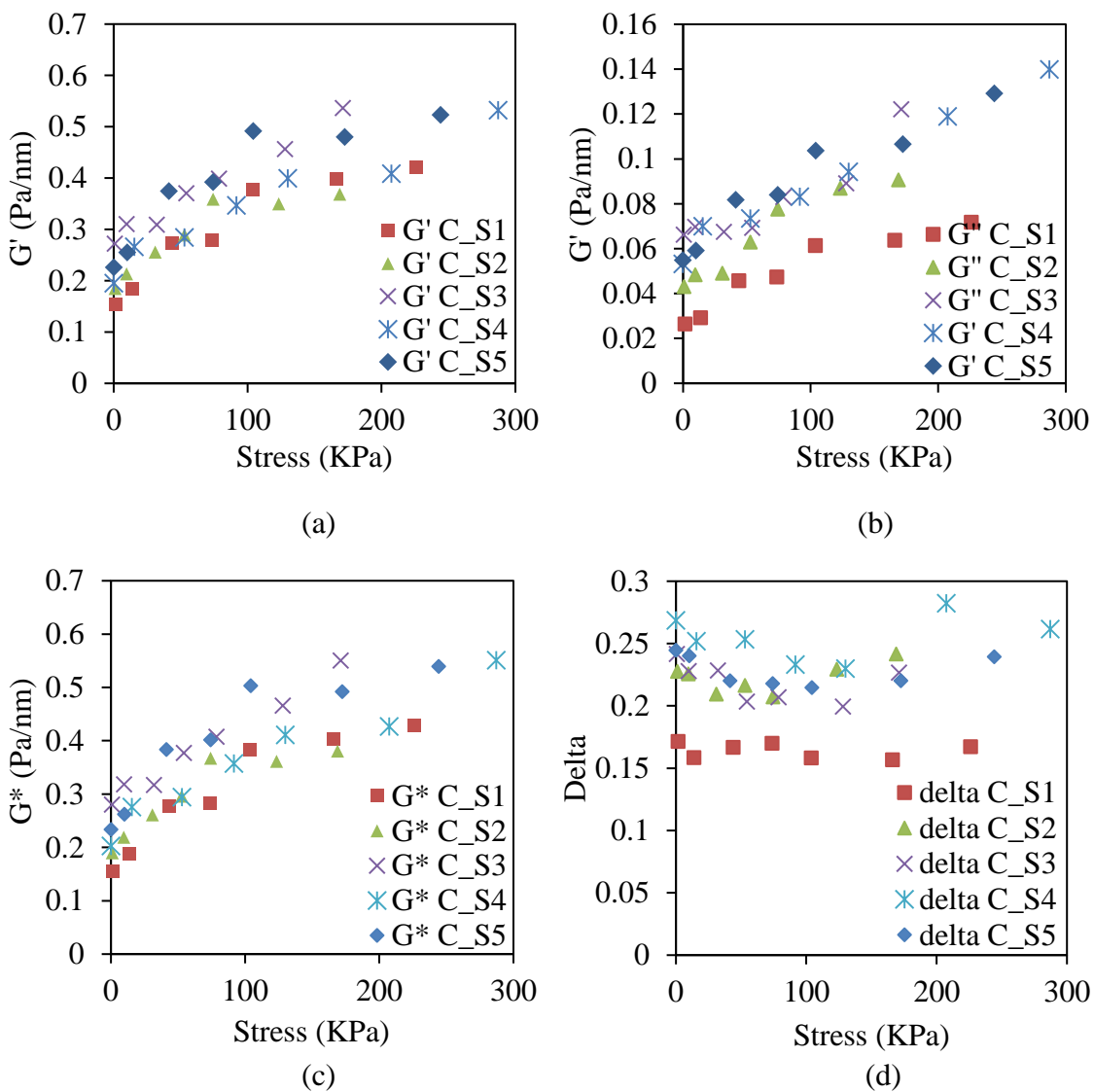


Figure 6.8: Apparent storage modulus (a), loss modulus (b), complex modulus (c), and phase angle (d) measured by OMTC vs. macroscopic biaxial stretch.



**Figure 6.9: Apparent storage modulus (a), loss modulus (b), complex modulus (c), and phase angle (d) measured by OMTC vs. macroscopic stress.**

## 6.5 Discussion

In this study, we established a novel multi-scale experimental approach that integrates OMTC and biaxial tensile testing experimental approaches to study the microscopic mechanical properties of collagen ECM when subjected to controlled global

biaxial mechanical loading. Multiphoton microscopy was used to visualize the structural changes of adventitial collagen during deformation. Our study shows structural heterogeneity, fiber orientation and recruitment play important roles in determining the multi-scale ECM mechanics.

The macroscopic properties of biological tissues are often related to its microscopic ECM structure (Tower, et al., 2002) (Voytik-Harbin, et al., 2003) (D'Amore, et al., 2014). As seen in many biological tissues, adventitia shows anisotropic and hyperelastic behavior (Figure 6.1a), which is associated with preferred fiber alignment and progressive recruitment of collagen fibers (Gasser, et al., 2006) (Tower, et al., 2002). The collagen fibers appear to be predominately circumferentially aligned in the unloaded state (Figures 6.2 and 6.3). It has been shown that fiber families could be obscured at low or no mechanical loading due to the large fiber waviness and become more evident when the fibers are straightened (Chow, et al., 2014). Similar results were shown from the multi-photon images of the separated adventitial layer (Figure 6.2). The appearance of multiple peaks from FFT analysis (Figure 6.3) is consistent with studies on either porcine (Chow, et al., 2014) (Mattson, et al., 2017) or human adventitia (Schriebl, et al., 2012). The preferred fiber distribution close to the longitudinal direction is correlated with the stiffer longitude than circumference beyond 1.1 stretch (Figure 6.1a).

The microscopic measurements from OMTC show a wide range distribution of stiffness (Figure 6.6). The collagen network contains regions of inhomogeneity arising from random interconnection of fibers into clusters. Structural heterogeneity in collagen network could be originated from a variation in fibril length, fibril diameter, and the pore

size between adjacent fibrils (Shayegan & Forde, 2013) (Yang & Kaufman, 2009) (Yang, et al., 2009). The structural heterogeneity was found to result in heterogeneity in microrheological characterization of collagen gels (Shayegan & Forde, 2013) (Latinovic, et al., 2010). The adventitia has an inhomogeneous hierarchical structure with thick and wavy collagen fibers (Chen, et al., 2011) (Chen, et al., 2016). The morphology of adventitia was found to be highly nonuniform from microCT studies (Walton, et al., 2015). It has been shown from atomic force measurements that the modulus of porcine adventitia has a distribution ranging four orders of magnitude due to its nature of structural heterogeneity (Grant & Twigg, 2013).

Collagen fiber orientation may play an important role in the way that the magnetic beads deform the collagen fibers during magnetic twisting. Before OMTC testing, ferromagnetic beads were remagnetized once the tissue sample was loaded, in order to keep the magnetizing direction of the beads remain circumferentially. When the fiber orientation coincides with the bead magnetizing direction, the fibers tend to be stretched and straightened during magnetic twisting. On the other hand, ferromagnetic beads tend to bend or twist the fibers when the magnetization direction is perpendicular to the fiber orientation. This case often results in a relatively large lateral bead displacement, which was interpreted as lower stiffness. However, in most cases, it is likely that both fiber straightening and bending play a role in the OMTC measurements, and thus contribute to the heterogeneity in local stiffness measurements (Figure 6.6).

Interestingly, the bead displacement orientation distribution in Figures. 6.4b and 6.4c mirrors the multiple fiber family distribution in adventitial collagen (Figures 6.2 and

6.3). A minor portion of ferromagnetic beads moves along  $\pm 70$  degrees, deviating from the circumferential magnetizing direction. This could be due to an interplay between the twisting of circumferentially magnetized ferromagnetic beads and the longitudinally preferred distributed collagen fibers under applied magnetic field. Measurements from beads move along the directions under the major peaks show a stronger dependency on global stretch (Figure 6.5). Such results further indicate that the complex interaction between ferromagnetic beads and collagen fiber orientation distribution plays an important role in determining the local ECM mechanical properties and in contributing to the heterogeneity in local ECM mechanical property measurements.

The gradual engagement of collagen fibers plays an important role in determining the local ECM stiffness as well. At low equal biaxial stretch levels (under 1.05), most collagen fibers are wavy and do not take much mechanical load (Figure 6.2). These wavy “floppy” fibers have little restriction to the movement of the magnetic beads. As seen in Figure 6.6a, the local stiffness is relatively small at no loading or low stretch levels (1.01), represented as a dominant peak distributed between 0.05 – 0.1 Pa/nm. Thus it is not a surprise that the portion of local measurements with smaller stiffness ( $< 0.2$  Pa/nm) dominates. As the global stretch increases, collagen fibers are gradually engaged to bear more mechanical loading. The gradual engagement can be seen obviously at 1.1 and 1.15 stretch levels from multiphoton images (Figure 6.2), which consists of a network of both stretched and wavy fibers. The ferromagnetic beads bound to straight fibers will be more difficult to rotate and resulted in a stiffer local mechanical property. The portion of measurement with low stiffness decreases significantly and the median moves toward the

stiffer region (Figures 6.6b and 6.6c).

Heterogeneity in local mechanical property measurements increases with global stretch, as reflected in the increasing MAD with global stretch (Figure 6.7). The engagement of collagen fibers results in gradual fiber straightening, which results in a redistribution of local stiffness. At higher stretch levels, the proportion of measurements with low stiffness gradually decreases, but still exists. Furthermore, the higher stiffness region starts to emerge (Figure 6.6), and result in a more spread distribution of the local modulus and increase of MAD (Figure 6.7).

Both global tangent modulus and local apparent complex modulus increase with applied biaxial stretch (Figures 6.1b and 6.8c). However, we find a much faster increase in global tangent modulus, which is possibly due to the lower strain experienced at the microscopic level. The global tangent modulus in the circumferential direction increases around 7 times at 1.15 global stretch (Figure 6.1a), whereas the local complex modulus increases only about 3 times (Figure 6.8c). Previous study has shown that the local strain is lower compared with the global applied strain, especially pronounced at applied strains above 0.1 (Roeder, et al., 2009). In their study, the local strain is measured on a scale, of approximately 10 – 20 $\mu\text{m}$ , which represent an average behavior of a group of collagen fibrils. It was also shown that the individual fibril strain is considerably lower when compared to overall tissue strain (Fratzl, et al., 1997) (Puxkandl, et al., 2002) (Screen, et al., 2004). Nonaffine fiber rearrangement has been shown to contribute to the lower fiber level strain from both experimental (Screen, et al., 2004) (Roeder, et al., 2009) and numerical approaches (Chandran & Barocas, 2005) (D'Amore, et al., 2014). Fibers

reorient to loading direction gradually, resulting in an increasing number of load bearing elements and a reduction of strain experienced by each fiber. Since equibiaxial tension was used in the present study, the effect of fiber realignment may play a role. Secondly, the lower strain at microscopic level could be due to the hierarchical structure of collagen fiber bundles. Deformation including intra- and inter-fibril sliding, and fiber-interstitial fluid interactions may occur simultaneously upon tissue level stretching (Fratzl, et al., 1997) (Puxkandl, et al., 2002) (Screen, et al., 2004). The deformation at these different sublevels regulates the multi-scale transfer of deformation from macro- to micro- scale. Dimensionless quantity phase angle provides a measure of the dissipated energy relative to the stored energy. Resulted from a proportional increase for both local storage and loss modulus, the phase angle measured from OMTC does not change significantly with global ECM loading (Figures 6.8d and 6.9d).

We would like to point out some limitations in our study. The unit of local stiffness is Pa/nm. External stretch may inevitably affect bead internalization, which may influence the local apparent modulus. A geometric factor is need to covert the apparent modulus from OMTC measurements to shear modulus (Fabry, et al., 2003) (Mijailovich, et al., 2002) (Ohayon & Tracqui, 2005). The geometric factor is usually obtained from computational modeling which assumes the bead is embedded in a homogeneous and continuous matrix (Mijailovich, et al., 2002) (Ohayon & Tracqui, 2005) (Li, et al., 2017). The geometric factor was not considered in the present study. Considering the discrete nature of collagen ECM, discrete network model is required to better understand the bead-matrix interaction considering nonaffine matrix reorganization under mechanical

loading. The bead-matrix binding was achieved by bio-conjugation between collagen and streptavidin in present study. Tight binding between collagen and other proteins including fibronectin and collagen specific targeted antibody could be used in future work to verify the dependency of measured local stiffness on the binding strength. Finally, viscoelastic deformation, such as creep, could occur during the local stiffness measurement, and its effect on the local mechanical property measurements is unknown.

## **6.6 Summary**

A novel experimental approach is established to study the multi-scale ECM mechanics that allows the measurements of local ECM mechanical properties with controlled tissue-level biaxial mechanical loading. Multiphoton imaging reveals interesting structural changes that involve gradual straightening and recruitment of collagen fibers with biaxial stretch. The heterogeneous local mechanical properties were attributed to the complex interplay among magnetic twisting, structural heterogeneity, and collagen fiber orientation and engagement. Both global tangent modulus and local apparent complex modulus increase with biaxial loading, however the local apparent complex modulus increase at a lower rate than the global tangent modulus, indicating the scale dependency of ECM mechanics.

## CHAPTER 7: CONCLUSIONS AND OUTLOOK

### 7.1 Conclusions

The ECM provides a principal avenue for mechanical communication between tissue and cells. This dissertation studies the multi-scale mechanics of ECM using both experimental and modeling approaches. The information gained in this study sheds light on understanding the multi-scale mechanics of ECM, which is important when studying the force translation from the tissue to cellular level.

Viscoelastic materials contain a continuous spectrum of relaxation time constants. Investigating the spectrum in terms of number of peaks, peak intensity and time constants sheds light on the main intrinsic properties of viscoelastic materials. In present study, a theoretical framework was developed to determine both discrete and continuous relaxation spectrum of viscoelastic soft biological material based on dynamic rheological measurements. Using collagen gel as an example, we have shown that the discrete spectrum, Prony Series, obtained by a nonlinear regression procedure, is not unique and highly dependent on the fitting criteria. The continuous relaxation spectrum, obtained through solving ill-posed inversion problem with Tikhonov regularization, however, is more reliable when studying the main properties (number of peaks, relaxation time constant and peak intensity) of a continuous spectrum, which is important when correlating with intrinsic structural properties and relaxation mechanisms of viscoelastic materials. The relaxation spectrum of collagen matrix obtained from our study consists for peaks, correlated with the relaxation mechanisms involving fluid flow, inter-fiber,

inter-fibril and intra-fibril sliding, respectively. Moreover, since finite element method is broadly used to solve problems that involve material and geometric nonlinearities as well as structural complexities, here we demonstrate that continuous relaxation spectrum can also be used in finite element modeling to characterize the behaviors of viscoelastic material.

Besides the macroscopic mechanics, the microscopic mechanical properties of collagen matrix were studied using OMTC. The mechanical properties of ECM, known to have a 3D hierarchical structure, have been shown to be highly dependent on the scale of measurement. However, to date, the understanding on the multi-scale ECM mechanical properties is still limited. Our study on the multiscale mechanics of collage matrix suggested several interesting differences between the macro and microscopic mechanical properties originated from the scales of measurements. In the macroscale rheometer measurements, the storage and loss modulus increases and the phase angle decreases as the collagen concentration increases. The nonaffine deformation of the fibril structural network plays an important role. At the microscopic scale, the apparent storage and loss modulus are less sensitive to changes in collagen concentration. However, the apparent loss modulus is more affected by the local interstitial fluid environment, leading to an increase in viscosity at high frequencies. Moreover, a 3-D finite element model was developed to study the geometric factors in the OMTC measurements when the collagen matrix was considered to be hyperelastic. Our results show that the geometric factors are dependent on collagen concentration, or the stiffness of matrix, when nonlinear material properties of the matrix are considered, thus interpretation of the apparent modulus from

OMTC measurements should be conducted carefully.

A novel experimental approach is established to study the multi-scale ECM mechanics that allows the measurements of local ECM mechanical properties with controlled tissue-level biaxial mechanical loading. Multiphoton imaging reveals interesting structural changes that involve gradual straightening and recruitment of collagen fibers with biaxial stretch. To our understanding, this is the first study that quantifies both structural and mechanical changes due to external stretch. The heterogeneous local mechanical properties were attributed to the complex interplay among magnetic twisting, structural heterogeneity, and collagen fiber orientation and engagement. Both global tangent modulus and local apparent complex modulus increase with biaxial loading, however the local apparent complex modulus increases at a lower rate than the global tangent modulus, indicating the scale dependency of ECM mechanics. Our study provides a novel experimental approach for studying the force translation from tissue to cellular level in the future.

## **7.2 Outlook**

The mechanical function of three-dimensional biological materials, such as the ECM network, is inherently multiscale, ranging from tissue to molecular level. Results from Chapter 5 suggested that it is necessary to consider the discrete fibrous network in order to understand the interesting differences between the macro- and micro-scopic mechanical properties of collage matrix. Discrete network models have been developed to model the tissue behavior considering its fibrous microstructure. (Heyden, 2000)

(Onck, et al., 2005) (Chandran & Barocas, 2005) (Chandran & Barocas, 2007) (Huisman, et al., 2007) (Stein, et al., 2011) (Nair, 2012) (D'Amore, et al., 2014). Discrete network model has the advantages of characterizing the topological properties of network, and allowing non-affine fiber network deformation. In order to gain a better understanding of multiscale ECM mechanics, discrete network modeling of a fibrous ECM network is necessary in future studies.

2D experiment was performed in measuring the microscopic mechanical properties of collagen matrix in the present study. However, cells are embedded in the ECM and senses the mechanical signals in a 3D configuration. Future studies on 3D measurements of the local mechanics of collagen matrix can be done by embedding ferromagnetic beads within the gel during polymerization.

Collagen is one of major ECM constituents, and other components exist in the ECM. Hyaluronic acid (HA) is a linear disaccharide glycosaminoglycan (GAG) found in various connective tissues. It has extraordinary water retaining capacity and plays an important role in determining the mechanical properties of tissues (Yang & Kaufman, 2009). Fabricating a co-gel system by combining HA and reconstituted Type-I collagen makes it possible for not only constructing biomaterials with particular structure and mechanical properties but also better reproducing the ECM environment than collagen itself alone. Future studies on the multiscale mechanical property measurements of HA-Collagen co-gel system would be interesting from the tissue engineering perspective. Moreover, recent studies suggested a pre-stressed model system that mimics the residue stress in biological tissue can be obtained when exposing HA-Collagen co-gel system to

hypotonic solution (Lai, et al., 2016). Co-gel swells as HA imbibes water, resulting in stretching the collagen network. This will allow studies on understanding the local mechanical properties of collagen matrix at different residue stress levels.

## BIBLIOGRAPHY

- Abhilash, A. et al., 2014. Remodeling of Fibrous Extracellular Matrices by Contractile Cells. *Biophysical Journal*, 107, 1829–1840.
- Aghvami, M., Barocas, V. & Sander, E., 2013. Multiscale Mechanical Simulations of Cell Compacted Collagen Gels. *Journal of Biomechanical Engineering*, 135(7), 071004-1-071004-8.
- Aifantis, K., Shrivastava, S. & Odegard, G., 2011. Transverse mechanical properties of collagen fibers from nanoindentation. *Journal of Materials Science. Materials in Medicine*, 22, 1375–1381.
- Alberts, B. et al., 2002. *Molecular Biology of the Cell*. 4th ed. New York: Garland Science.
- Arevalo, R., Urbach, J. & Blair, D., 2010. Size-dependent rheology of type-I collagen networks. *Biophysical Journal*, 99(8), L65–L67.
- Arevalo, R., Urbach, J. & Blair, D., 2011. Four-dimensional structural dynamics of sheared collagen networks. *Chaos*, 21(041102), 041102-1.
- Babaei, B. et al., 2016. Remodeling by fibroblasts alters the rate-dependent mechanical properties of collagen. *Acta Biomaterialia*, 37, 28–37.
- Bailey, A., 2001. Molecular mechanisms of aging in connective tissues. *Mechanisms of Ageing and Development*, 122(7), 735–755.
- Baker, B. et al., 2015. Cell-mediated fibre recruitment drives extracellular matrix mechanosensing in engineered fibrillar microenvironments. *Nature Materials*, 14, 1262–1268.
- Baker, E., Bonnecaze, R. & Zaman, M., 2009. Extracellular Matrix Stiffness and Architecture Govern Intracellular Rheology in Cancer. *Biophysical Journal*, 97, 1013–1021.
- Baniasadi, M. & Minary-Jolandan, M., 2015. Alginate-Collagen Fibril Composite Hydrogel. *Materials*, 8, 799–814.
- Bartenev, G., Shelkovichova, L. & Akopyan, L., 1973. Relaxation spectrum in polymer. *Polymer Mechanics*, 9(1), 133–136.
- Baumgaertel, M. & Winter, H., 1989. Determination of discrete relaxation and retardation time spectra from dynamic mechanical data. *Rheologica Acta*, 28, 511–519.

Bell, B., Nauman, E. & Voytik-Harbin, S., 2012. Multiscale Strain Analysis of Tissue Equivalents Using a Custom-Designed Biaxial Testing Device. *Biophysical Journal*, 102(6), pp. 1303–1312.

Bhattacharjee, S., Swamy, A. & Daniel, J., 2012. Continuous relaxation and retardation spectrum method for viscoelastic characterization of asphalt concrete. *Mechanics of Time-Dependent Materials*, 16(3), 287–305.

Bilston, L., Liu, Z. & Phan-Thien, N., 1997. Linear viscoelastic properties of bovine brain tissue in shear. *Biorheology*, 34(6), 377–385.

Bilston, L., Liu, Z. & Phan-Thien, N., 2001. Large strain behavior of brain tissue in shear: some experimental data and differential constitutive model. *Biorheology*, 38(4), 335–345.

Brands, D., Bovendeerd, P. & Peters, G., 2000. The Large Shear Strain Dynamics Behavior of In-Vitro Porcine Brain Tissue and the Silicone Gel Model Material. *Stapp Car Crash Journal*, 44, 249–260.

Brown, R., 1999. *Handbook of Polymer Testing*. New York: Marcel Dekker, Inc.

Brown, T., 2000. Techniques for mechanical stimulation of cells in vivo: A review. *Journal of Biomechanical Engineering*, 33, 3–14.

Chandran, P. & Barocas, V., 2005. Affine versus non-affine fibril kinematics in collagen networks: theoretical studies of network behavior. *Journal of Biomechanical Engineering*, 128(2), 259–270.

Chandran, P. & Barocas, V., 2007. Deterministic Material-Based Averaging Theory Model of Collagen Gel Micromechanics. *Journal of Biomechanical Engineering*, 129(2), 137–147.

Chaturvedi, R. et al., 2010. Passive stiffness of myocardium from congenital heart disease and implications for diastole. *Circulation*, 121, 979–988.

Chen, H., Guo, X., Luo, T. & Kassab, G., 2016. A validated 3D microstructural-based constitutive model of coronary artery adventitia. *Journal of Applied Physiology*, 121(1), 333–342.

Chen, H. et al., 2011. The Layered Structure of Coronary Adventitia under Mechanical Load. *Biophysical Journal*, 101, 2555–2562.

Chen, P., Herath, S., Wang, D. & Asada, H., 2012. *Active Manipulation of ECM Stiffness and Its Effect on Endothelial Cell Migration during Angiogenesis*. London, Proceedings of the World Congress on Engineering.

- Chow, M., Turcotte, R., Lin, C. & Zhang, Y., 2014. Arterial Extracellular Matrix: A Mechanobiological Study of the Contributions and Interactions of Elastin and Collagen. *Biophysical Journal*, 106, 2684–2692.
- Costa, K., Ho, M. & Hung, C., 2003. *Multi scale measurement of mechanical properties of soft samples with atomic force microscopy*. Florida, 2003 Summer Bioengineering Conference.
- D'Amore, A. et al., 2014. From single fiber to macro-level mechanics: A structural finite element model for elastomeric fibrous biomaterials. *Journal of the Mechanical Behavior of Biomedical Materials*, 39, 146–161.
- Darvish, K. & Crabdall, J., 2001. Nonlinear viscoelastic effects inn oscillatory shear deformation of brain tissue. *Medical Engineering and Physics*, 23(9), 633–645.
- Davies, A. & Anderssen, R., 1997. Sampling localization in determining the relaxation spectrum. *Journal of Non-Newtonian Fluid Mechanics*, 73(1–2), 163–179.
- Dealy, J. & Larson, R., 2006. *Structure and rheology of molten polymers*. Cincinnati, Ohio: Hanser Gardner Publications.
- Deng, L. et al., 2004. Localized mechanical stress induces time-dependent actin cytoskeletal remodeling and stiffening in cultured airway smooth muscle cells. *American Journal of Physiology. Cell Physiology*, 287(2), C440–C448.
- Duan, X. & Sheardown, H., 2006. Dendrimer crosslinked collagen as a corneal tissue engineering scaffold: Mechanical properties and corneal epithelial cell interactions. *Biomaterials*, 27, 4608–4617.
- Elster, C., Honerkamp, J. & Weese, J., 1991. Using regularization methods for the determination of relaxation and retardation spectra of polymeric liquids. *Rheologica Acta*, 31(2), 161–174.
- Engler, A. et al., 2008. Embryonic cardiomyocytes beat best on a matrix with heart-like elasticity: scar-like rigidity inhibits beating. *Journal of Cell Science*, 121, 3794–3802.
- Engler, A., Sen, S. & Sweeney, H., 2006. Matrix elasticity directs stem cell lineage specification. *Cell*, 126(4), 677–689.
- Even-Ram, S., Artym, V. & Yamada, K., 2006. Matrix control of stem cell fate. *Cell*, 126(4), 645–647.
- Fabry, B. et al., 2001. Scaling the Microrheology of Living cells. *Physical Review Letters*, 87(14), 148102.

- Fabry, B. et al., 2003. Time scale and other invariants of integrative mechanical behavior in living cells. *Physical Review. E*, 68, 041914-1-041914-18.
- Fabry, B. et al., 1999. Implications of heterogeneous bead behavior on cell mechanical properties measured with magnetic twisting cytometry. *Journal of Magnetism and Magnetic Materials*, 194, 120–125.
- Fabry, B. et al., 2001. Signal Transduction in Smooth Muscle Selected Contribution: Time course and heterogeneity of contractile responses in cultured human airway smooth muscle cells. *Journal of Applied Physiology*, 91, 986–994.
- Feng, Z. et al., 2003. Investigation on the mechanical properties of contracted collagen gels as a scaffold for tissue engineering. *Artificial Organs*, 27(1), 84–91.
- Ferry, J., 1980. *Viscoelastic properties of polymers*. 3rd ed. New York: John Wiley&Sons.
- Franck, C., Maskarinec, S., Tirrell, D. & Ravichandran, G., 2011. Three-Dimensional Traction Force Microscopy: A New Tool for Quantifying Cell-Matrix Interactions. *PLoS One*, 6(3), e17833.
- Fratzl, P., 2008. *Collagen: Structure and Mechanics*. New York: Springer.
- Fratzl, P., Misof, K. & Zizak, I., 1997. Fibrillar Structure and Mechanical Properties of Collagen. *Journal of Structural Biology*, 122, 119–122.
- Fredberg, J. & Fabry, B., 2006. The cytoskeleton as a soft glassy material. In: *Cytoskeleton Mechanics: Models and Measurements in Cell Mechanics*. Cambridge University Press.
- Gasser, T., Ogden, R. & Holzapfel, G., 2006. Hyperelastic modelling of arterial layers with distributed collagen fibre orientations. *Journal of the Royal Society, Interface*, 3(6), 15–35.
- Gautieri, A. & Vesentini, S., 2011. Hierarchical structure and nanomechanics of collagen microfibrils from the atomistic scale up. *Nano Letters*, 11(2), 757–766.
- Gautreau, Z., Griffin, J., Peterson, T. & Thongpradit, P., 2006. *Characterizing viscoelastic properties of polyacrylamide gels*, B.S. Project Report, Worcester Polytechnic Institute.
- Georges, P. et al., 2007. Increased stiffness of the rat liver precedes matrix deposition: implications for fibrosis. *American Journal of Physiology. Gastrointestinal and Liver Physiology*, 293, 1147–1154.
- Grant, C. & Twigg, P., 2013. Pseudostatic and Dynamic Nanomechanics of the Tunica Adventitia in Elastic Arteries Using Atomic Force Microscopy. *ACS Nano*, 7(1), 456–464.

- Grillet, A., Wyatt, N. & Gloe, L., 2012. Polymer gel rheology and adhesion. In: J. D. Vicente, ed. *Rheology*. Croatia: InTech, 59–80.
- Groetsch, C., 1984. *The theory of Tikhonov regularization for Fredholm equations of the first kind*. Boston: Pitman.
- Guo, C. & Kaufman, L., 2007. Flow and magnetic field induced collagen alignment. *Biomaterials*, 28(6), 1105–1114.
- Gupta, H. et al., 2010. In situ multi-level analysis of viscoelastic deformation mechanisms in tendon collagen. *Journal of Structural Biology*, 169(2), 183–191.
- Hansen, P., 1992. Numerical tools for analysis and solution of Fredholm integral equations of the first kind. *Inverse Problems*, 8(6), 849–872.
- Hansen, P., 1994. Regularization tools: A MATLAB package for analysis and solution of discrete ill-posed problems. *Numerical Algorithms*, 6(1), 1–35.
- Hansen, S., 2008. Estimation of the relaxation spectrum from dynamic experiments using Bayesian analysis and a new regularization constraint. *Rheologica Acta*, 47(2), 169–178.
- Hatami-Marbini, H., Shahsavari, A. & Picu, R., 2013. Multiscale modeling of semiflexible random fibrous structures. *Computer Aided Design*, 45(1), 77–83.
- Herath, S. et al., 2014. Characterization of uniaxial stiffness of extracellular matrix embedded with magnetic beads via bio-conjugation and under the influence of an external magnetic field. *Journal of the Mechanical Behavior of Biomedical Materials*, 30, 253–265.
- Heyden, S., 2000. Network modelling for the evaluation of mechanical properties of cellulose fibre fluff. *Doctoral dissertation – Lund University*.
- Honerkamp, J., 1989. Ill posed problems in rheology. *Rheologica Acta*, 28(5), 363–371.
- Honerkamp, J. & Weese, J., 1989. Determination of the relaxation spectrum by a regularization method. *Macromolecules*, 22(11), 4372–4377.
- Hrapko, M., van Dommelen, J., Peters, G. & Wismans, J., 2006. The mechanical behaviour of brain tissue: large strain response and constitutive modelling. *Biorheology*, 43(5), 623–636.
- Hrapko, M., van Dommelen, J., Peters, G. & Wismans, J., 2008. The influence of test conditions on characterization of the mechanical properties of brain tissue. *Journal of Biomechanical Engineering*, 130(3), 31003.1–31003.10.

- Hsu, H., Jamieson, A. & Blackwell, J., 1994. Viscoelastic studies of extracellular-matrix interactions in a model native collagen gel system. *Biorheology*, 31, 21–36.
- Huisman, E., VanDillen, T., Onck, P. & Van der Giessen, E., 2007. Three-Dimensional Cross-Linked F-Actin Networks: Relation between Network Architecture and Mechanical Behavior. *Physical Review Letters*, 99(20), 2–5.
- Jordan, A. et al., 2010. Cell-collagen networks breakdown by collagen remodelling. *Biorheology*, 47(5–6), 277–295.
- Jackson, J., DeRosa, M. & Winter, H., 1994. Molecular weight dependence of relaxation time spectra for the entanglement and flow behavior of monodisperse linear flexible polymers. *Macromolecules*, 27(9), 2426–2471.
- Janmey, P. & Miller, R., 2011. Mechanisms of mechanical signaling in development and disease. *Journal of Cell Science*, 124, 9–18.
- Jensen, E., 2002. Determination of discrete relaxation spectra using Simulated Annealing. *Journal of Non-Newtonian Fluid Mechanics*, 107(1), 1–11.
- Jhun, C., Evans, M., Barocas, V. & Tranquillo, R., 2009. Planar Biaxial Mechanical Behavior of Bioartificial Tissues Possessing Prescribed Fiber Alignment. *Journal of Biomechanical Engineering*, 131(8), 81006-1-081006-8.
- Julias, M., Edgar, L. T., Buettner, H. M. & Shreiber, D. I., 2008. An in vitro assay of collagen fiber alignment by acupuncture needle rotation. *Biomedical Engineering Online*, 7(19).
- Kamgoue, A., Ohayon, J. & Tracqui, P., 2007. Estimation of Cell Young's Modulus of Adherent Cells Probed by Optical and Magnetic Tweezers: Influence of Cell Thickness and Bead Immersion. *Journal of Biomechanical Engineering*, 129, 523–530.
- Kang, H. et al., 2009. Nonlinear elasticity of stiff filament networks: strain stiffening, negative normal stress, and filament alignment in fibrin gels. *Journal of Physical Chemistry. B*, 113, 3799–3805.
- Knapp, D., Barocas, V. & Moon, A., 1997. Rheology of reconstituted type I collagen gel in confined compression. *Journal of Rheology*, 41(5), 971–993.
- Komatsu, K., 2010. Mechanical strength and viscoelastic response of the periodontal ligament in relation to structure. *Journal of Dental Biomechanics*, 2010:502318.
- Kontogiorgos, V., 2010. Calculation of relaxation spectra from mechanical spectra in MATLAB. *Polymer Testing*, 29(8), 1021–1025.

- Kontogiorgos, V. & Dahunsi, O., 2014. Relaxation dynamics in hydrated gluten networks. *Journal of Cereal Science*, 59(1), 101–108.
- Kontogiorgos, V., Jiang, B. & Kasapis, S., 2009. Numerical computation of relaxation spectra from mechanical measurements in biopolymers. *Food Research International*, 42(1), 130–136.
- Kontogiorgos, V. & Kasapis, S., 2010. Temperature dependence of relaxation spectra for highly hydrated gluten networks. *Journal of Cereal Science*, 52(1), 100–105.
- Kurniawan, N. A., Wong, L. H. & Rajagopalan, R., 2012. Early stiffening and softening of collagen: Interplay of Deformation Mechanisms in Biopolymer networks. *Biomacromolecules*, 13(3), 691–698.
- Lai, V. et al., 2016. Swelling of Collagen-Hyaluronic Acid Co-Gels: An In Vitro Residual Stress Model. *Annals of Biomedical Engineering*, 44(10), 2984–2993.
- Latinovic, O., Hough, L. & Ou-Yang, H., 2010. Structural and micromechanical characterization of type I collagen gels. *Journal of Biomechanics*, 2010(43), 500–505.
- Laun, H., 1978. Description of the non-linear shear behavior of a low-density polyethylene. *Rheologica Acta*, 17(1), 1–15.
- Laurent, V. et al., 2002. Assessment of mechanical properties of adherent living cells by bead micromanipulation: comparison of magnetic twisting cytometry vs optical tweezers. *Journal of Biomechanical Engineering*, 124(4), 408–421.
- Lee, C., Singla, A. & Lee, Y., 2001. Biomedical applications of collagen. *International Journal of Pharmaceutics*, 221(1–2), 1–22.
- Lee, K. & Yuk, S., 2007. Polymeric protein delivery systems. *Progress in Polymer Science*, 32(7), 669–697.
- Leung, L. et al., 2007. A new microrheometric approach reveals individual and cooperative roles for TGF-beta1 and IL-1beta in fibroblast-mediated stiffening of collagen gels. *Federation of American Societies for Experimental Biology Journal*, 21(9), 2064–2073.
- Li, H. et al., 2017. Multiscale Measurements of the Mechanical Properties of Collagen Matrix. *ACS Biomaterials Science & Engineering*. Articles ASAP. DOI: 10.1021/acsbiomaterials.6b00634
- Li, H. & Zhang, Y., 2014. Modeling of the viscoelastic behavior of collagen gel from dynamic oscillatory shear measurements. *Biorheology*, 51(6), 369–380.

- Li, W., Dobraszczyk, B. & Schofield, J., 2003. Stress relaxation behavior of wheat dough, gluten and gluten protein fractions. *Cereal Chemistry*, 80(3), 333–338.
- Lu, P., Weaver, V. & Werb, Z., 2012. The extracellular matrix: A dynamic niche in cancer progression. *Journal of Cell Biology*, 196(4), 395–406.
- Maksym, G. et al., 2000. Mechanical properties of cultured human airway smooth muscle cells from 0.05 to 0.4 HZ. *Applied Physiology*, 89, 1619–1632.
- Malkin, A., 1990. Some inverse problems in rheology leading to integral equations. *Rheologica Acta*, 29(6), 512–518.
- Malkin, A., 2002. The sense of a relaxation spectrum and methods for its calculation. *Vysokomolekuljarnye Soedinenija (Polymers-in Russian)*, 44(9), 1698–2005.
- Malkin, A., 2006. Continuous relaxation spectrum-its advantages and methods of calculation. *International Journal of Applied Mechanics and Engineering*, 11(2), 235–243.
- Mao, R., Tang, J. & Swanson, B., 2000. Relaxation time spectrum of hydrogels contin analysis. *Journal of Food Science*, 65(3), 374–381.
- Marquez, J., Genin, G., Pryse, K. & Elson, E., 2006. Cellular and Matrix Contributions to Tissue Construct Stiffness Increase with Cellular Concentration. *Annals of Biomedical Engineering*, 34(9), 1475–1482.
- Mattson, J., Turcotte, R. & Zhang, Y., 2017. Glycosaminoglycans contribute to extracellular matrix fiber recruitment and arterial wall mechanics. *Biomechanics and Modeling in Mechanobiology*, 16(213).
- Mckee, C., Last, J., Russell, P. & Murphy, C., 2011. Indentation Versus Tensile Measurements of Young's Modulus for Soft Biological Tissues. *Tissue Engineering. Part B, Reviews*, 17(3), 155–164.
- Mezger, T., 2006. *The Rheology Handbook*. 2nd ed. Hannover: Vincentz Network.
- Mijailovich, S. et al., 2002. A finite element model of cell deformation during magnetic bead twisting. *Journal of Applied Physiology*, 93, 1429–1436.
- Motte, S. & Kaufman, L., 2012. Strain stiffening in collagen I networks. *Biopolymers*, 99(1), 35–46.
- Mow, V., Bachrach, N., Setton, L. & Guilak, F., 1994. Stress, strain, pressure and flow fields in articular cartilage and chondrocytes. In: V. Mow, N. Bachrach, L. Setton & F. Guilak, eds. *Cell Mechanics and Cellular Engineering*. New York: Springer-Verlag.

- Mustapha, S. & TN, P., 2000. A dynamics nonlinear regression method for the determination of discrete relaxation spectrum. *Journal of Physics D: Applied Physics*, 33(10), 1219–1229.
- Nair, A., 2012. Discrete Micromechanics of Random Fibrous Architectures. *Doctoral Dissertaion – National University of Singapore*.
- Nasseri, S., Bilston, L. & Phan-Thien, N., 2002. Viscoelastic properties of pig kidney in shear, experimental results and modelling. *Rheologica Acta*, 41(1), 180–192.
- Nerurkar, N., Elliott, DM & Mauck, R., 2010. Mechanical Design Criteria for Intervertebral Disc Tissue Engineering. *Journal of Biomechanics* 43(6), 1017–1030.
- Nicolle, S., Lounis, M., Willinger, R. & Paliarne, J., 2005. Shear linear behaviour of brain tissue over a large frequency range. *Biorheology*, 42(3), 209–223.
- Nicolle, S. & Paliarne, J., 2012. On the efficiency of attachment methods of biological soft tissues in shear experiments. *Journal of the Mechanical Behavior of Biomedical Materials*, 14, 158–162.
- Ohayon, J. & Tracqui, P., 2005. Computation of Adherent Cell Elasticity for Critical Cell-Bead Geometry in Magnetic Twisting Experiments. *Annals of Biomedical Engineering*, 33(2), 131–141.
- Onck, P., Koeman, T., Dillen, T. & Giessen, E., 2005. Alternative explanation of stiffening in cross-linked semiflexible networks. *Physical Review Letters*, 95(17), 178102.
- Orbey, N. & Dealy, J., 1991. Determination of the relaxation spectrum from oscillatory shear data. *Journal of Rheology*, 35(6), 1035–1049.
- Parekh, A. & Velegol, D., 2007. Collagen gel anisotropy measured by 2-D laser trap microrheometry. *Annals of Biomedical Engineering*, 35(7), 1231–1246.
- Pelham, R. & Wang, Y., 1997. Cell locomotion and focal adhesions are regulated by substrate flexibility. *Proceedings of the National Academy of Sciences of the United States of America*, 94(25), 13661–13665.
- Peyton, S., Ghajar, C., Khatiwala, C. & Putman, A., 2007. The emergence of ECM mechanics and cytoskeletal tension as important regulators of cell function. *Cell Biochemistry and Biophysics*, 47(2), 300–320.
- Pizzo, A. et al., 2005. Extracellular matrix (ECM) microstructural composition regulates local cell-ECM biomechanics and fundamental fibroblast behavior: a multidimensional perspective. *Journal of Applied Physiology*, 98(5), 1909–1921.

- Pourati, J. et al., 1998. Is cytoskeleton tension a major determinant of cell deformability in adherent endothelial cells. *American Journal of Physiology*, 274, C1283–C1289.
- Provencher, S., 1982. A constrained regularization method for inverting data represented by linear algebraic or integral equations. *Computer Physics Communications*, 27(3), 213–227.
- Ptaszek, A. et al., 2009. Viscoelastic properties of waxy maize starch and selected non-starch hydrocolloids gels. *Carbohydrate Polymers*, 76(4), 567–577.
- Ptaszek, P. & Grzesik, M., 2007. Viscoelastic properties of maize starch and guar gum gels. *Journal of Food Engineering*, 82(2), 227–237.
- Puxkandl, R. et al., 2002. Viscoelastic properties of collagen: synchrotron radiation investigations and structural model. *Philosophical Transactions of the Royal Society of London. Series B, Biological Sciences*, 357, 191–197.
- Raub, C. B. et al., 2007. Noninvasive Assessment of collagen gel microstructure and mechanics using multiphoton microscopy. *Biophysical Journal*, 92(6), 2212–2222.
- Roeder, B., Kokini, K., Robinson, J. & Voytik-Harbin, S., 2004. Local, three-dimensional strain measurements within largely deformed extracellular matrix constructs. *Journal of Biomechanical Engineering*, 126(6), 699–708.
- Roeder, B. et al., 2002. Tensile mechanical properties of three-dimensional type I collagen extracellular matrices with varied microstructure. *Journal of Biomechanical Engineering*, 124(2), 214–222.
- Roeder, B., Kokini, K. & Voytik-Harbin, S., 2009. Fibril microstructure affects strain transmission within collagen extracellular matrices. *Journal of Biomechanical Engineering*, 131(3), 031004-1–031004-11.
- Rosenblatt, N. et al., 2004. Distending stress of the cytoskeleton is a key determinant of cell rheological behavior. *Biochemical and Biophysical Research Communications*, 321(3), 617–622.
- Rosenblatt, N. et al., 2007. Contributions of the Active and Passive Components of the Cytoskeletal Prestress to Stiffening of Airway Smooth Muscle Cells. *Annals of Biomedical Engineering*, 35(2), 224–234.
- Roths, T. et al., 2000. Determination of the relaxation time spectrum from dynamic moduli using an edge preserving regularization method. *Rheologica Acta*, 39(2), 163–173.
- Rousseeuw, P. & Croux, C., 1993. Alternatives to the Median Absolute Deviation. *Journal of the American Statistical Association*, 88, 1273–1283.

Rowe, R. et al., 2015. Collective Matrix Remodeling by Isolated Cells: Unionizing Home improvement Do-It-Yourselfers. *Biophysical Journal*, 108, 2611–2612.

Sacks, M. & Sun, W., 2003. Multiaxial Mechanical Behavior of Biological Materials. *Annal Review of Biomedical Engineering*, 5, 251–284.

Sander, E., Stylianopoulos, T., Tranquillo, R. & Barocas, V., 2009. Image-based multiscale modeling predicts tissue-level and network-level fiber reorganization in stretched cell-compacted collagen gels. *Proceedings of the National Academy of Sciences of the United States of America*, 106(42), 17675–17680.

Schrader, J. et al., 2011. Matrix Stiffness Modulates Proliferation, Chemotherapeutic Response and Dormancy in Hepatocellular Carcinoma Cells. *Hepatology*, 53(4), 1192–1205.

Schriebl, A. et al., 2012. Determination of the layer-specific distributed collagen fibre orientations in human thoracic and abdominal aortas and common iliac arteries. *Journal of the Royal Society, Interface*, 9, 1275–1286.

Screen, H., Lee, D., Bader, D. & Shelton, J., 2004. An investigation into the effects of the hierarchical structure of tendon fascicles on micromechanical properties. *Proceedings of the Institution of Mechanical Engineers. Part H, Journal of Engineering in Medicine*, 218(2), 109–119.

Shayegan, M. & Forde, N., 2013. Microrheological Characterization of Collagen Systems: From Molecular Solutions to Fibrillar Gels. *PLoS One*, 8(8), e70590.

Shkumatov, A. et al., 2015. Matrix stiffness-modulated proliferation and secretory function of the airway smooth muscle cells. *American Journal of Physiology. Lung Cellular and Molecular Physiology*, 308(11), L1125–L1135.

Smith, P., Deng, L., Fredberg, J. & Maksym, G., 2003. Mechanical strain increases cell stiffness through cytoskeletal filament reorganization. *American Journal of Physiology. Lung Cellular and Molecular Physiology*, 285, L456–L463.

Sodhi, N., Sasaki, T., Lu, Z. & Kohyama, K., 2010. Phenomenological viscoelastic of some rice starch gels. *Food Hydrocolloids*, 24(5), 512–517.

Stein, A., Vader, D., Weitz, D. & Sander, L., 2010. The micromechanics of three-dimensional collagen-I gels. *Complexity*, 16(4), 22–28.

Sundararaghavan, H. et al., 2008. Genipin-induced changes in collagen gels: correction of mechanical properties to fluorescence. *Journal of Biomedical Materials Research. Part A*, 87(2), 308–320.

- Sun, Y., Luo, Z., Fertala, A. & An, K., 2004. Stretching type II collagen with optical tweezers. *Journal of Biomechanics*, 37(11), 1665–1669.
- Throm Quinlan, A. & Billar, K., 2012. Investigating the role of substrate stiffness in the persistence of valvular interstitial cell activation. *Journal of Biomedical Materials Research. Part A*, 100(9), 2474–2482.
- Throm Quinlan, A. et al., 2011. Combining Dynamic Stretch and Tunable Stiffness to Probe Cell Mechanobiology In Vitro. *PLoS One*, 6(8), e23272.
- Toms, S., Dakin, G., Lemons, J. & Eberhardt, A., 2002. Quasi-linear viscoelastic behavior of the human periodontal ligament. *Journal of Biomechanics*, 35(10), 1411–1415.
- Tower, T., Neidert, M. & Tranquillo, R., 2002. Fiber alignment imaging during mechanical testing of soft tissues. *Annals of Biomedical Engineering*, 30(10), 1221–1233.
- Toyjanova, J. et al., 2014. High Resolution, Large Deformation 3D Traction Force Microscopy. *PLoS One*, 9(4), e90976.
- Trepat, X., Grabulosa, M., Buscemi, L. & Rico, F., 2003. Oscillatory magnetic tweezers based on ferromagnetic beads and simple coaxial coils. *Review of Scientific Instruments*, 74(9), 4012–4019.
- Trepat, X. et al., 2004. Viscoelasticity of human alveolar epithelial cells subjected to stretch. *American Journal of Physiology. Lung Cellular and Molecular Physiology*, 287(5), 1025–1034.
- Vader, D., Kabla, A., Weitz, D. & Mahadevan, L., 2009. Strain-induced alignment in collagen gels. *PLoS One*, 4(6), e5902.
- Valberg PA, B. J., 1987. Magnetic particle motions within living cells. *Biophysical Journal*, 52, 537–550.
- Van Oosten, A. et al., 2016. Uncoupling shear and uniaxial elastic moduli of semiflexible biopolymer networks: compression-softening and stretch-stiffening. *Scientific Reports*, 6, 19270:1–9.
- Velegol, D. & Lanni, F., 2001. Cell Traction Forces on Soft Biomaterials. I. Microrheology of Type I Collagen Gels. *Biophysical Journal*, 81(3), 1786–1792.
- Voytik-Harbin, S. et al., 2003. Simultaneous mechanical loading and confocal reflection microscopy for three-dimensional microbiomechanical analysis of biomaterials and tissue constructs. *Microscopy and Microanalysis*, 9(1), 74–85.
- Wagenseil, J. et al., 2003. One-dimensional viscoelastic behavior of fibroblast populated collagen matrices. *Journal of Biomechanical Engineering*, 125(5), 719–725.

- Walton, L. et al., 2015. Morphological Characterisation of Unstained and Intact Tissue Micro-architecture by X-ray Computed Micro- and Nano-Tomography. *Scientific Reports*, 5(10074), 1–14.
- Wang, H. et al., 2014. Long-Range Force Transmission in Fibrous Matrices Enabled by Tension-Driven Alignment of Fibers. *Biophysical Journal*, 107, 2592–2603.
- Wang, H., Dembo, M. & Wang, Y., 2000. Substrate flexibility regulates growth and apoptosis of normal but not transformed cells. *American Journal of Physiology. Cell Physiology*, 279, 1345–1350.
- Wang, N., Butler, J. & Ingber, D., 1993. Mechanotransduction across the cell surface and through the cytoskeleton. *Science*, 260, 1124–1127.
- Weese, J., 1992. A reliable and fast method for the solution of Fredholm integral equations of the first kind based on Tikhonov regularization. *Computer Physics Communications*, 69(1), 99–111.
- Wells, R., 2008. The Role of Matrix Stiffness in Regulating Cell Behavior. *Hepatology*, 47(4), 1394–1400.
- Wenger, M., Bozec, L., Horton, M. & Mesquida, P., 2007. Mechanical Properties of Collagen Fibrils. *Biophysical Journal*, 93, 1255–1263.
- White, E., 2015. Lung Extracellular Matrix and Fibroblast Function. *Annals of the American Thoracic Society*, 12, S30–S33.
- Winter, H., 1997. Analysis of dynamic mechanical data: inversion into a relaxation time spectrum and consistency check. *Journal of Non-Newtonian Fluid Mechanics*, 68, 225–239.
- Wu, C., Ding, S. & Wang, Y., 2005. Mechanical properties of collagen gels derived from rats of different ages. *Journal of Biomaterials Science. Polymer Edition*, 16(10), 1261–1275.
- Xu, B., Chow, J. & Zhang, Y., 2011. Experimental and Modelling Study of Collagen Scaffolds with the Effects of Crosslinking and Fiber Alignment. *International Journal of Biomaterials*, 2011, 172389–172400.
- Xu, B., Li, H. & Zhang, Y., 2013. Understanding the viscoelastic behaviour of collagen matrices through relaxation time distribution spectrum. *Biomatter*, 3(3), e24651.
- Xu, D. & Craig, S., 2011. Strain hardening and strain softening of reversibly cross-linked supramolecular polymer networks. *Macromolecules*, 44, 7478–7488.

Yang, Y. & Kaufman, L., 2009. Rheology and confocal reflectance microscopy as probes of mechanical properties and structure during collagen and collagen/hyaluronan self-assembly. *Biophysical Journal*, 96(4), 1566–1585.

Yang, Y., Leone, L. & Kaufman, L., 2009. Elastic Moduli of Collagen Gels Can Be Predicted from Two-Dimensional Confocal Microscopy. *Biophysical Journal*, 97(7), 2051–2060.

Zaman, M., Trapani, L. & Sieminski, A., 2006. Migration of tumor cells in 3D matrices is governed by matrix stiffness along with cell-matrix adhesion and proteolysis. *Proceedings of the National Academy of Sciences of the United States of America*, 103(29), 10889–10894.

Zhou, E. et al., 2009. Universal behavior of the osmotically compressed cell and its analogy to the colloidal glass transition. *Proceedings of the National Academy of Sciences of the United States of America*, 106(26), 10632–10637.

Zou, Y. & Zhang, Y., 2009. An experimental and theoretical study on the anisotropy of elastin network. *Annals of Biomedical Engineering*, 37(8), 1572–1583.

**CURRICULUM VITAE**

